UNIVERSITEIT VAN PRETORIA
UNIVERSITY OF PRETORIA
YUNIBESITHI YA PRETORIA

THE CHARACTERISATION OF SPACE WEATHER EFFECTS ON CELLULAR AND MICROWAVE TELECOMMUNICATION

by

Jan Adam Vivian Zięba

Submitted in partial fulfilment of the requirements for the degree

Master of Engineering (Computer Engineering)

in the

Department of Electrical, Electronic and Computer Engineering
Faculty of Engineering, Built Environment and Information Technology
UNIVERSITY OF PRETORIA

January 2016

SUMMARY

THE CHARACTERISATION OF SPACE WEATHER EFFECTS ON CELLULAR AND MICROWAVE TELECOMMUNICATION

by

Jan Adam Vivian Zięba

Supervisor:	Prof. BJT Maharaj
Department:	Electrical, Electronic and Computer Engineering
University:	University of Pretoria
Co-Supervisor:	Dr. PJ Cilliers
Directorate:	Space Science
Institution:	SANSA (South African National Space Agency)

Degree:	Master of Engineering (Computer Engineering)
Keywords:	Space Weather Impacts, Mobile Phone, Microwave, Radio Telecommunications, e-Callisto, X-ray Flare, $F_{10.7}$, LTE, GSM, UMTS, Radio Interference, Radio Noise

To the knowledge of the authors, studies making use of cellular network counters to analyse the impact of solar originated radio waves on cellular telecommunication systems are a relatively unexplored area. This dissertation examines interference of solar originated radio waves with the radio aspect of terrestrial cellular telecommunications systems. A theoretical analysis was performed and real world data were also obtained from a cellular network. Solar parameters that have a potential relationship to noise generated on the cellular network were analysed, making use of the position of the sun relative to the radiation patterns of antennas of cellular network equipment.

The most sensitive cellular networks are those based on the long-term evolution (LTE) standard; radio bursts of as little as 10 solar flux units (SFU), though beyond the range of the equipment, are theoretically detectable by it and bursts of 100 000 SFU have been shown to be capable of producing noise levels of -88 dBm, 13 dBm above the thermal noise level at 300 K. A comparison between sun

incident hours and others, when the sun is not in direct line of sight of cellular basestation antennas, reveals increased interference, though the cellular network data do not correlate well with solar radio burst and X-ray flares, owing to lack of sample diversity and low granularity of telecommunications data and lack of extreme solar events during the period. However, potential susceptibly to solar radio interference exists, especially in the case of lower frequencies (900 MHz) in telecommunication bands (900–2100 MHz) with high bandwidth (20 MHz) applications.

OPSOMMING

DIE KARATERISERING VAN RUIMTEWEEREFFEKTE OP SELLULÊRE EN MIKROGOLFTELEKOMMUNIKASIE

deur

Jan Adam Vivian Zięba

Studieleier:	Prof. BJT Maharaj
Departement:	Elektriese, Elektroniese en Rekenaar-Ingenieurswese
Universiteit:	Universiteit van Pretoria
Mede-Studieleier:	Dr. PJ Cilliers
Direktoraat:	Ruimtewetenskap
Instituut:	SANSA (South African National Space Agency)

Graad:	Magister in Ingenieurswese (Rekenaaringenieurswese)
Sleutelwoorde:	Ruimteweerimpakte, Mobiele Telefoon, Mikrogolf, Radiotelekommunikasie, e-Callisto, X-straal fakkel, $F_{10.7}$, LTE, GSM, UMTS, Radiosteurings, Radio-ruis

Na die wete van die skrywer is studies wat van sellulêrenetwerktellers gebruik maak om die impak van radiogolwe van sonoorsprong op telekommunikasiestelsels te analiseer ’n relatief swak bestudeerde veld. Hierdie verhandeling ondersoek die steurings wat radiogolwe van son-oorsprong het op die radio-aspek van aard-sellulêre telekommunikasiestelsels. ’n Teoretiese analise is uitgevoer en gemete is verkry van ’n sellul êre netwerk. Sonparameters wat potensieel ’n verband het met ruis op die sellulêre netwerk opgewek is, is geanaliseer deur gebruik te maak van die posisie van die son relatief tot die stralingspatrone van antennas van sellulêrenetwerktoerusting.

Die sensitiefste sellulêre netwerke is gebaseer op die langtermynevolusiestandaard (LTE); radiouitbarstings van so min as 10 sonvloedeenhede (SFE) is waarneembaar met LTE en daar is bewys dat uitbarstings van 100 000 SFE in staat is om ruisvlakke van -88 dBm te veroorsaak, 13 dBm bo die termiese ruisvlak by 300 K.’n Vergelyking tussen son-insidensie-ure en ander, wanneer die son nie

in direkte siglyn is nie, toon verhoogde inmenging, alhoewel die sellulêrenetwerkdata nie goed met sonradio-uitbarstings en X-straal fakkels korreleer nie, te danke aan die lae granulariteit van telekommunikasiedata en die afwesigheid van uiterste son-insidente gedurende die tydperk. Daar is nietemin potensieel vatbaarheid vir son-radio-steurings, veral in die geval van laer frekwensies (900 MHz) in telekommunikasiebande (900–2100 MHz) met hoë bandwydtetoepassing (20 MHz).

ACKNOWLEDGEMENTS

In no particular order, many thanks to:

- Institute of Astronomy, ETH Zurich, and FHNW Brugg/Windisch, Switzerland
- SANSA (South African National Space Agency) - www.sansa.org.za
- The helpful engineers at the cellular network operator
- Prof. Sunil Maharaj of the University of Pretoria
- Dr Pierre J. Cilliers from SANSA
- Dr David Perez-Suarez from SANSA
- Dr Donald W. Danskin from Geomagnetic Laboratory, Natural Resources Canada
- Sebastian Monstein from eCallisto
- Dr Danie Louw from the University of Pretoria

LIST OF ABBREVIATIONS

2G	Second Generation Network: CDMA One, GSM
3G	Third Generation Network: UMTS, CDMA2000, LTE
4G	Fourth Generation Network: LTE, HSPA+
ADC	Analogue-to-digital Converter
AGC	Automatic Gain Control
AMR	Adaptive Multi-rate
BAO	Baryon Acoustic Oscillations
BER	Bit Error Rate
BSC	Base Station Controller
C/A	Coarse Acquisition
Callisto	Compound Astronomical Low-cost Low-frequency Instrument for Spectroscopy and Transportable Observatory
CDMA	Code Division Multiple Access
CGN	Coloured Gaussian Noise
CME	Coronal Mass Ejection
CS	Circuit Switched
dBm	Decibel relative to a milli-Watt
DCR	Dropped Call Rate
DL	Downlink
DONKI	Database of Notification, Knowledge, Information
eNB	E-UTRAN Node B
E-UTRAN	Evolved UTRAN
$F_{10.7}$	Penticton Canada 10.7 cm / 2.8 GHz Solar Radio Flux
EDGE	Evolved GPRS
EGPRS	Enhanced Data Rates for GSM Evolution

EFR	Enhanced Full Rate
ETSI	European Telecommunications Standards Institute
EUV	Extreme Ultraviolet
FCC	Federal Communication Commission (USA)
FDD	Frequency Division Duplex
FDMA	Frequency Division Multiple Access
FEC	Forward Error Correction. Also called channel coding
FER	Frame Error Rate
FITS	Flexible Image Transport System
FR	Full Rate
GOES	Geostationary Operational Environmental Satellite
GNSS	Global Navigation Satellite System
GPS	Global Positioning System
GPRS	General Packet Radio Service
GSM	Global System for Mobile Telecommunication
HR	Half Rate
ISDN	Integrated Services for Digital Network
IP	Internet Protocol
HSDPA	High Speed Downlink Packet Access
KPI	Key Performance Indicator
LTE	Long-term Evolution
LOS	Line of Sight
MIMO	Multiple Input Multiple Output
MF	Medium Frequency
MSC	Mobile Switching Centre
NOAA	National Oceanic and Atmospheric Administration (USA)
OFDMA	Orthogonal Frequency Division Multiple Access
OVSF	Orthogonal Variable Spreading Factor
P(Y)	Precise Code
PCA	Polar Cap Absorption
PTP	Precision Timing Protocol
QAM	Quadrature Amplitude Modulation
QPSK	Quadrature Phase Shift Keying

RAN	Radio Access Network
RHCP	Right-hand Circularly Polarised
RNC	Radio Network Controller
RSCP	Received Signal Code Power
RSSI	Received Signal Strength Indication
RSTN	Radio Solar Telescope Network
RTWP	Received Total Wideband Power
RxQual	Received Quality
SID	Sudden Ionospheric Disturbance
SMS	Short Message Service
SNR	Signal-to-noise Ratio
SSN	Sun Spot Number
SWF	Short Wave Fade
SWPC	Space Weather Prediction Centre (USA)
TDD	Time Division Duplex
TDMA	Time Division Multiple Access
True 4G	IMT-Advanced 4G: LTE Advanced, Wimax Advanced
TRX	Tranceiver
UL	Uplink
Um	User Mobile
UMTS	Universal Mobile Telecommunication System
UTRAN	Universal Terrestrial Radio Access Network
UV	Ultraviolet
UWB	Ultra-wideband
VAS	Value Added Services

TABLE OF CONTENTS

CHAPTER 1

INTRODUCTION

Indications of interference of space weather with radio waves of radio frequency systems and telecommunication networks exist [1, 2]. Studies of the influence of solar radiation on communications systems exist [3, 4] primarily for:

- High-frequency (HF) radio and other waveguide systems.
- Satellite systems influenced by the space environment, atmosphere and ionosphere. For example, GPS operates in a similar band to cellular telecommunications systems and has been seen to be susceptible to solar radio bursts [5][6].
- Wired systems, such as telegraph and power systems influenced by geomagnetic storms.

Some studies have been done on wireless systems with frequencies near to telecommunication bands [7] and a study inspected the dropped call rate [1], indicating that there may be interference affecting cellular base stations at sunrise and sunset. Cellular telecommunications network performance indicators do not seem to have been analysed, probably because private communication company network data are often proprietary [8], giving little opportunity for analysis [1]. Cellular telecommunications are used extensively (especially for emergency services and disaster response [9, 10]) and are more prone to interference than wired systems [11]. Interference from solar radio noise in cellular telecommunications networks, including the microwave backhaul systems[1], can result from an increased noise floor.

Making use of information from the actual cellular telecommunications equipment that is being interfered with is important, as it could contribute to creating a clearer picture, regarding the problems experienced, than by making use of data from related systems, such as receivers in similar, but not

[1] Backhaul connects the radio access network (RAN) to the portion of the network which routes calls, the core network.

identical bands or transmission technologies.

In this thesis, susceptibility of the radio network of cellular telecommunication networks (as a function of primary frequency, bandwidth, system design specifications and typical configuration values) to solar radio noise is investigated. The mechanism of interference is expected to be an increase in the noise floor and thus influence the signal-to-noise ratio (SNR), decreasing throughput. Comparisons between space weather data (X-ray flares, 245 MHz solar radio burst and 2695 MHz solar radio burst data) and cellular telecommunications network data (microwave backhaul, Global System for Mobile Communications (GSM), Universal Mobile Telecommunications System (UMTS) and long-term evolution (LTE)) are performed.

1.1 TELECOMMUNICATIONS PARAMETERS

The network counter data types selected were based on recommendations from the cellular network operator and manufacturer, given the goal of measuring radio noise, see Table 1.1. Cellular data which characterised network quality were made available by a South African network operator under an agreement, which restricted the distribution and publication of detailed data. The cells selected were based on recommendations from the cellular operator - the area chosen is considered stable from an equipment integrity, network quality and infrastructure change point of view. The period of data are related to infrastructure constraints of the cellular network operator.

The cellular network used in this study makes use of technologies that operate in the frequency ranges of 880 – 960 MHz (GSM), 1710 – 1880 MHz (LTE), 2110 – 2170 MHz (UMTS) and 26 GHz (microwave backhaul). Other implementations do exist where systems operate at different frequencies.

Data were available summarised hourly or daily, as specified, for a given number of sectors, indicated by the samples column. Cellular telecommunication network sites are sectored, typically three sectors of 120° each.

Overall, in the case of GSM, UMTS and LTE, sectors cover 360° over the sample. Microwave backhaul makes use of four sectors of 90° each, typically oriented north, south, east and west. Antennas, excluding microwave links, which are point to point, are often oriented downwards slightly, as the target coverage area is at ground level; the angle is referred to as downtilt, see Figure 2.11.

Table 1.1: Particulars of data used in analysis. The abbreviation TR means time resolution. In this document average is used interchanably with mean.

Source	Data	Samples	TR.	Period
Cellular Network	Microwave RSSI	12	Daily	2013-02-17 to 2014-04-01
Cellular Network	LTE UL interference	32 sectors	Hourly	2014-02-22 to 2014-05-23
Cellular Network	UMTS RTWP	35 sectors	Hourly	2014-02-22 to 2014-05-23
Cellular Network	GSM RxQual	47 sectors averaged	Hourly	2014-04-20 to 2014-07-01
NOAA SWPC	Solar radio bursts	NA	Second	2001-04-06 to 2014-06-30
NASA DONKI	GOES-15 SEM/XRS 1.0-8.0	NA	Second	2013-07-25 to 2014-07-10

The data used are as follows:

- Microwave backhaul received signal strength indication (RSSI) is a measure of total received signal strength in dB.
- LTE UL[2] interference, measured in dBm, is the total power of the noise floor and neighbouring cell interference received by each physical resource block in the UL for a time period.
- UMTS Received Total Wideband Power (RTWP), in decibels, can be used to determine the noise floor.
- GSM TRX UL RxQual is an indication of bit errors over the hour. Errors are grouped into two groups (good: bit error rate (BER) $< 2.7\%$ and bad: BER $> 3.8\%$ [12]).

A full discussion of the data is available in Section 2.7.

[2]Downlink (DL) indicates communication in the direction of user equipment, typically a handset or data modem, from the base station. Uplink (UL) indicates the inverse.

1.2 SPACE WEATHER PARAMETERS

Space weather data used in this study are the intensity for the periods during the events listed in Table 1.1. The first data set is the peak of solar radio bursts as measured by terrestrial observatories at 245 and 2695 MHz. Solar radio burst flux density is measured in solar flux units (SFU), 1 SFU = $10^{-22} Wm^{-2} Hz^{-1}$. Wideband radio noise is produced by the sun.

In addition, periods of time when flux levels of soft X-ray have significant value are included in this study. X-ray flares are classified according to the NOAA scale [13]. Only X and M-class flares are considered. X-ray flare data are from the Geostationary Operational Environmental Satellite-15 (GOES-15).

1.3 SOLAR AND TELECOMMUNICATIONS RELATIONSHIP

Radio noise of solar events and in wireless telecommunications systems are relatable, because solar radio emissions can occupy a wide range of frequencies, including those used by wireless telecommunications systems, and can occur at levels sufficiently high enough to cause interference with telecommunications systems.

Although solar radio noise measurements used in the study are not from the specific frequencies of interest in the cellular telecommunications networks, the noise is wideband and affects a broad frequency spectrum.

Peak intensity of radio events differs on an event basis, but a relationship between flux density and frequency has been presented by [14], as in Figure 1.1. Measurements of between 67 MHz – 9.5 GHz [15] appear to agree with the linear relationships G and A, where flux density decreases as frequency approaches 2 GHz and increases as it approaches 10 GHz. Measurements of a similar distribution are provided by [1]. Observations for 1.2 – 18 GHz [16] appear to agree with lines G and C - flux density increases and peaks at 2 GHz, decreases until 5 GHz and increases again until 10 GHz. Frequency sampling spacing is not uniform.

Based on Figure 1.1 [14], statistically, the flux density measured at 245 MHz should be larger than in the bands in which the cellular telecommunication services operate (900 MHz, 1800 MHz, 2100 MHz); flux density should be similar at 1800 and 2100 MHz; flux density at 2695 MHz would be

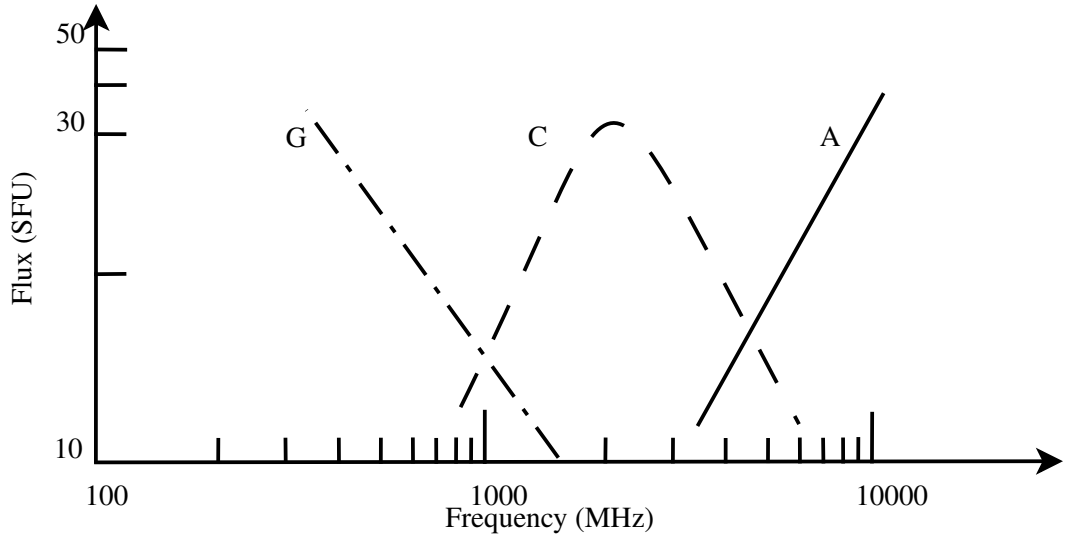

Figure 1.1: Burst spectra predominantly have a single parabolic component with intensity decreasing at high and low frequencies, as in line C. At low frequencies, as in line G, and higher frequencies, as in line A, intensity decreases and increases with an increase in frequency. The profile is similar for different magnitudes of flux density. Adapted from [14], with permission.

larger than at 900 MHz and similar to flux density at 1800 and 2100 MHz. In all cases, flux density should be in the same order of magnitude, making it possible to use 245 and 2695 MHz bursts as a proxy for in-band solar noise measurements in cellular telecommunication networks. However, as seen, frequency emissions vary per radio event. Variations may also exist within an event.

In cellular telecommunications, because of the higher gain antennas used and being less sheltered from the sun by natural and man-made structures, base stations are more likely to be affected than handsets. Base station antennas tend to be installed on elevated sights out of the way of obstructions, in order to provide handsets with line of sight connection. Sun-facing antennas are more likely to be affected than others. This would likely happen at sunrise and sunset. Received solar flux levels (at the base station) of 250 SFU, 1000 SFU and 150 000 SFU (defined by [17] as an intense event) could cause noise levels of 1, 3 and 22 dB [2] in systems with bandwidth of 0,2 – 20 MHz operating at 900 MHz.

The occurrence of X-ray flares correlates to radio emissions in the centimetre band ($\sim$10 and $\sim$3 GHz) [18]. Non-terrestrial detectors are necessary to record X-ray flares, because of atmospheric attenuation [8].

Type IV events (approximately $\leq$250 MHz – 2 GHz with flux density of approximately $\leq 10^4$ SFU for periods of hours to minutes) are deci-metre (300 MHz – 3 GHz) radio waves, usually associated with solar flares [19].

Solar radio waves are circularly polarised [20]. In this study, antennas used in LTE, GSM and UMTS are linearly polarised and deployed in a cross-polarised configuration. A circularly polarised signal can be detected at full power by a linearly polarised antenna with a cross-polarised configuration. The circularly polarised wave can be decomposed into two perpendicular linear waves [21]. For convenience, it can be decomposed at the orientation of the perpendicular antenna elements. The antenna is therefore always aligned with the signal with regard to polarisation. In a case where the antenna only had one element, there would be a 50% loss, as only one of the linear components would align with the antenna.

1.4 RESEARCH GAP

Most studies on the topic of solar radio interference do not appear to include telecommunications counters and do not seem to address the specific telecommunications systems in detail with regard to theoretical impact.

Making use of information (called counters) from the actual cellular telecommunications equipment that is being interfered with is important, as it could contribute to creating a clearer picture, regarding the problems experienced, than by making use of data from related systems, such as receivers in similar, but not identical, bands or transmission technologies. Furthermore, it will be very interesting to be able to determine how severe interference is. Interference could slightly increase the noise floor, decreasing Erlang/Hz/km^2, or affect the system more seriously by increasing BER, frame error rate (FER), perceived call quality and finally increasing dropped call rate (DCR) in the case of voice or affecting data throughput for data services.

1.5 RESEARCH OBJECTIVE AND QUESTIONS

The goal of the dissertation was, by performing theoretical calculations and an empirical study on existing and primary numeric data, to determine if an association could be found between solar radio noise and increases in interference on GSM, UMTS, LTE and microwave backhaul radio access networks (RANs). Furthermore, based on the results, mitigation strategies should be proposed and

suggestions for further studies presented.

In order to address the engineering hypothesis of what the characterisation and impact of solar generated radio noise on the quality of service of cellular telecommunications and microwave backhaul is , the susceptibility of the radio network of cellular telecommunication networks (as a function of primary frequency, bandwidth, system design specifications and typical configuration values) to solar interference was investigated. The mechanism of interference was expected to be an increase in the noise floor and thus an impact on signal-to-noise ratio (SNR), decreasing throughput. Correlation between space weather data (X-ray flares, 245 MHz solar radio burst and 2695 MHz solar radio burst data) and cellular telecommunications network data (microwave backhaul, GSM (2G), UMTS (3G) and LTE (4G) network counters) is performed.

1.6 RESEARCH CONTRIBUTION

The contribution to research is twofold. Firstly, determining that cellular networks are potentially susceptible to solar radio noise. Initial analysis was performed by a theoretical analysis specific to cellular network technologies, using typically configured values, as well as those from technology specifications. Secondly, examination of real world cellular network data and solar indices, as well as performing correlation between cellular network data and solar indices, gives insight into the requirements for future studies.

1.7 OVERVIEW OF STUDY

The dissertation is arranged into six chapters and an appendix. Chapter 2 is a literature study describing space weather, wideband radio noise and antennas and also includes an investigation of space weather data sources and cellular radio network antennas and counters.

An overview of the data selected, as well as the methodology of the study, is presented in Chapter 3. Both theoretical susceptibility of telecommunications systems to space weather and an analysis of real world data are examined.

Chapter 4 presents the results of the experiments and Chapter 5 discusses them. Finally a conclusion, including suggestions for future work, forms Chapter 6. The appendix contains analysis done to gain understanding of related systems and data.

CHAPTER 2

LITERATURE STUDY

2.1 SPACE WEATHER OVERVIEW

Space weather refers to the changes in the interplanetary medium between the sun and the earth, as well as the magnetosphere, ionosphere and thermosphere of the earth, due to phenomena such as coronal mass ejection (CME) and solar flares [8]. Both phenomena originate near sunspots, which are regions of intense magnetic field strength of both positive and negative polarity called active regions. Sunspot activity has an 11-year cycle [22][23] and is characterised by the sunspot number [8] and other indices, such as $F_{10.7}$, which is a measure of the radio flux emanating from the sun. The occurrences of CME and X-ray flares vary due to the cycle in general. These events cause heat, light, radio waves, X-rays and plasma to be produced by the sun.

In addition to the 11-year cycle, the sun rotates once every $\sim$27 days, as can be observed by motion of sunspots and active regions across the face of the sun [24][25]. These active regions are also the primary source of X-rays and solar radio noise.

The interaction between the sun and earth can be summarised as [8] :

- When an open field line region on the sun occurs, a coronal hole or CME forms, causing plasma to exit the sun at a high speed. The fast travelling plasma ($> 700\ km \cdot s^{-1}$) interacts with the slow moving plasma ($\sim 400\ km \cdot s^{-1}$), causing turbulence. When the turbulent solar wind reaches earth it causes a destabilisation in the magnetosphere and plasma due to the interplanetary magnetic field (IMF) in the solar wind. A magnetospheric substorm occurs. Aurora are a visual indicator of the event.
- Disturbances on the sun can cause radio wave emissions. When arriving at earth, geomagnetic

storms can occur, in turn producing ionospheric storms. Radio waves above ∼10 MHz are not significantly filtered by the ionosphere and reach the surface of the planet.

- A solar flare causes X-ray emissions, solar wind and radio emissions.

The magnetic field of the sun is too weak to free itself from the solar plasma. The solar magnetic field becomes frozen in the ionised plasma from the sun's corona. Since the sun's plasma is one with the magnetic field and the plasma rotates faster at the equator than at the poles, the magnetic fields in the plasma become contorted, causing the magnetic field to move from the poles to the equator [8]. The twisted magnetic field causes turbulence in the convection zone. The normally dominant force exerted by the plasma on the magnetic field becomes overwhelmed by the magnetic field, causing dark sunspots.

At the beginning of a solar cycle, sunspots are found at higher latitudes than at the end [26]. The number of sunspots vary with an approximately 11-year period. Eventually the activity at the equator reduces and the cycle ends. The areas around sunspots are brighter than normal. It is possible for these regions to increase in brightness abruptly, which can be followed by a solar flare. A high sunspot area is indicative of high magnetic activity [8].

Solar flares are magnetic flux tubes that rise rapidly and erupt, releasing X-rays when magnetic reconnection occurs. A flux tube is a prominence that rises out of the corona of the sun, forming a loop [26], see Figure 2.1. Solar flares produce radio emissions and solar winds[1]. Radio bursts can last for tens of seconds to hours [6].

Solar flares are classified according to flux intensity according to the NOAA scale, see Table 2.1. X-ray flare data are quantised as intensity levels are placed into classes. Flares in the classes A – C are not of concern for most space weather applications. GOES satellites are a source of X-ray flare measurements.

CME are sun-based magnetic discharge events. A typical CME can carry 10 billion tons of solar material away from the sun [27]. CME are accompanied by, but are not the cause of, type II or type IV (broad band emission) metric radio bursts [28], see Section 2.1. X-rays, non-thermal particles and broad spectrum radiation are produced by the shock wave. If directed at earth, CME are responsible for causing geomagnetic storms and disrupting the magnetosphere of the earth. CME and solar flares

[1] Plasma from the sun.
[2] 1 Angstrom = 10^{-10} m.

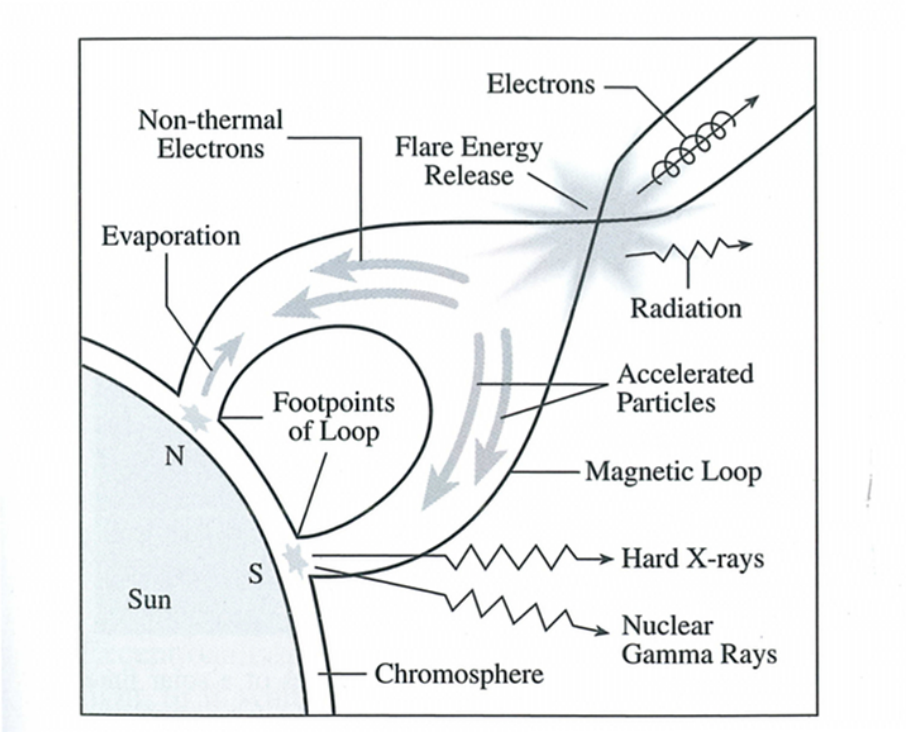

Figure 2.1: Depiction of a solar flare, producing radio and X-ray emissions. Taken from [27], with permission.

are not dependent, but may be related [29]. Solar flares often occur with CME, see Figure 2.2, but can also occur without them. In this type of event mass slowly moves away from the sun.

A varying stream of particles, called the solar wind, also emanates from the sun. The solar wind also carries with it a magnetic field [8]. Approximately three days are required for the traversal from the sun to earth [30]. This magnetic field has a complex interaction with the magnetic field of the earth and may cause a geomagnetic storm when the field is oriented in a southward direction.

The solar wind is, as described by current models, due to the difference in pressure between the corona of the sun and space [26]. The solar wind typically travels at 450 $km \cdot s^{-1}$, but can travel at much higher speeds (2000 $km \cdot s^{-1}$) during a CME, which are caused by eruptions on the sun. Large solar wind speeds and the turbulence of fast-moving wind interacting with earth's magnetosphere lead to auroral displays.

Wideband radio emissions are produced by the sun. A radio wave can be defined as an electromagnetic wave of a frequency between about 10 kHz and 10 THz, some of which may be used for

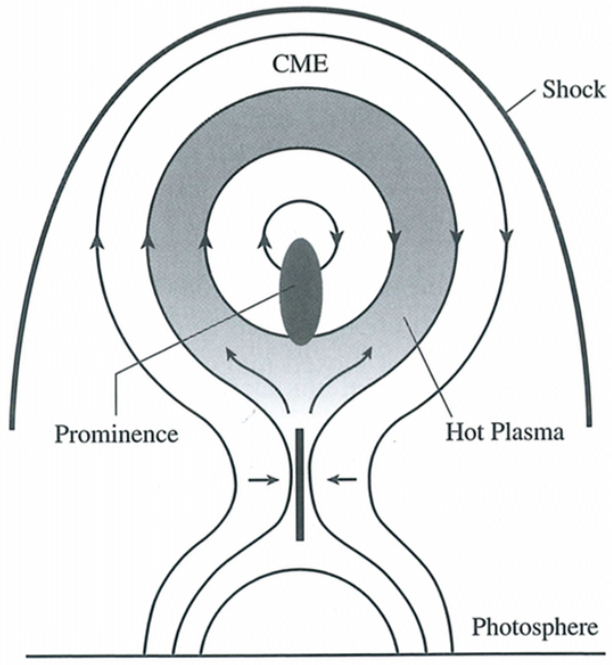

Figure 2.2: In the illustration, a reconnection occurs producing a solar flare and CME. The round bubble of plasma is ejected from the sun. Taken from [27], with permission.

long-distance communication. The frequencies cover long-wave radio to infrared. Five spectral types of solar radio bursts exist and are denoted by numerals I to IV [31][19], see Figure 2.3.

Type I radio bursts seem to be caused by ion sound turbulence (shock waves) and occur in narrowband storm bursts [31] of < 300 MHz [19]. Type I bursts are not normally associated with solar flares and have extremely narrow bandwidth. The duration of single bursts is seconds and storms can occur for hours to days [32].

Type II are due to shock waves [19] and storm bursts [31] and are associated with faster moving CME [33]. These occur as slow drift bursts; frequency changes slowly from high to low frequencies at a rate of 1 MHz s^{-1} [27]. Type II and III bursts may occur simultaneously during times of high activity [34] and seem to be at frequencies of tens of KHz to hundreds of MHz [34]. Type II events of the highest magnitude are most unlikely to occur during solar maximum [31]. Durations are 3 - 30 minutes [32].

Type III are caused by the excitation of the solar wind along magnetic field lines [34] and e-beams [19]. Frequency and intensity rapidly (10^{-1} – 10^{4} MHz s^{-1} and $\lesssim$ 5 – 80 minutes respectively)

shift in time from high to low. These bursts occur between 10 kHz and 1 GHz [33][32] and can be accompanied at a second harmonic of the plasma. Because of attenuation caused by the earth's atmosphere, measurements > 10 MHz can be made from terrestrial stations. Measurements < 10 MHz must be made from above the ionosphere. Flux levels as high as 10^7 – 10^8 SFU for frequencies of 200 KHz – 9 MHz have been observed by satellites [34]. U-type bursts are a variation in which frequency decreases, then rises [27].

Type IV events are usually associated with solar flares and are caused by trapped electrons [19]. Type IV events are broadband [32], often partly [27] circularly polarised and often preceded by type III bursts and X-ray radiation. Variations in intensity and frequency are smooth. The components of the type IV bursts range from $\lesssim$20 – 2 GHz with flux density of $\lesssim 10^4$ SFU for periods of minutes to hours. The biggest type IV events are twice as likely to occur during the decline of the solar cycle than at solar maximum [31]. Geomagnetic storms are associated with 85% of large type IV events. A type IV event is most likely to cause a geomagnetic storm if the flux density level is larger than 4000, 500 and 1000 at frequencies of 200, 500 and 3000 MHz.

Type V are due to e-beams [19] and consist of broad band radiation, mostly below 150 MHz [35] or between 10 – 200 MHz lasting 1 – 3 minutes. The intensity is often larger than that of type III events, which they often follow [35]. Two other types of bursts are [27] centimetre bursts, which are impulsive continuum radiation, lasting a few minutes, and are caused by gyrosynchrotron radiation at centimetre wavelengths. Millisecond bursts are the other type. Millisecond bursts occur between 200 and 1400 MHz and consist of thousands of spikes lasting milliseconds.

The frequencies of most interest, in view of the operating frequencies of terrestrial telecommunications systems, see Table 2.3, are near 1, 2 and 26 GHz. Type I ($\sim$ 100 MHz), III ($\sim$30 kHz – 300 MHz) and IV (10 MHz – 100 GHz) appear to be the most applicable storm types [27].

2.2 NEAR EARTH ENVIRONMENT

Earth is surrounded by a number of zones or regions, see Table 2.2. The ionosphere and magnetosphere are of most interest.

The geomagnetic field of earth is composed of the field produced in the core, ionosphere and mag-

Table 2.1: Solar flare class and associated released X-ray energy measured at earth for X-rays in the 1-8 Å range[2]. The order of magnitude is indicated by the the letter (B, C, M, X) and a number n is used for more precision. For example, $13 \times 10^{-4}\ W \cdot m^{-2}$ would be designated X13. Classes other than X are given magnitudes between 1 and 9.9. X can be larger.

Flare Class	E = X-Ray Energy at earth ($W \cdot m^{-2}$)
Xn	$E < 10^{-4}$
Mn	$10^{-5} < E < 10^{-4}$
Cn	$10^{-6} < E < 10^{-5}$
Bn	$E < 10^{-6}$

Table 2.2: Height (km) of regions above the surface of earth. The regions overlap and change during the night and day.

Height from surface of earth (km)	Region
$\sim$ 70 - 90	Ionosphere, D-region (during day only)
90 - 130	E_s-region
90 - 130	Ionosphere, E-region (during day only)
130 - 210	Ionosphere, F1-region (day only)
200 - $\sim$1000	Ionosphere, F2-region (day only)
200 - $\sim$1000	Ionosphere, F-region (night only)
500 - 800	Exosphere
800 - 2000	Protonosphere or plasmasphere
480 - 66000	Magnetosphere

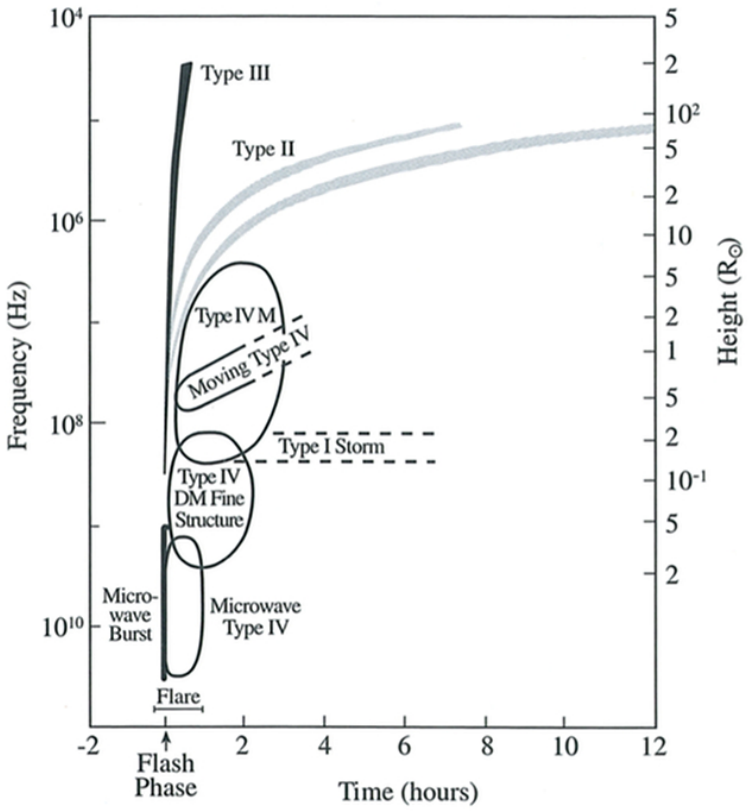

Figure 2.3: A depiction of the height, frequency and duration of type I to IV radio bursts. Taken from [27], with permission.

netosphere. No magnetic field lines are present beyond the magnetopause[3]. The geomagnetic field shields the ionosphere from direct interaction with particles from space and the sun, except at the polar cusp and when polar cap absorption (PCA) occurs, see Figure 2.4. The collision of the solar wind with the magnetosphere at the bowshock causes the magnetic field of earth to be compressed on the sunward side and a tail reminiscent of a comet to form on the other.

Under normal circumstances, the solar wind interaction with earth is constant. When solar wind speed rapidly fluctuates, the magnetosphere and plasma of the earth become unsettled. Energy builds up and is then released towards earth into the plasma [8]. These disturbances in the plasma sheet produce aurora at high latitudes $\sim 23^{\circ}$. The auroral ring is wider on the night side of the earth, see Figure 2.5. The auroral oval becomes thicker and can descend to lower latitudes when magnetic activity is high, thus an aurora is a visual indicator of magnetic activity.

[3]The magnetopause is the border between the solar wind and the magnetosphere

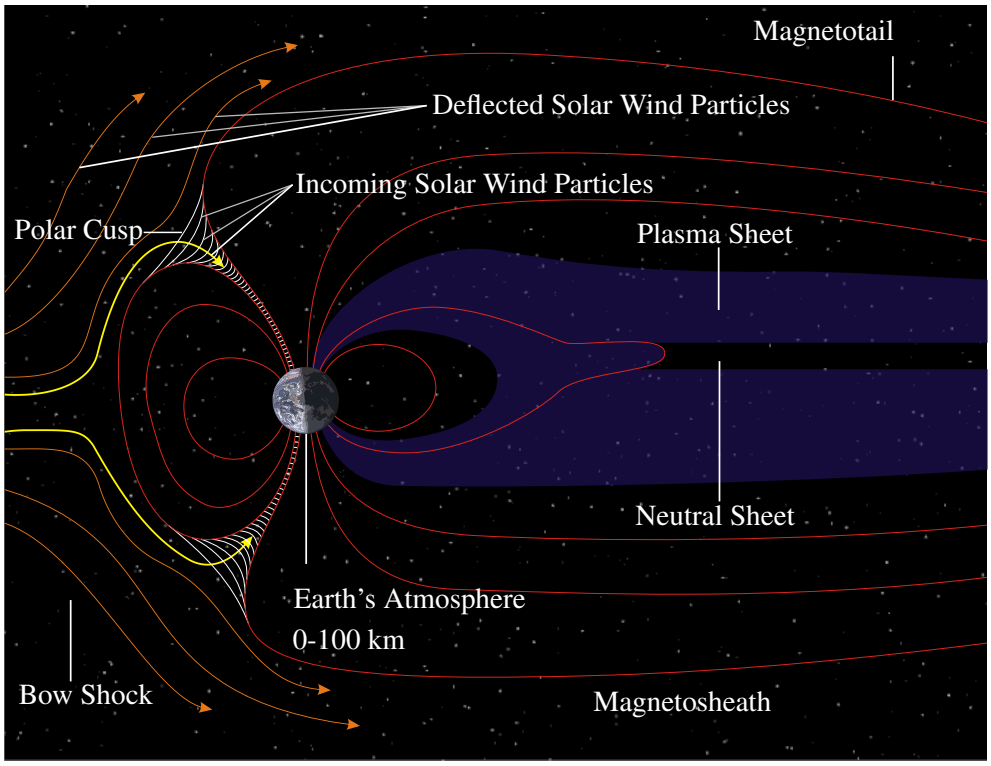

Figure 2.4: Structure of the magnetosphere of earth, adapted from [36].

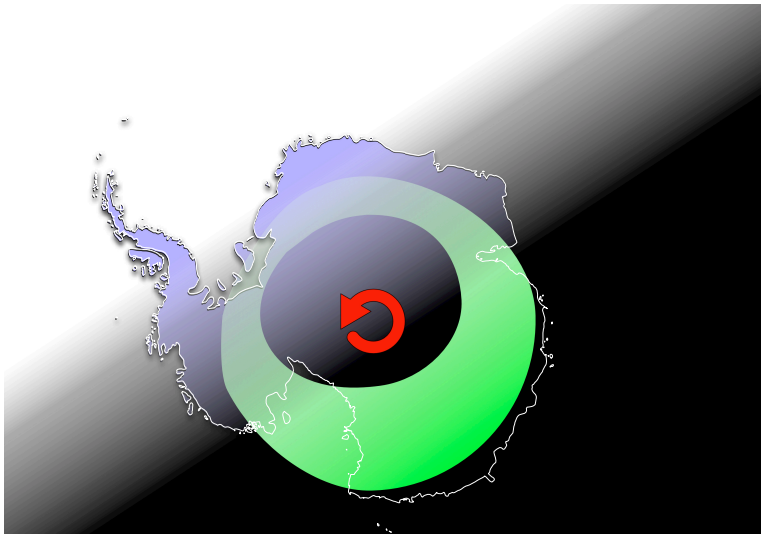

Figure 2.5: Illustration of rotation of the auroral oval over Antarctica. The aurora is most active and only visible at night time.

Seventy percent of space weather occurs in the ionosphere. The ionosphere is influenced by both solar and non-solar space weather [8]. The ionosphere is a region above earth that is ionised by solar radiation. It acts as an attenuator to electromagnetic waves and also a transmission medium, in the

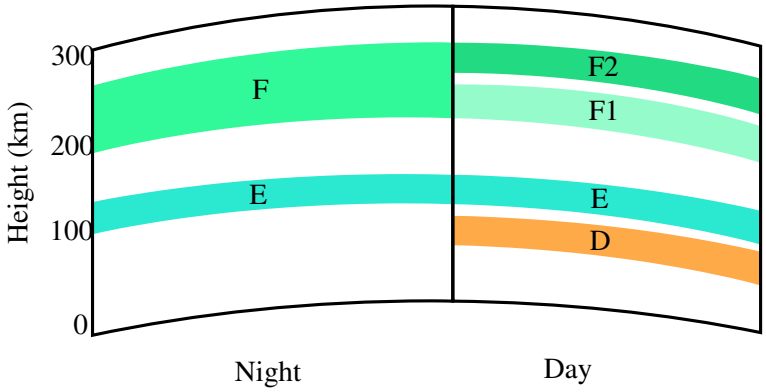

Figure 2.6: Layers of the ionosphere differ depending on the time of day, adapted from [37].

case of earth-to-satellite communications and systems using the ionosphere as a waveguide or bounce path, respectively. It is comprised of a number of layers, see Figure 2.6.

The D region of the ionosphere affects short-wave radio owing to absorption loss. Ionisation can occur in the D region from proton absorption from PCA. The absorption of the D region is used in skywave models to predict HF propagation.

Sunspot number and zenith angle influence electron production in the E and F1 regions. The midday sun causes the highest production. The higher the sunspot number, the higher the expected production. The critical frequency (E and F regions) and absorption level (at 4 MHz in dB, for the D region) increase proportionally to sunspot number [4].

F1 merges with F2 to produce F on the night side of the planet. Variations in the layers occur due to the time of the day and year. Ionospheric storms occur in two forms: positive, which increase the ionospheric critical frequency (also called f_0F_2), and negative, which decrease the ionospheric critical frequency. The F region is also known as the Appleton layer. The ionospheric critical frequency cannot be modelled easily, therefore sets of pre-calculated static values are selected based on sunspot number by telecommunication prediction codes. The F region is important for HF communications and other systems that use the ionosphere to reflect radio waves.

The sporadic E region (Es) is correlated to magnetic substorms, aurora (during the night) and the

[4] Critical frequency is the maximum frequency at which reflection still occurs and can be determined by Chapman theory.

equatorial electrojet (during the day).

An ionospheric storm is the response of the ionosphere to a geomagnetic storm. The fact that ionospheric storms are delayed with respect to geomagnetic storms means that geomagnetic storms could be used as early warning system or forecast for ionospheric storms [8]. Sudden ionospheric disturbances (SID) are predisposed to occurring during the increase of solar activity in the 11-year cycle [26]. SID are directly related to X-ray flares. SID appear to occur in the initial portion when sunspot numbers are on the increase [8]. Variations due to ionospheric storms are directly proportional to the occurrence of magnetic storms. Ionospheric storms appear to occur more often during the decline of sunspots in the solar cycle [8].

The high-latitude portion of the atmosphere is more complicated than lower latitudes. Magnetospheric and interplanetary events instead of variations in solar flux cause variation in these regions. Kp and Q indices can be used to represent auroral activity. Changes associated with visible and radio auroras influence terrestrial and satellite radio systems at high latitudes.

2.3 EFFECTS OF SPACE WEATHER ON RADIO PROPAGATION SYSTEMS

Three groups of systems that can be interfered with by solar and space weather activity are:

- Those that depend on the ionosphere. HF and medium-wave exploit the skywave mode of propagation [8]. A large number of propagation prediction models exist for HF and over-the-horizon communications systems.
- Those that propagate through and for which the ionosphere causes interference (e.g. satellite) [8]
- Systems operating using line of sight (e.g. cellular communications), which would not normally interact with the ionosphere.

Solar events and the effects felt on earth are not trivial to link together [8], in part because:

- The solar rotation period of 27 days and the 11-year cycle are considered the predictable components of the sun. Short-term activity is more random in appearance.
- A high sunspot number is not indicative of large ionospheric storms or flares.
- Large radiation storms, X-ray flares and magnetic storms are sparsely distributed events.
- Major activity can occur from a sunspot in high or low sunspot number periods [8].

The Appleton-Lassen (also known as Appleton-Hartree) expressions detail the relationship between plasma and signals, such as short and long-wave communications, in the ionosphere [8]. Ionospheric storms are due to the solar wind producing geomagnetic storms in the magnetosphere, which then triggers an ionospheric storm. Geomagnetic storms can produce enhanced auroral effects.

Propagation prediction models such as VOACAP consider sunspot number and Kp in calculations [8]. High Kp values inhibit communication, while high sunspot numbers enhance it. Magnetic indices have been used to explain the effects of high-speed solar winds, which are linked to geoeffective coronal holes and CME, on the surface of the earth [8].

A direct relationship between ionospheric activity and sun spot number does not seem to exist. Solar flares, coronal holes and CME do, but a time lag exists [8]. Coronal holes, solar wind activity and magnetic disturbances are highly correlated [8]. Coronal holes are long-lived and coupled with the 27-day cycle, it is possible to predict magnetic disturbances.

The ionosphere causes dispersion, absorption, birefringence[5] and anisotrophy[6] to radio signals.

Solar flares are responsible for interference with telecommunications, especially HF radio [8]. Short wave fade (SWF) is caused by SID and affects HF communication circuits on the sunward side of the earth. X-ray or other pulse (electromagnetic radiation) emissions from the sun, probably caused by solar flares, cause the D region to produce higher loss when HF radio waves pass through it. The phenomenon is due to increased ionisation of the D region [8].

PCA events caused by high energy solar particles a few hours after the eruption of a flare and may cause problems with HF communications at the poles. PCA are twice as likely to occur during the decline in the solar cycle than at the maximum. PCA are associated with 85% of large type IV events [31].

Because of the wide range of phenomena at polar regions (PCA, auroral zone, Es region), HF communications at the poles have been studied extensively. Large-scale D-region (sunlit earth only) absorption events (PCA or SWF) can reduce atmospheric noise [8], increasing SNR, at least in the medium frequency [7] band.

[5] A wavelength is refracted along two paths due to birefringence.
[6] Anisotrophy is when refraction differs, depending on where the propagation takes place.
[7] 300 kHz to 3 MHz

The body of the literature focuses on the HF, medium-wave radio and satellite systems, such as mentioned on GPS, see Section 1.3. The technologies of interest in this dissertation make use of terrestrial line of sight or subionospheric rectilinear propagation [8], excluding the ionosphere as a propagation medium. It appears from the literature that line of sight technologies will be affected by environmental noise, see Section 2.5. The ionosphere does not appear to be a factor.

2.4 SPACE WEATHER INDICATORS

Space weather and its effects can be represented by indices. These are captured by terrestrial or satellite monitoring stations. Indices of relevance are those that indicate the level of radio noise in or near the frequency bands of interest.

According to OGO-A and OGO-B satellite data, X-ray events larger than $3\text{x}10^{-7}$ ergs cm^{-2} s^{-1} in the range of 10 – 50 keV have been seen to accompany 10 and 3 cm radio bursts of 80 SFU or larger [18]. The decay rates and duration of X-ray and the 10 and 3 cm bursts are similar. Decay rates are exponential and their duration is between 1 and 10 minutes.

Because of the absorption of the atmosphere and brightness of the sun, observations of the corona are best done by satellite-based X-ray monitors [8]. GOES is a potentially good data source, as satellites are geostationary and an almost uninterrupted data feed is available. The NASA Database of Notification, Knowledge, Information (DONKI) database, see [38], provides a collection of event dates and magnitudes of radio flares captured by GOES-15 SEM/XRS 1.0-8.0. SWPC also provides the data. X-ray flares do not correlate with solar radio bursts [17].

Sunspot number is counted by hand and is the number of sunspots on the sun at a given time [8]. $F_{10.7}$ is strongly correlated to sunspot number [39] and second to sunspot number in terms of longest historic record [40]. Sunspot measurements are accurate to within 1% of daily average $F_{10.7}$ solar flux.

$F_{10.7}$ is the measurement of the flux density in a 100 MHz band centred at 2.8 GHz or 10.7 cm and describes the variation of solar intensity over hours to years [24]. The incident solar radio energy on a surface at a given frequency is measured in SFU[8]. The quiet component of the solar cycle is 64 SFU. The bursty components of solar activity can cause a flux density of 120 – 200 SFU during active

[8] 1 SFU = $10^{-22} W m^{-2} Hz^{-1}$

periods [24]. The slowly varying component is observable at wavelengths of 1 – 50 cm, but is most prominent at ∼10 cm wavelengths [39].

Sunspots can be related to solar flux,

$$\phi_{12} = 63.7 + 0.728R_{12} + 8.9(10^{-4})R_{12}^2, \tag{2.1}$$

where R_{12} and ϕ_{12} indicate the running mean values of $F_{10.7}$ and sunspot number for 12 months, respectively.

A large body of data and literature exists for the $F_{10.7}$ index, which is collected at Penticton, British Columbia, Canada. Data points are produced three times daily at 19:00, 22:00 and 02:00 UTC+2 or at 20:00, 22:00 and 24:00 UTC+2 during winter [40, 41, 42]. Measurements may not be suitable for use in correlating interference owing to the bursty solar component, as samples of solar interference will need to be taken when the antenna is in line of sight with the sun. The index is a good indication of average daily measurements. Three data points are produced per day, with 30 – 40% of time used for sampling. Under-sampling can occur if solar flux varies rapidly.

Bursts in solar activity could skew $F_{10.7}$ results; though attempts are made to remove the contribution of solar flares from the final result, they appear despite manual intervention. It is recommended to apply a low-pass filter to $F_{10.7}$ before making a comparison with other data to remove bursty components. Making use of $F_{10.7}$ to estimate flux density at other wavelengths may be unreliable, since a single wavelength is measured. The index has an error of ∼2% when used as an estimate for sunspot number whereas ∼20% error for estimating average daily solar flux [40].

The monthly median is considered stable enough to be used as the standard measurement. The average of five days of measurements is considered poor, but an acceptable compromise between granularity and accuracy [8].

The significant error for short periods, poor prediction ability [8], slow sampling rate and recommendation to smooth data may reduce the usefulness of the index, especially considering that the radio interference of most interest in cellular networks is likely to take place in minutes to an hour.

The Space Weather Prediction Center (SWPC) [43] produces the Radio Burst Event List and con-

tains solar flux density measurements (in SFU) for bursts and noise storms of 245 MHz and 2695 MHz. Levels for 2695 MHz are given for events that are double or more than the magnitude of the background flux. Data are available at second resolution; polarisation is not stored.

Data are from the following observing stations:

- Culgoora, Australia
- Holloman AFB, NM, USA
- Learmonth, Australia
- Palahua, HI, USA
- Ramey AFB, PR, USA
- Sagamore Hill, PA, USA
- San Vito, Italy.

2.5 NOISE INTERFERENCE

In wireless communications, assuming constant bandwidth, topology, weather conditions (such as lightning [44][45]) and increasing environmental noise [46], at a given frequency, can reduce channel capacity and eventually make communications impossible if the SNR[9] becomes too low [47]. For example, satellite systems could potentially cause interference with earth-based systems, if operating frequencies are similar [48][49].

Noise consists of a number of components such as the noise figure of the receiver, antenna gain, polarisation of noise and antenna, ambient temperature, transmission power and environmental conditions [6]. Since the operating environment varies, noise must often be dealt with differently in different situations for optimal results [49]. For example, interference with GPS differs from that experienced by systems operating purely in the troposphere. However, GPS appears less susceptible to interference than other wireless systems [7][25].

Bursts and continuous noise in the band of interest can be dealt with by temporal, frequency and spacial filtering [48], thus increasing SNR. In order to increase throughput, especially in applications such as data transfer, for which ever higher demand is predicted [50], high modulation schemes are used. The higher the modulation scheme, the more important SNR becomes [51]. Short noise

[9] Noise is additive white Gaussian noise.

bursts have been found to be simpler and influence a narrower frequency range than long ones, which are spectrally and temporally more varied [1]. Low magnitude noise could cause interference by increasing the BER [7]. Although an increased BER may not be fatal to communications, efficiency will be reduced and battery life may suffer on mobile devices.

Interestingly, because of typical antenna orientation, it would be necessary for interference to occur when the sun is low on the horizon (sunrise or sunset) [25]. For this reason, a seasonal component may exist. The noise is Gaussian, if the antenna beam width is greater than the diameter of the sun. The rule is generally true for lower frequencies and effective antenna widths (applicable to cellular user equipment). At high frequencies, such as those used in microwave backhaul, noise could be considered Gaussian.

2.5.1 Interference due to UWB

Ultra wideband (UWB) communications systems have been designed to operate in bands of other communication systems (3.1 – 10.6 GHz). The Federal Communication Commission (FCC) classifies a system with bandwidth of $\geq$500 MHz at -10 dB as UWB [52]. UWB communications use very short bursts (500 ps) and a wide frequency range [53] to reduce power levels so as to reduce possible interference with other systems [54]. UWB transmissions appear as wideband noise to other systems. Since the sun produces wideband noise, UWB as a noise source for other technologies was investigated. A channel model used as reference for IEEE802.15.3a is Saleh-Valenzuela. An interference model used is coloured Gaussian noise.

UWB interference in the lower residual band (0 – 3.1 GHz) can be tolerated by UMTS (with 1% capacity reduction), if levels produced by a single device are below -92.5 $dBm \cdot MHz^{-1}$ and if noise is produced by multiple devices, -94.5 $dBm \cdot MHz^{-1}$. For this measurement, UWB transmissions must be $\geq$1 m from user equipment. For every 3 dB increase in noise, reduction in capacity doubles [55].

If noise is above -100 dBm to -95 dBm, UMTS can begin to suffer from degradation. Under simulation conditions, achieving a BER of $10^{-}3$ requires the delta of node-B transmitted power and UWB noise to be $\geq$ 62 dB (assuming SNR of -4 dB, distance between user equipment and UWB source of 1 m and distance between user equipment and node-b of 600 m) [56]. If noise becomes too high, the base station will not be able to increase power sufficiently to provide the desired BER.

UWB interference at a distance of 1 m from a mobile station at levels less than -100 $dBm \cdot MHz^{-1}$ causes very little interference with GSM [57]. Interference of -70 $dBm \cdot MHz^{-1}$ severely reduces transmission range compared to a minimal decrease at -80 $dBm \cdot MHz^{-1}$. UWB systems do not appear to interfere with GSM, UMTS or GPS systems, though time hopping UWB has greater impact on GPS than direct sequence UWB [54]. FCC and European Telecommunications Standards Institute (ETSI) masks may be lower than recommended by some researchers [55][57]. Degradation is linear and due to interference power levels. A transmission power increase could negate degradation [56], since UMTS is an interference limited system.

In the U-NII lower (5.12-5.25 GHz) and U-NII middle (5.25-5.35 GHz) bands, UWB interference is insignificant [53].

2.5.2 Antennas

For ease of use, antenna radiation patterns are decomposed into horizontal and vertical radiation patterns, rather than viewing the radiation pattern in 3D. The most sensitive portion of the antenna is in the primary lobe, see Figure 2.10(b) at boresight[10]. The effect of noise or gain depends on the antenna design, which will vary per vendor.

When describing radio systems, an ideal antenna can be used to simplify calculations. A theoretical antenna that radiates uniformly is called an isotropic radio frequency source or a point source. It has a power gain of unity or 0 dBi. The effective area of an antenna is related to the gain and the operating wavelength [6].

Because of the reciprocity theorem of electromagnetics and materials used, antenna characteristics (gain, radiation pattern, bandwidth, resonant frequency and polarisation) are identical for transmission and reception[11] [58]. This means that the direction in which an antenna is excellent at transmitting signal is also where it will excel at receiving. An antenna radiation pattern is often made up of a number of lobes, see Section 2.5.2.1. In the context of noise reception, a directional antenna would be better at receiving noise in a lobe with high gain than low gain, meaning that though an antenna is pointed in a certain direction, the design causes it to be be able to receive signal and interference from directions other than where it is pointed directly, though it will not be as sensitive at that angle

[10] Boresight is the direction of maximum antenna gain.

[11] This is may not always be the case. Ferrite is an example of a non-reciprocal material.

as in the primary lobe.

Solar radio waves are circularly polarised [20]. In this study, antennas used in LTE, GSM and UMTS are linearly polarised, but configured in a cross-polarised configuration; a circularly polarised signal will not experience a loss, since the antenna is always receiving the full signal. The circularly polarised wave can be decomposed into two perpendicular linear waves [21]. For convenience, it can be decomposed at the orientation of the perpendicular antenna elements. The antenna is therefore always aligned with the signal with regard to polarisation. If the antenna only had one element, there would be a 50% loss, as only one of the linear signal or noise components would align with the antenna.

2.5.2.1 GSM/LTE/UMTS antenna design

Cellular telecommunication networks make use of antennas that are constructed from an array of elements. The effect of noise or gain in general depends on the antenna design, which will vary per vendor. The horizontal beam width of a cellular network base station antenna typically has 3 dB less gain at 30° on either side of boresight than at boresight and roughly 6 dB less gain at 60° on either side of boresight, depending on the antenna [59]. In other words, power is half at 30° and a quarter at 60°.

In a simplified form, cells are put together either as an omni-directional cell, covering 360°, or as three sectors each covering 120°, see Figure 2.7(b), producing a clover pattern. This is done to provide capacity to an area and to allow reuse of scarce radio spectrum. In practice, some interference will occur between sectors, as the radiation pattern has larger coverage than the sector, see Figure 2.7(a) and 2.9(a).

Vertical beam width is quite narrow, typically 3° on either side of boresight. In other words, the half power beam width is taken between the points where the radiation pattern is 3 dB below the value at boresight or approximately 6° in total, see Figure 2.10(b) and 2.9(b) for horizontal and vertical radiation patterns, respectively. A specification of 20 dB down can be visualised as in Figure 2.10(a) and 2.9(b) for vertical and horizontal patterns respectively. The specification for a Kathrein 742241 directional multiband antenna states that the half power beam width of the primary lobe is between 6.8 and 8.1° wide, depending on frequency [60]. Many antennas in busy areas use downtilt[12] to

[12]Either a mechanical tilting of the antenna towards the ground or electrical downtilt (a change in the phase between

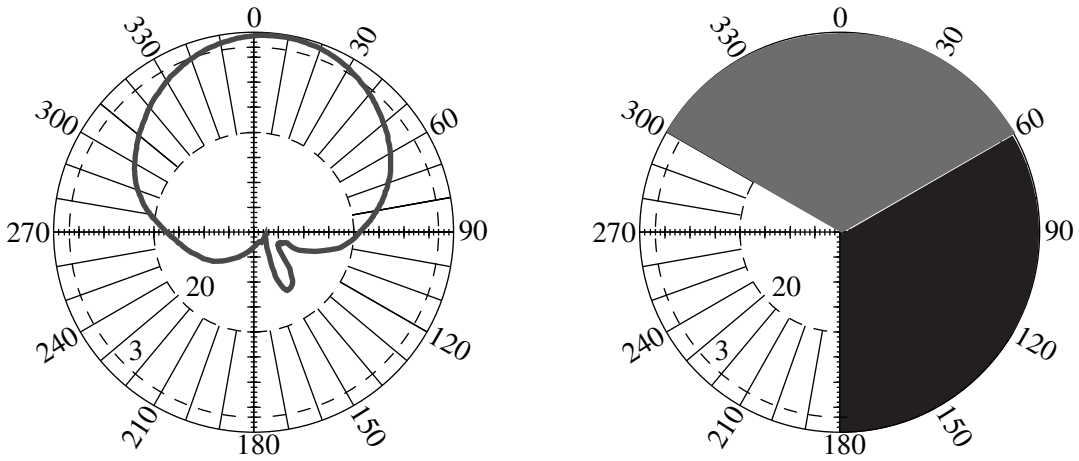

(a) (b)

Figure 2.7: Practical single horizontal radiation pattern and theoretical cell layout of three sectors. The angles indicate azimuth. In practice, antennas with radiation patterns similar to that of the left image would be oriented to 0° or north, 120° and 240°, the three sectors would overlap, adapted from [60]. Combining of sectors produces a cell. (a) A realistic representation of the horizontal radiation pattern of a sector. The 3 and 20 indicate 3 and 20 dB down, respectively. (b) Theoretical three-sector cell. Sectors are represented by the white, grey and black areas.

reduce interference between neighbouring transmitters, see Figure 2.11. For this reason, boresight could point below the horizon, therefore the antenna would point towards the ground. The primary lobe is not the full representation of the antenna. Most antennas have side lobes that could have 10 dB less gain than the primary lobe. A typical antenna has a vertical pattern of Figure 2.8(a) or Figure 2.8(b).

Antennas are often deployed in a cross-polarised configuration. Antennas are deployed at different polarisations in order to contend with the varying alignment of the antenna of a mobile phone. Sectored antenna, as used for sectors of cells, are cross-polarised. Omni-directional cells are not cross-polarised and not included in this study.

antenna elements).

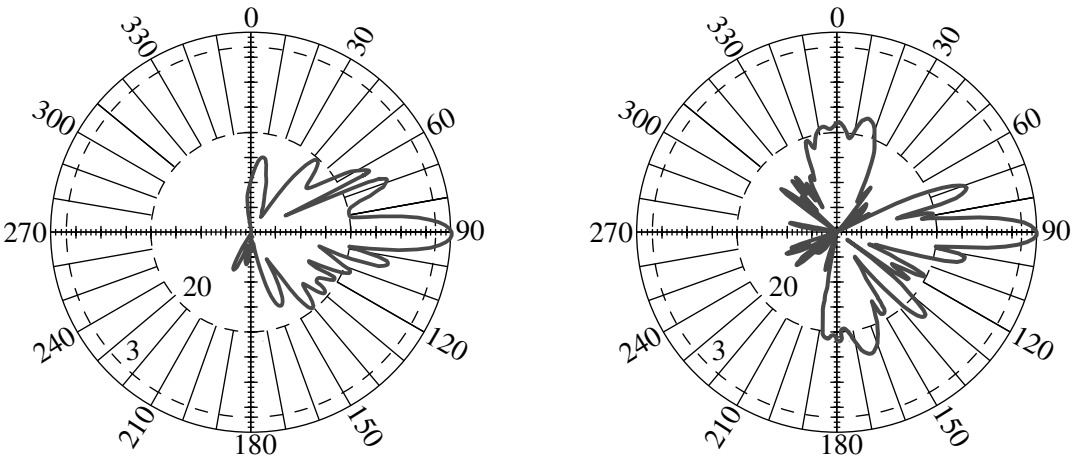

(a) (b)

Figure 2.8: Vertical radiation patterns from directional cellular antennas, adapted from [60], with permission. The angle indicates zenith angle, 0° indicates pointing straight up into the sky, perpendicular to a tangent plane to a spherical earth. (a) Vertical radiation pattern for a base station antenna operating at 824 – 960 MHz, the GSM range. (b) Vertical radiation pattern for a base station antenna operating at 1710 – 2170 MHz displays large side lobes. UMTS and LTE may make use of such an antenna.

2.5.2.2 Microwave antenna design

Microwave backhaul systems, as made use of in this study, are directional point-to-multipoint systems in which the hub covers 360° in four sectors of 90° each, typically facing north, south, east and west. Designs aim for radiation patterns to be biased towards the ground, not having high gain above the horizontal (90° zenith) and having 3 dB gain loss at 95°. Horizontal radiation patterns aim for maximum gain at 90°. End points would have narrow vertical beam widths of around 2.5°.

Antennas are typically polarised either horizontally or vertically, as all points are stationary and can be aligned easily. Handsets are less likely to be susceptible to solar interference because of low antenna gain and being shielded by the environment (buildings and trees etc.). However, handsets on cell boundaries, from where the received signal at a basestation could be weak, could be affected [2].

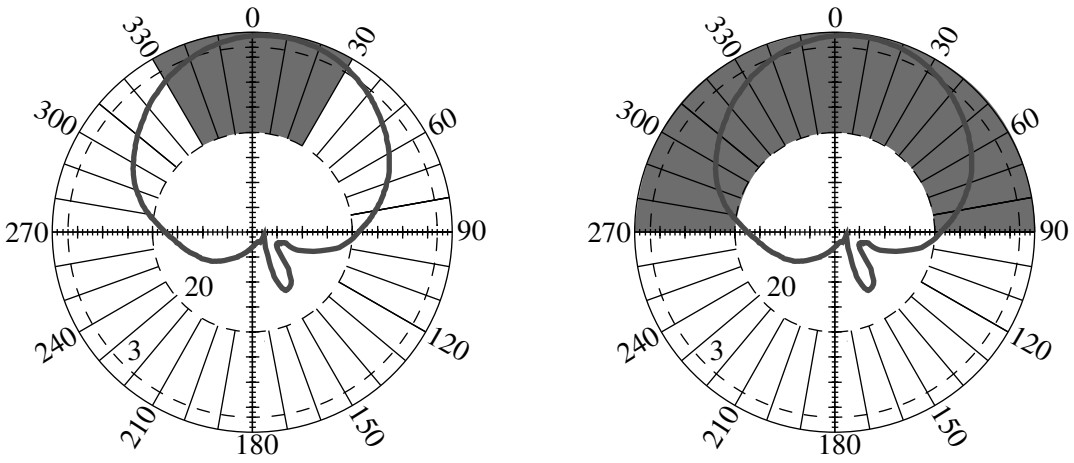

(a) (b)

Figure 2.9: Horizontal radiation pattern for antenna operating and 824 – 960 and 1710 – 2170 MHz as would be used for GSM, UMTS and LTE base stations, adapted from [60], with permission. (a) The shaded area indicates the theoretical region that will receive with a gain 3 dB down 330 – 30°. However, practically it is 320 – 35°. (b) The shaded area indicates the region that will receive with a gain 20 dB down 270 – 90°.

2.6 RADIO TECHNOLOGIES

Modern wireless terrestrial telecommunications systems operate in the L, S and C, X, K_u, K and K_a bands[13], see Table 2.3 [61][62]. The bands of interest can also be classified as ultra-high frequency, super high frequency and extremely high frequency bands[14]. Bursts of $> 10^3$ SFU, produced during solar maximum, can create interference with telecommunications systems operating in the $\sim$1 GHz region. Lower radio frequencies $\sim$1 – 2.6 GHz appear to be affected most [16]. Intensity of bursts is higher at high frequencies, e.g. $\sim$10 – 18 GHz, but of shorter duration than at lower frequencies, e.g. $\sim$1 GHz, where more low flux density events are reported [63]. High antenna gain and environmental temperature reduce and increase flux density respectively. Bursts exceeding 10^3 SFU can be expected roughly every six days during solar maximum and monthly during solar minimum [64] or 3.5 and 18.5 days apart respectively [1]. Bursts of 2×10^3 SFU occur every 244 days during a solar cycle and every 86 days during solar maximum.

[13] $\sim$1 – 2, 2 – 4, 4 – 8, 8 – 12, 12 – 18, 18 – 27, and 26.5 – 40 GHz respectively

[14] 0.3 – 3, 3 – 30 and 30 – 300 GHz respectively

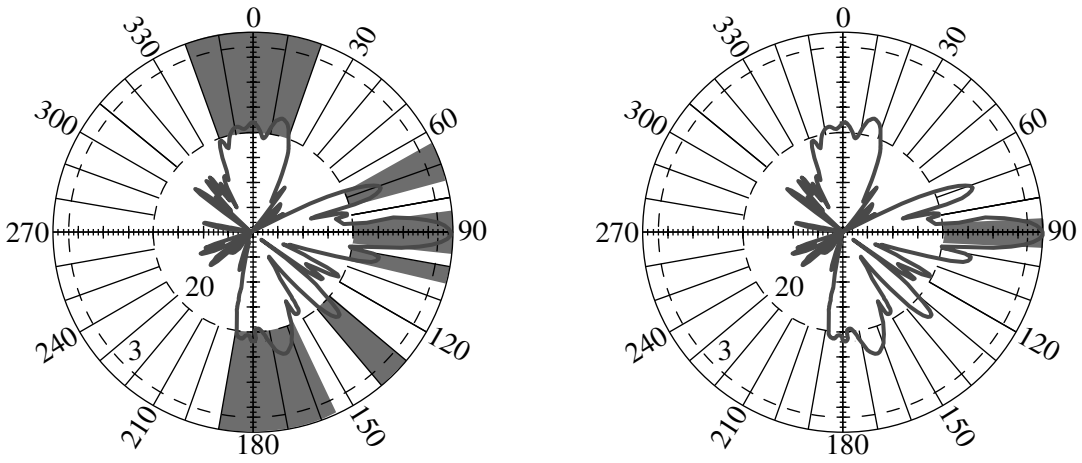

(a) (b)

Figure 2.10: Vertical radiation patterns from directional cellular antennas indicating antenna coverage for 20 and 3 dB down, adapted from [60], with permission. (a) Note the large number of areas where gain is above or close to 20 dB. (b) Only the primary lobe need be considered for 3 dB down.

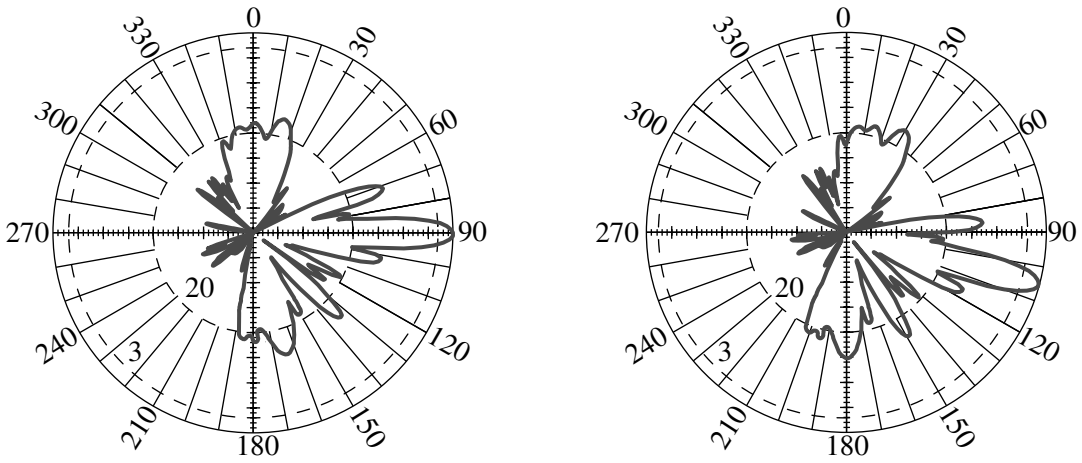

(a) (b)

Figure 2.11: Downtilt is the amount that the antenna is pointed downwards from the vertical or zenith of 90°, adapted from [60], with permission. (a) The antenna at 0° downtilt. (b) Downtilt of 15° degrees would mean that the antenna faces 90° + 15° = 105°.

Table 2.3: Typical telecommunications frequency usage and band indication per technology.

	Technology	GPS	GSM	UMTS	LTE	WiFi	Microwave backhaul
Band	Frequency (MHz)						
L	800			x			
L	850		x				
L	900		x	x	x		
L	1200	x					
L	1600	x					
L	1800		x		x		
L	1900			x			
S	2100			x	x		
S	2400					x	
S	2600				x		
C	5000					x	x
C	5800						x
C	7000						x
X	10500						x
K_u	15000						x
K	26000						x
K_a	28000						x
K_a	38000						x

To understand how noise affects cellular radio equipment, it is necessary to discuss the design of the equipment briefly.

2.6.1 GPS

GPS is discussed separately in Section A.1. GPS is susceptible to solar radio interference. How it is affected is similar to how terrestrial systems would be affected with respect to antenna gain and angle of interference, as in Section 2.5.2. On 6 December 2006, the two GPS frequencies, L1 and L2 (1.228 and 1.575 GHz , respectively) were estimated to have received a flux density of above 1 000 000 SFU [65]. The interference was right-hand circularly-polarised. The impact of the 6

December 2006 event was a CIR change of over 25 and 30 dB on the GPS L1 and L2 frequency. GPS service was affected. In total, the event lasted approximately an hour. On 14 December 2006, for approximately 25 minutes, flux density of 10 000 to 100 000 SFU was reported for GPS L1 and L2 bands. Polarisation was right-hand circularly-polarised. The event, in total, lasted for approximately 1 hour and 10 minutes.

Measurements from GPS L1 and L2 can be used to detect radio bursts at 1415 MHz with RSTN radio burst data [17]. The radio noise appears to be wideband with comparable flux density in the 1.4 and 1.6 GHz bands [17].

2.6.2 GSM/GPRS/EDGE

Cellular telecommunication systems are complicated collections of nodes. The air interface[15] is the focus, therefore core and value added services (VAS) systems will be omitted.

The Um interface of the GSM RAN makes use of frequency division multiple access (FDMA) with radio frequency channels of 200 MHz bandwidth in combination with time division multiple access (TDMA) with eight time slots. Time slots contain channels to manage the connection to the network and to send and receive user voice or data [66].

A traffic channel (TCH) carries voice data. When a full TCH is used to carry voice data, it is referred to as a full rate channel. A TCH can be split into two by making use of a technology called half rate (HR), enhanced full rate (EFR) and adaptive multi-rate make this possible.

A packet data channel (PDCH) is the data equivalent of TCH. Modern data communications on GSM are made possible by general packet radio service (GPRS) and evolved GPRS (EDGE). Improved data rates and resilience are provided by different coding schemes CS1-4 (for GPRS) and MSC1-9 (for EDGE).

Dedicated control channels (DDCH) are a family of channels used mainly for controlling the call. These are equivalent to Integrated Services for Digital Network (ISDN) D channel. DCCH makes short message service (SMS) possible. Common control channels (CCCH) are a group of channels used mostly for radio resource management. Broadcast control channels (BCCH) broadcast information used by the user equipment to initiate and maintain connection to the network

[15] The air interface is the wireless communication portion of a telecommunication network

GSM makes use of frequency hopping [67], micro-cells, adaptive antennas and advanced detection techniques to increase channel capacity [68]. AMR voice encoding and eight-phase shift keying have allowed GSM voice and enhanced GPRS (EGPRS) to operate at 6 and 30 dB carrier-to-interference ratio (CIR), respectively [69]. Under normal conditions AMR and enhanced full rate (EFR) codecs increase voice channel capacity. If radio channel throughput becomes constrained, voice quality is sacrificed and forward error correction (FEC) is increased; channel capacity may decrease. AMR has been adopted by ETSI as the standard for GSM and UMTS.

Radio network planners configure network parameters and design the network with the goal of minimising interference [70].

A time slot resource is reserved entirely for a single device when a call is set up. In this context, a TCH or PDCH can be considered a call. Noise reduces the capacity of each time slot or half time slot in the case of HR. When interference becomes severe, HR channels will be converted to full rate and the AMR codec will become more robust. In the case of data, the coding scheme used becomes more robust if interference or a poor connection is experienced.

If the control channel cannot be maintained, the connection will be lost. The control channel could also fail because of a core or VAS network failure. If payload data cannot be delivered fast enough, the call quality will become poor and eventually unusable. It may be possible to hand over from one cell to another to attempt to continue carrying a call. Handover may fail if no resources are available on the receiving cell; the call may eventually be dropped. New calls will not be established if the base station controller (BSC) determines that radio resources are limited.

2.6.3 UMTS/HSPA

UMTS was designed to be a progression from 2G, providing higher data speeds and theoretically easier radio planning; it begins the transition to an all internet protocol (IP) network.

The air interface of the UMTS terrestrial radio access network (UTRAN) is called Uu. UMTS radio communications make use of wideband code division multiple access, allowing simultaneous transmission of different channels on the same frequency. UMTS may operate in time division duplex (TDD) or frequency division duplex (FDD). The latter requires separate frequencies for the UL and DL. The former interleaves the UL and DL in time and uses a 5 MHz band, including two guard bands

of 0.58 MHz, effectively leaving a bandwidth of 3.84 MHz available. Capacity depends on the available power and code tree; allocation of these resources is managed by the radio network controller (RNC).

UMTS continues with the GSM concept of control and data channels. Channels are separated by channellisation codes.

Multiple users transmit simultaneously on a single frequency by use of orthogonal variable spreading factor (OVSF) scrambling codes, controlling code tree usage. Code tree allocation can be thought of as user bandwidth and is described by the spreading factor. The smaller the spreading factor, the more bits are allocated to a single user. Quadrature phase shift keying (QPSK) is used for modulation.

UMTS operates in a self-created environment of radio noise. The cell operating environment is limited to a maximum power, thus noise cannot be infinite. In order to limit noise, a cell will reduce transmit power, reducing cell size and excluding further away users. Power utilisation is more limiting than code tree utilisation.

If noise begins to cause interference, the encoding, for example AMR, can be more robust: more code can be allocated to a user. Users can be excluded from the cell by reducing power and therefore cell size. This is called cell breathing. To manage decreased capacity further, users may be handed over to other cells or new resource requests may be denied. These functions are managed by the RNC.

UMTS supports circuit-switched voice and packet-switched data. The high speed packet access (HSPA) and HSPA+ enhancements to UMTS provide increased data throughput. HSPA+ is considered a 4G technology [71].

As applicable to GSM, if the channels providing resource management to the system fail, transmission of the payload will fail.

2.6.4 LTE

LTE is a progression from 3G technology towards an all-IP core, as well as faster and more cost-effective data services for the operator. LTE moves more intelligence closer to the antenna into the eNode B (eNB). LTE is considered a 4G technology [71].

The radio access network was labelled E-UTRAN. QPSK, 16QAM (quadrature amplitude modulation) and 64QAM are used for modulation. Orthogonal frequency division multiplexing was chosen as the signal bearer on the DL partly because of inherent resilience to interference. Single carrier frequency division multiple access is used for the UL, allowing cheaper, less complicated user terminals [72] with a better peak-to-average power ratio. Single user multiple input multiple output, spatial division multiple access, beam forming, space-frequency block coding (SFBC) and frequency switched transmit diversity are techniques using multiple antennas, which improve system efficiency. Similar to UMTS, LTE allows FDD and TDD modes.

Continuing the design of GSM and UMTS, LTE groups channels into control and traffic channels. Channel degradation in LTE will cause speed to be reduced, as the modulation scheme will switch to one where data transmission is possible. Handover and prevention of resource allocation may be used to improve or maintain channel usability.

2.6.5 Microwave backhaul

Microwave backhaul technologies are proprietary. Little information appears to be available; however the technology used in the available data operates at 26 GHz with a channel bandwidth of 14 or 28 MHz. The modulation used is QPSK, 16-QAM or 64-QAM and the channel is FDD/TDMA.

Microwave backhaul is used to carry GSM, UMTS and LTE traffic bearers from the sectors at the network sites base transceiver station, NodeB and eNodeB in the direction of the core network towards the BSC, RNC and mobility management entity, respectively.

2.7 PERFORMANCE COUNTERS

Performance counters are data produced by cellular network equipment in order to give an indication of the status of the equipment. The selection of counters was based on the desire for counters most closely representing radio noise level.

The progression of noise in a cellular network can be viewed as follows: Assume no or little initial interference. Gradually, interference is introduced into a system; the noise floor begins to increase. The system compensates by raising transmit power and gain. When these features can no longer compensate, the BER increases. In other words, bits in some frames will have to be corrected [73].

When the BER becomes too high, entire frames become unrecoverable and the FER increases. Lost frames cause data to be lost. In a data system this requires retransmission, causing the data rate to drop. In a voice system the result is reduced voice quality due to the dropped frames. The AMR codec can adapt rate during a conversation to make best use of the channel. If the degradation becomes high enough the network may attempt to hand over the subscriber to a different cell or different network (GSM to UMTS). If too many frames are lost, the call or connection is likely to be dropped.

Potentially useful performance counters are phase jitter, synchronisation, loss of lock and clock error related counters, received signal and noise power indicators, SNR, BER (for example RxQual), FER, error-free seconds, retransmission rate, DCR and Erlang. The counters were mentioned in order of increase in impact of noise in a telecommunications system. Interference would initially manifest as an increase in the noise floor.

Counters are typically summarised over a period of time using averaging, or selecting minimum or maximum values for the period. Averaging may hide some information, such as making outliers appear less extreme, which may be good in the case of errors in the data, but can also mask legitimate data. Summarising using the minimum method has the advantage that it gives an indication of the lowest value in a period. If measurements, overall, for the period are higher than usual, this measure would provide a good indication. The maximum level type summary is good for detecting unusually high measurements in a given period.

Because of the infrastructure of the cellular network operator that was available, the following counters could be provided.

2.7.1 GSM counters/KPIs

Counters or key performance indicators (KPIs) for the 900 MHz (880 – 960 MHz [74]) used for the GSM network are summarised hourly and per cell. Counter data summarised daily stretches back over approximately a year and hourly summarised counters stretch over three months. Statistics were chosen for 47 cells.

Radio noise indicators were not available for GSM, because of the model and manufacturer of network equipment used. Average TRX UL RxQual is the best substitute available. Average TRX UL RxQual is an indication of bit errors over the hour. Errors are grouped into two groups (good: BER $< 2.7\%$

and bad: BER $>$ 3.8% [12]). The UL is more susceptible to interference owing to lower handset power (2W), relative to the base station (20W), thus the UL data were chosen.

2.7.2 UMTS counters/KPIs

UMTS operates at 2100 MHz[16]. UMTS cells are co-located with GSM. DL indicates communication in the direction of user equipment, typically a handset or data modem. UL indicates the inverse. Data are available summarised hourly.

The available counter, which is a potential indicator of the noise floor level, is received total wideband power (RTWP):

- **Average RTWP** is the mean of the RTWP of the bandwidth for a cell, measured in dB for a time period.
- **Minimum RTWP** is the minimum power of totally received bandwidth for cell, measured in dB for a time period.
- **Maximum RTWP** is the maximum power of totally received bandwidth for cell, measured in dB for a time period.

2.7.3 LTE counters/KPIs

LTE counters and KPIs are available for the same periods, locations and sites as GSM and UMTS. The LTE network operates at 1900 MHz (1710 – 1880 MHz [74]).

UL interference, measured in dBm, is the total power of the noise floor and neighbouring cell interference received by each physical resource block in the UL for a time period. High interference level would indicate that the eNodeb is picking up an interference/noise signal of a particular signal strength over its bandwidth. The available counter is summarised as:

- **Power/Quality Max UL interference**, the maximum total UL power over a time.
- **Power/Quality Average UL interference**, the average total UL power over a time.

UL counters were chosen above DL counters, because the antenna of a cellular phone is omni-

[16]The operating frequency for 2100 MHz UMTS is 1920 – 1980, 2010 – 2025 and 2110 – 2170 MHz in South Africa [74].

directional, as the handset may be oriented in any direction by the user. Signal strength on the UL is lower than on the DL, owing to mobile device limitations, therefore UL interference is more likely and is considered. The stronger DL signal could, in times of high loss and interference, cause the handset to be able to receive signal, but be unable to transmit it to the base station.

2.7.4 Microwave backhaul transmission counters

Microwave backhaul transmission counters [75] are available hourly for 60-day periods and summarised daily for approximately one year. Counters for hubs and end nodes of 13 links have been received. The system is a $\sim$26 GHz point-to-multipoint system. Endpoints face mainly east and south, but since hub data are available, a 360° view exists. The microwave network is provisioned by the network operator to function at a minimum of 99.98 or 99.95% availability because of interference. For this reason, it is unlikely to observe significant service-affecting interference.

RSSI appears to be the most useful counter available for microwave backhaul. Data was available summarised hourly per sector. RSSI is a measure of all signals: thermal noise, environmental noise and actual signal. Three variations are available:

- **AirlinkMinRSSI** The minimum RSSI.
- **AirlinkAvgRSSI** The average of the RSSI.
- **AirlinkMaxRSSI** The maximum RSSI.

CHAPTER 3

METHOD

3.1 CHAPTER OVERVIEW

The problem was approached in four stages. A theoretical analysis was performed in order to determine what flux density level could affect the cellular radio network, based on the parameters of different technologies. Antennas and potential susceptibility to solar interference were investigated next. Data were then obtained from various sources, filtered and combined with software tools to form usable datasets, which were processed extracting descriptive statistics, so that an understanding of the data could be developed. Finally, correlation of radio noise producing event magnitudes with cellular telecommunications performance indicator values was performed.

In order to perform the study, data needed to be extracted from data sources, transformed, cleaned and loaded into a database, which occupied a large portion of the study. The counters chosen in Section 2.7, were originally in a de-pivoted form with a date time index and cell identifiers as column headings. The sets were manipulated into the form of three columns: a date and cell index, and counter value (such as max UL interference) and dates were formatted. Sector names were altered to match the format in the cellular network metadata (azimuth, tilt, height above ground and coordinates) and a join was performed between the cellular network metadata and counter sets, so that the associated metadata were available to calculate line of sight with the sun. Identical column formats were created for the different technologies, where possible, in order to allow generic data processing.

Initial statistical analysis was performed for solar indices and cellular network counters to gain an understanding of the requirements for processing. All data, initially in text files, were processed by extracting data and concatenating the results into a single database. Timestamps and database column

formats were standardised in order to allow generic data processing.

Solar event data are trustworthy, since it is manually inspected by professionals. Cellular network radio access network data are normally reliable, as companies base performance on it and missing data within the supplied periods were not evident. The cellular network operator maintains that during the period of data gathering, the area was stable and did not experience network planning changes or upgrades that would alter the noise experienced. The study was concerned with higher than normal noise events; outliers to the left of the bell curve could safely be ignored and where necessary, outliers to the right were removed by inspection. It was not possible to identify and omit noise caused by external interference sources, such as malfunctioning electronics in the area.

The time of occurrence of solar events was used to match solar activity and cellular network data. Filtering was performed to exclude nighttime hours and non-sunfacing hours. X-ray flares of class lower than M were excluded and only solar radio bursts larger than or equal to 100 SFU were used. Telecommunications counters were not excluded based on magnitude. The filtered and unfiltered sets were then compared.

3.2 THEORETICAL SENSITIVITY TO SOLAR FLUX

Analysis was performed to determine what flux density level of radio burst could cause interference, based on system design specifications, in the case of a user handset. Real world sensitivity levels as configured in the network were used for the base station. Flux density, in SFU, is spectral irradiance and can be used to determine what the power on a surface is, given the frequency band and surface area.

Assuming an isotropic antenna and making use of an approximation [76], the equivalent received noise power in dBm (P_{dBm}) can be calculated from the flux density level of a 245 or 2695 MHz radio burst. For example, to calculate the noise power in dBm of 1 SFU, as received by a GSM 1800 system, calculate antenna aperture (A) from the wavelength (λ) of the primary frequency and use the 200 kHz bandwidth (B) as per the GSM specification. Multiplying flux density (S) by bandwidth (B)

and antenna aperture (A) produces the power level in Watts (P_W)

$$P_W = S \times B \times A \tag{3.1}$$

$$B \approx 200\,kHz$$

$$\lambda \approx 0.167\,m$$

$$A = \lambda^2/4\pi$$

$$1\,SFU = 10^{-22} W m^{-2} Hz^{-1}$$

$$S = 1\,SFU$$

$$= 10^{-22} W m^{-2} Hz^{-1} \times B \times A$$

$$\approx 4.4 \times 10^{-20}\,W$$

$$P_{dBm} = 10\log(4.4 \times 10^{-20}\,W \times 1000)$$

$$= -164\,dBm.$$

Results produced by applying Equation 3.1 to parameters of different technologies can be found in Section 4.3.

3.3 DESCRIPTION OF DATA AND CELLULAR NETWORK

The area from which data were obtained covers ~25 km^2 for GSM, UMTS and LTE sectors. UMTS data consists of 34 sectors on two different RNCs, 13 and 21 sectors, respectively. Microwave backhaul links are distributed around South Africa.

An analysis of the orientation of sectors from the GSM, LTE and UMTS radio as well as microwave networks reveals sector orientation is as expected, see Figure 3.1(a). GSM and LTE/UMTS site azimuth distributions are similar. Microwave transmission hub sites are made up of four sectors, as opposed to the cellular network layout of three, see Figure 3.1(b). Further discussion of the microwave systems is not presented, as the available data are summarised daily and antenna tilt was not available. Attempting to determine the influence of the sun by making use of network data that is summarised daily is not sensible.

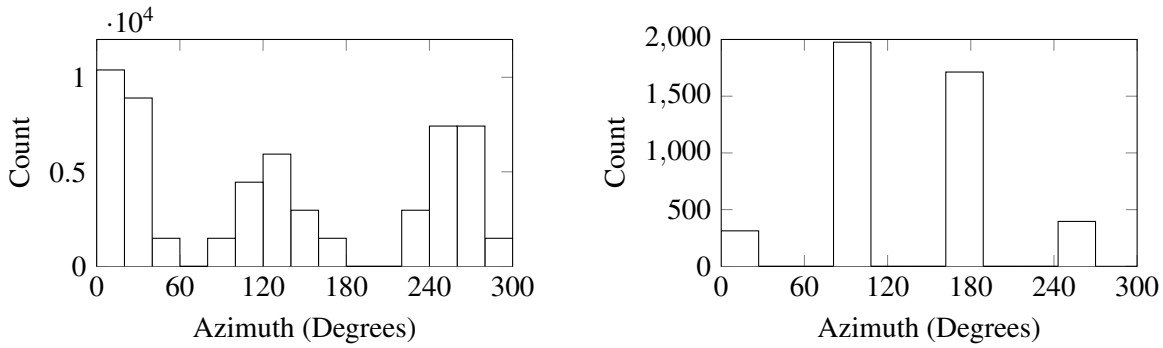

(a) (b)

Figure 3.1: Site azimuths for cellular network towers (a) and the microwave network (b). (a) Histogram of bucketed cell azimuth for the GSM network. The sectors face roughly 0° (north), 120° and 260°, which is expected. (b) Histogram of microwave transmission HT site azimuths. Sectors face north, east, south and west. The data set contains predominantly west and east facing towers.

An assumption was made that in the most extreme case, after 20 dB down (a 100x reduction in gain), noise would not be a significant influence on an antenna. Using 20 dB down, as opposed to 3 dB, increases the area over which the antenna could detect a signal or noise. The vertical radiation pattern of the GSM antenna used, see Figure 2.8(a), is less sensitive at 20 dB down than the LTE/UMTS case see Figure 2.8(b). Determining at which angle the antenna can detect signal or noise is performed by consultation of antenna manufacturer radiation patterns, see Table 3.1, and considering antenna tilt, see Table 3.2. As a simplification, a Katherein 742241 antenna is assumed for the entire network.

Shuttle Radar Topography Mission (STRM) is a NASA project that mapped global earth elevation, providing horizontal resolution of 90 m and vertical resolution of 16 m. STRMv4 data [77], released by CGIAR[1]-CSI (CGIAR Consortium for Spatial Information), were used to calculate the altitude of cells (and by association, sectors), if latitude and longitude were present. For calculating total height, antenna height was added to altitude at the antenna location. UTMS sector latitude and longitude information was not available, thus sites were assumed to be co-located with LTE sectors/sites.

The United States Naval Observatory (USNO) [78] provides daily sunrise and sunset hours for a given latitude and longitude, see Figure 3.2(a) and 3.2(b). Daylight and nighttime hours were differentiated by allocating the hours of 06:00 to 18:59:59 and 20:00 to 05:59:59, respectively.

[1] CGIAR Consortium of International Agricultural Research Centers

Table 3.1: Approximate angles for antenna gain of 3 dB, 20 dB down or assuming the maximum angle where reception is possible, from [60]. Some simplifications were made when interpreting radiation patterns.

Orientation	**Frequency**	**20 dB Down ∠**	**Max ∠**	**3 dB Down ∠**
Horizontal	824 – 960 MHz	270 – 90°	0 – 170°, 210 – 360°	330 – 30°
Horizontal	1710 – 2170 MHz	270 – 90°	0 – 170°, 210 – 360°	330 – 30°
Vertical	824 – 960 MHz	55 – 115°	0 – 170°	87.3 – 93.7°
Vertical	1710 – 2170 MHz	350 – 360°, 0 – 20°, 65 – 75°, 85 – 95°, 100 –105°, 130 – 140°, 155 – 175°	305 – 190°	87.3 – 93.7°,

	GSM	**UMTS**	**LTE**
Mode	7	5	6
Mean	7.16	4.47	5.3
Max	10	9	9
Min	4	0	0
Standard Deviation	1.42	1.89	1.89

Table 3.2: Descriptive statistics for total antenna downtilt for sample GSM, UMTS and LTE sectors. Mostly, antennas face downward.

Sun zenith and azimuth can be calculated with coordinates, altitude, date and hour as inputs [79][80]. Because of the data granularity being hourly, a sector is indicated as being in line of site with the sun if it is found that the sun was in line of sight with the sector at any point in the hour. Obstructions have not been considered, therefore If an antenna is blocked by an object, such as a building, then it is possible that line of sight with the sun may be lost, but it was not possible to correct for it.

Times when antennas would be in line of sight with the sun during the day were identified by considering the position of the sun and radiation patterns, see Figure 3.3 and 3.4. All times are in South African Standard Time, which is the same as UTC+2. The graphs include all hours of the day for clarity, rather than just daylight hours. Time is bucketed such that, for example 09:00:00–09:59:59 is represented by 09:00.

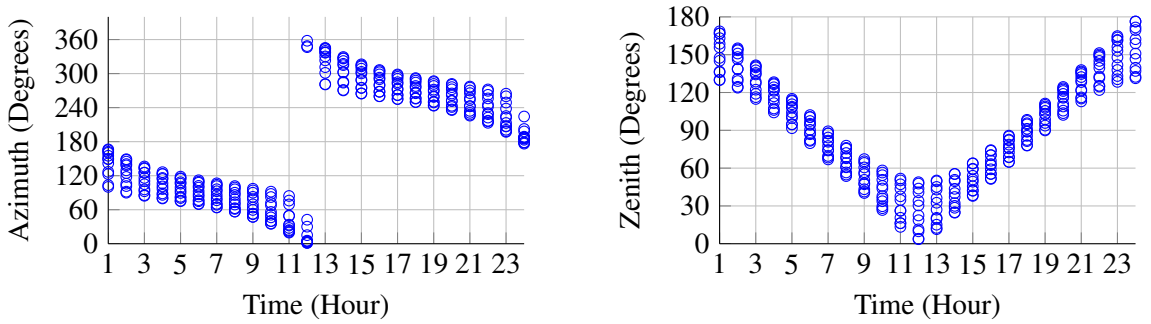

(a) (b)

Figure 3.2: Azimuth (a) and zenith (b) of the sun relative to a site in the sample area for 2013 – 2014. (a) The variation due to month of year can be seen. Variation is approximately 20-25°. The discontinuity from low to high azimuth at 12:00 is due to the counter-clockwise path of the sun. (b) Variation due to month of year is approximately 30-50°, depending on time of day. Zenith indicates the angle from the vertical. Facing straight up indicates 0°. Straight down is equivalent to 180°.

For the period 2014-01-25 to 2014-03-28, sun exposure for 3 dB down and using the available network layout, results were similar for GSM, UMTS and LTE. The 20 dB down case was different; the secondary lobe of the 1710–2170 MHz antenna was visible in observations at midday for 20 dB down, see Figure 3.5 and 2.8(b). The number of LTE sectors in line of sight with the sun during daylight hours was 3% of the sample. For 20 dB down, during daylight hours, 25% of sectors were in line of sight with the sun. The results were used to exclude hours when towers were not in direct line of sight with the sun for the 3 dB and 20 dB down cases. The radiation pattern for UMTS was identical to LTE, therefore sun exposure was very similar. In the GSM case, Figure 3.6 and 2.8(a), (for 20 dB down) 22.8% of sectors were in line of sight with the sun during the day. For 3 dB down on GSM, the percentage of sectors in line of sight with the sun during daylight hours was 3.18%. In both cases, line of sight with the sun occurs predominantly when the sun is low at sunrise and sunset. A figure of 100% would mean that all sectors in the sample would have been in line of sight with the sun in every hour of the day when the sun was above the horizon.

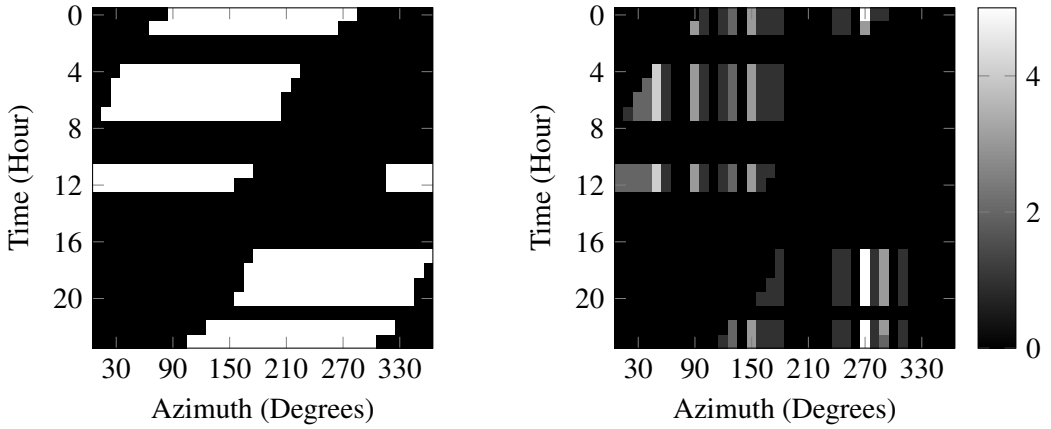

(a) (b)

Figure 3.3: Given the radiation patterns for LTE and UMTS at 20 dB down, comparing a perfectly distributed network with results produced from available data, it is seen that over the entire day, hours where the sun is in line of sight with an antenna are 00:00, 01:00, 04:00–07:00, 11:00, 12:00, 17:00–20:00, 22:00 and 23:00 in both cases, even though some azimuth are not covered, due to the distribution of the network. (a) A single location with one antenna oriented at 10° intervals (in azimuth) and constant zenith of 90°. White indicates one site in line with the sun, black indicates none. (b) The actual network zenith and azimuth are used, for a single 24 hour period. The legend indicates the number of cells in line with the sun for a given hour and azimuth. Hours when the sun is below the horizon and cannot be in line of sight with the antenna are included to make the image easier to understand.

3.4 INITIAL SPACE WEATHER DATA ANALYSIS

It can be seen for solar radio bursts, that larger events occur less often than smaller ones and that fewer events are detected at higher frequencies, Table 3.3. The number of unique and good[2] data points for 245 and 2695 MHz and radio bursts in the period 2013-07-25 to 2014-07-11 was 1578, using SWPC data [81], see Figure 3.7. For the same period, the number of events producing a flux greater than or equal to 1000 was 101, see Figure 3.8. Flux density of greater than or equal to 10 000 SFU was found 13 times at 245 MHz and never at 2695 MHz. Only five occurrences of greater than or equal to 100 000 SFU were recorded and only for 245 MHz. Table 3.4 agrees that the range of values is large, skewing the mean value relative to the median.

[2]Data are indicated as good, corrected or uncertain in the dataset

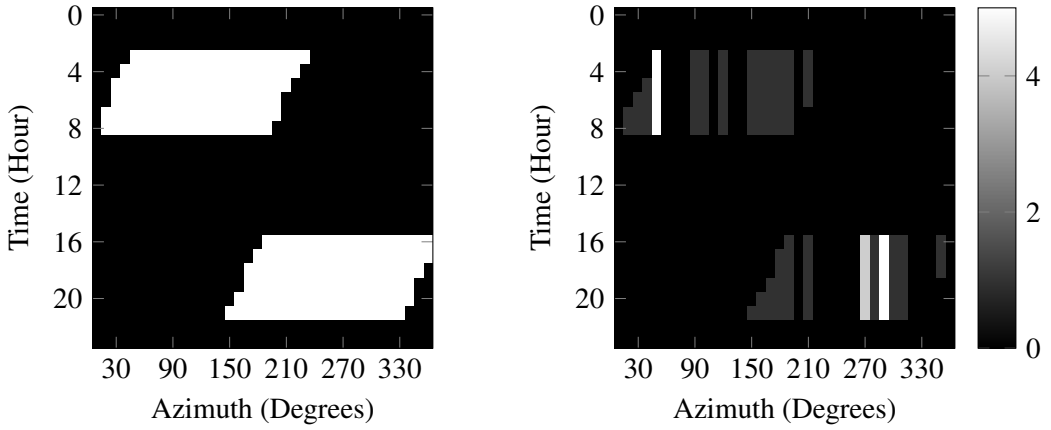

(a) (b)

Figure 3.4: Given the radiation patterns for GSM at 20 dB down, for a single location, it is seen that over the entire day, the antenna could come into contact with the sun at 03:00–08:00 and 16:00–21:00. (a) A single location with one antenna oriented at 10° intervals (in azimuth) and zenith of 90°. White indicates one site in line with the sun, black indicates none. (b) The actual network zenith and azimuth are used, for a single 24 hour period. Hours when the sun is below the horizon and cannot be in line of sight with the antenna are included to make the image easier to understand.

Table 3.3: The mean monthly occurrence of solar radio bursts greater than the specified flux density as calculated using a subset of the data. The subset for the periods 2013-05 to 2014-06.

Radio Burst	**>100 SFU**	**>1000 SFU**	**>10000 SFU**	**>100000 SFU**
245 MHz	117.72	8.27	1.18	0,45
2695 MHz	3.64	0.91	–	–

Solar flux levels for both 245 and 2695 MHz occur predominantly at levels lower than 400 SFU, but some high value outliers do occur. Both distributions, Figure 3.10 and 3.11, show large positive outliers. The standard deviation is large, mean radio burst durations are 6.8 and 11.88 minutes, for 245 and 2695 MHz events, respectively, see Figure 3.12 and Table 3.5. A few events of many hours' duration were recorded for 245 MHz, but events are predominantly of sub-minute durations.

From analysis, it can be seen that flares of greater magnitude occur less often than those of smaller magnitude, see Table 3.6. For the period 2013-04 to 2014-07-11, 18 X-class flares were reported, see Figure 3.13 [38], with a magnitude of up to 4.9, see Table 3.7 and Figure 3.14. The distribution

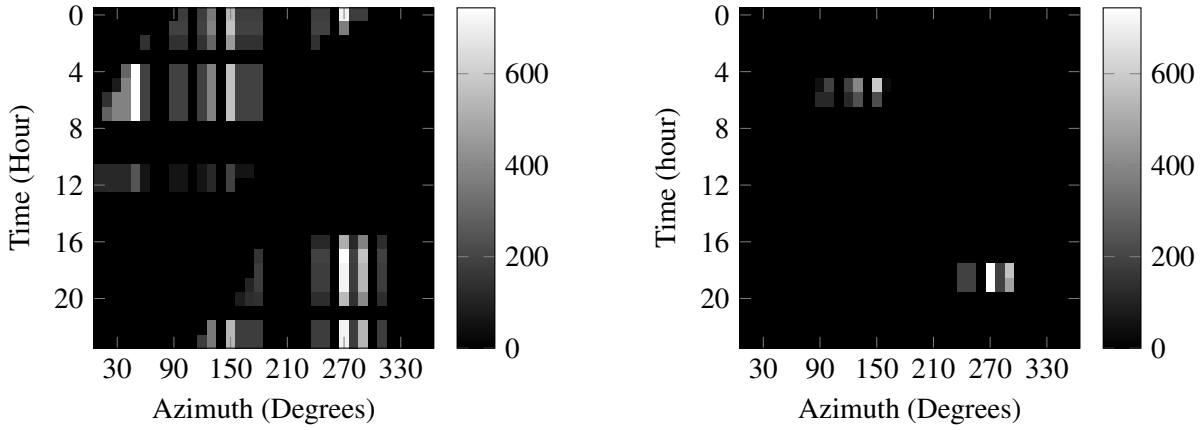

(a) (b)

Figure 3.5: The heatmap indicates the number of sectors, facing a particular direction, in line of sight with the sun at a given time of day. North is represented by 0°. Zenith angle or downtilt is not represented, but is considered. Line of sight with the sun was plotted hourly for LTE sectors with 1710–2170 MHz radiation patterns as per Figure 2.8(a) and 2.9(a) in the sample set for 20 (a) and 3 dB (b) down angles. An analysis of the UTMS network is likely to yield a similar result, as the same antenna could be used. (a) For 20 dB down, a large number of LTE sectors are in line of sight with the sun at 06:00, 07:00, 11:00, 12:00, 16:00–18:00. During daylight hours 25% of sectors are in line of sight with the sun. Azimuth indicates azimuth of the cell. (b) For 3 dB down, LTE sectors were in line of sight with the sun at 17:00 and 18:00. The percentage of sectors in line of sight with the sun during daylight hours is 3%.

Table 3.4: Descriptive statistics for 245 and 2695 MHz flux density measurements.

	245 MHz	**2695 MHz**
Mode	100	170
Median	150	360
Mean	871	906
Max	13000	8300
Min	100	150
Standard Deviation	6840	1718

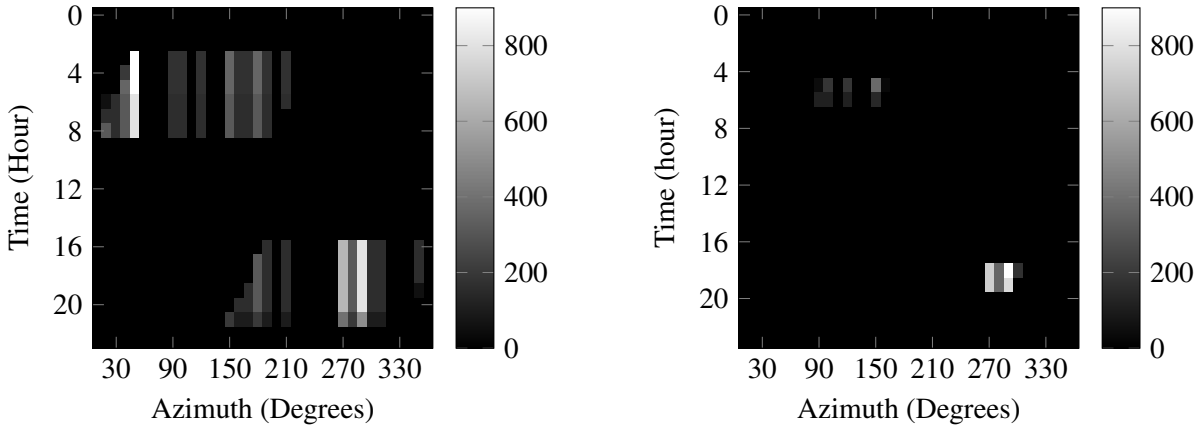

(a) (b)

Figure 3.6: The heatmap indicates the number of sectors, facing a particular direction, in line of sight with the sun at a given time of day. North is represented by 0°. Zenith angle or downtilt is not represented, but is considered. Line of sight with the sun is plotted hourly for GSM sectors with 824–960 MHz radiation patterns as per Figure 2.8(a) and 2.9(a) in the sample set for 20 (a) and 3 dB (b) down angles. (a) For 20 dB down, GSM sectors are in line of sight with the sun at 07:00, 08:00 and 16:00, 17:00 and 18:00. The percentage of sectors in line of sight with the sun during daylight hours is 22.8%. (b) For 3 dB down, GSM sectors are in line of sight with the sun at 17:00 and 18:00. The percentage of sectors in line of sight with the sun during daylight hours is 3.2%.

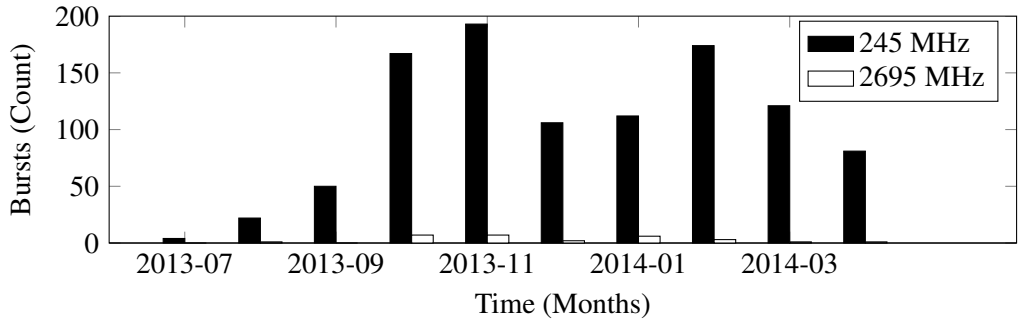

Figure 3.7: Total number of 245 and 2695 MHz radio bursts per month for the period 2013-07-25 to 2014-04-16. The number of 245 MHz events is an order of magnitude greater than for 2695 MHz events.

of event magnitude is negatively skewed, as can be seen in Figure 3.14, with some occasional large positive outliers.

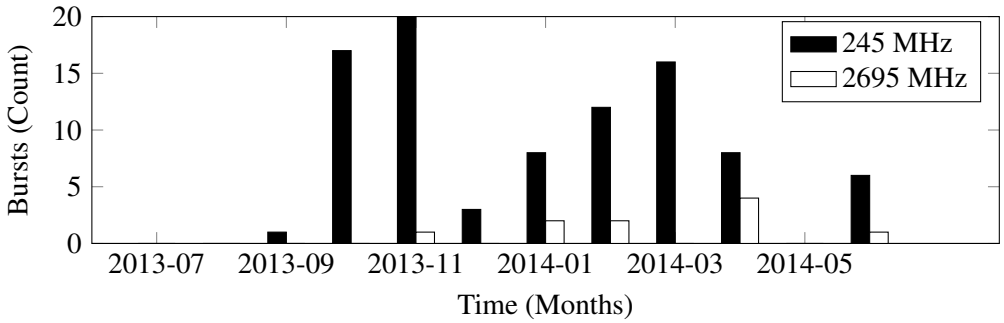

Figure 3.8: Number of 245 and 2695 MHz radio bursts monthly where flux density is more than 1000 SFU for the period 2013-07-25 to 2014-07-11. The number of 245 MHz events is an order of magnitude greater than for 2695 MHz.

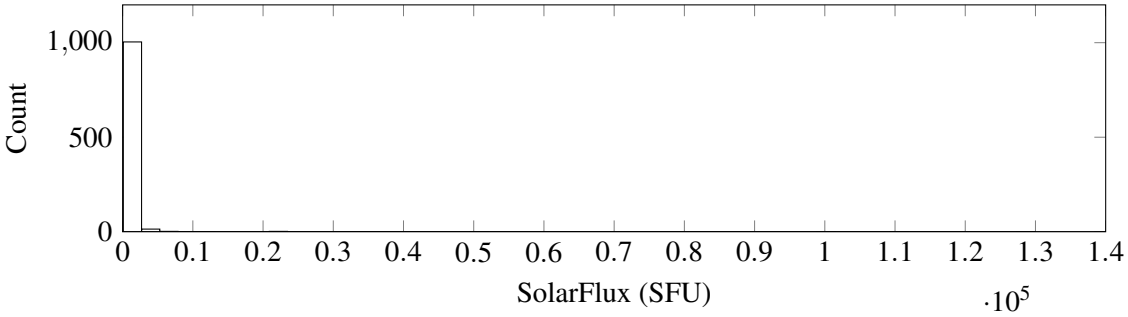

Figure 3.9: The complete distribution of good 245 MHz radio bursts showing flux density for the period 2013-07-25 to 2014-04-16 showing a large amount of negative skewness. The first two bins have been excluded to place emphasis on outliers.

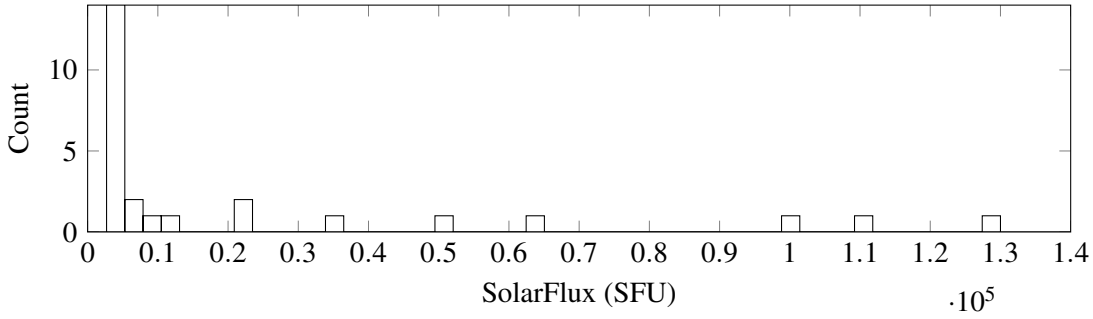

Figure 3.10: The complete distribution of good 245 MHz radio bursts showing flux density for the period 2013-07-25 to 2014-04-16 showing a large amount of negative skewness.

Between 1997 and 2013 there were four earth-facing X-class X-ray flares X10 or larger, magnitudes were 10, 14.4, 17, 17.2. The three largest occurred during daylight hours. All events lie outside dates

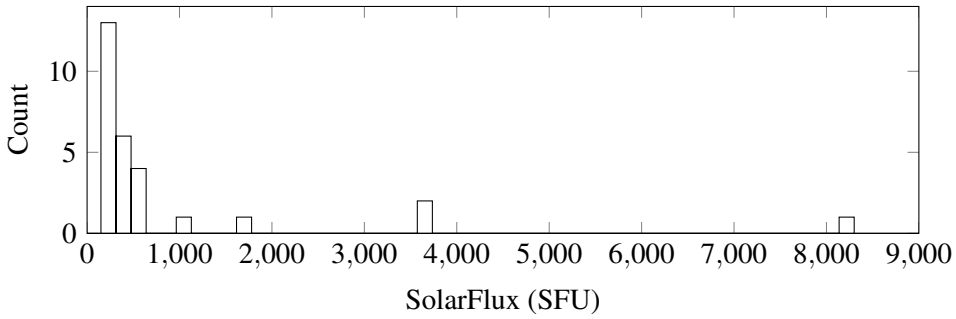

Figure 3.11: Distribution of all good 2695 MHz radio bursts. The plot shows the flux density for the period 2013-07-25 to 2014-04-16.

Table 3.5: Descriptive statistics for 245 and 2695 MHz radio burst duration (minutes) for the period 2013-07-25 to 2014-07-11.

	245 MHz	**2695 MHz**
Mode	0	1
Median	0	5.50
Mean	6.8	11.88
Max	796	50
Min	0	0
Standard Deviation	42.66	12.73

Table 3.6: The mean monthly occurrence of X-ray flares greater than the specified flare magnitude. A data subset of 2013-08 to 2014-06 was used.

Solar Flare	**>1**	**>2**	**>4**	**>6**
M-class	8.50	3.21	1.43	0.79
X-class	1.36	0.50	0.07	–

for which hourly telecommunication counter data are available. Mean, see Figure 3.15 and Table 3.8, flare durations were 19.1 and 23.43 minutes long for M and X-class events, respectively. Maximum observed durations are just under an hour for both classes of events.

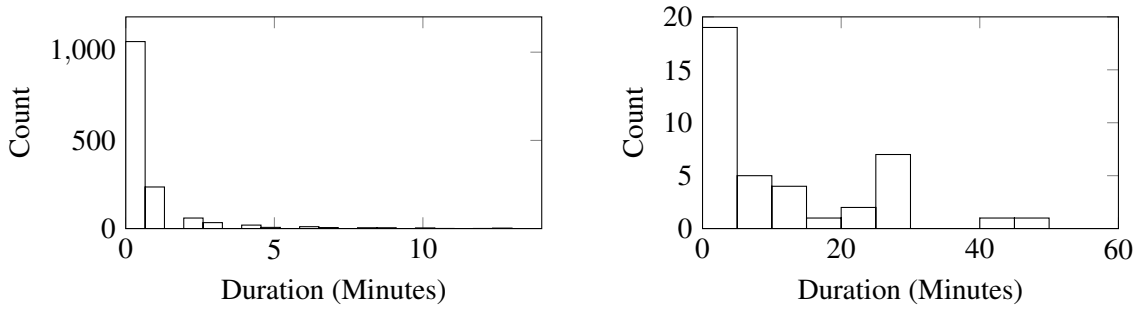

(a) (b)

Figure 3.12: Histograms of event duration (minutes) of 245 and 2695 MHz solar radio bursts. (a) Duration of 245 MHz solar radio burst is skewed toward zero. The histogram includes only values below 15 minutes. (b) Duration of 2695 MHz solar radio burst. The distribution is skewed towards zero.

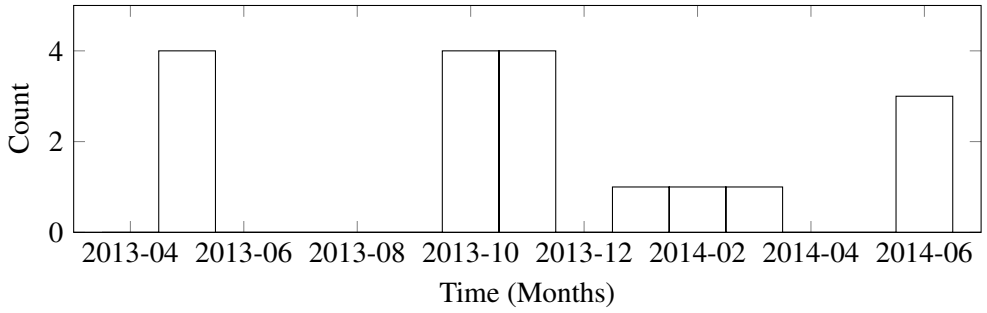

Figure 3.13: Count X-class flares monthly for the period 2013-04 to 2014-07-11.

Table 3.7: Descriptive statistics for M and X-class flares for the period 2013-04 to 2014-07-11.

	M-class	**X-class**
Mode	1	1
Median	1.7	1.5
Mean	2.52	1.87
Max	9.90	4.90
Min	1	1
Standard Deviation	2	1.05

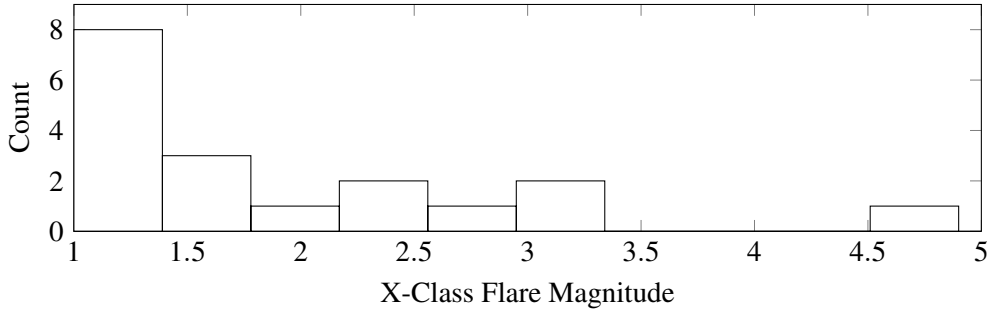

Figure 3.14: Histogram of magnitude of X-class flares for the period 2013-04 to 2014-07-11.

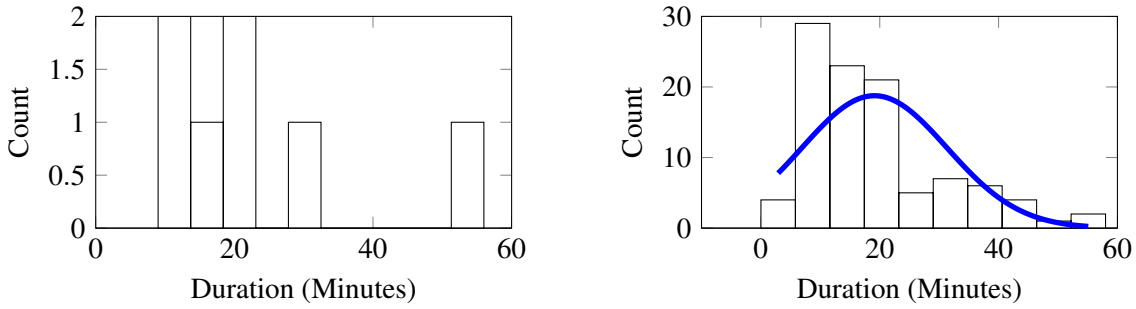

(a) (b)

Figure 3.15: Histograms of duration of X and M-class flares. (a) X-class flare duration. It is possible that not enough samples exist for a distribution to be seen. (b) M-class flare duration with Gaussian fit. The distribution appears possibly bi-modal; however a larger data set might reveal a different distribution.

Table 3.8: Descriptive statistics for duration of M and X-class flares for the period 2013-04 to 2014-07-11.

	M-class	**X-class**
Mode	9	9
Median	16	20
Mean	19.1	23.43
Max	58	56
Min	0	9
Standard Deviation	12.21	15.82

3.5 INITIAL CELLULAR NETWORK DATA ANALYSIS

Descriptive statistics and histograms are used to describe cellular network data. Analysis of the same counter during the day and night is used to investigate if potential interference due to the sun exists, regardless of antenna orientation. GSM data was excluded as inconsistencies were found with the data, however the theoretical analysis regarding line of sight with the sun as well as potential susceptibility to radio noise were included.

3.5.1 UMTS radio network counter statistics

Values of hourly UMTS RTWP, measured in dB, seem to form a normal bell-curve, perhaps slightly skewed with some large outliers, see Figure 3.16 and Table 3.9. Zero values are assumed to be erroneous, as some cells have long periods of zeros. The sample contains 1266 observations for 35 sectors over the period of 2014-02-22 to 2014-05-23.

Table 3.9: Descriptive statistics for average, minimum and maximum UMTS RTWP in dB for the period 2014-02-22 to 2014-05-23.

	Average	**Minimum**	**Maximum**
Mode	-105.90	-105.90	-105.80
Median	-104.70	-105.60	-97.0
Mean	-104.25	-105.30	-95.65
Max	-72.79	-73.40	-50.30
Min	-112.02	-112.10	-107.90
Standard Deviation	2.25	2.10	7.53

A comparison of UMTS RTWP during the daytime versus nighttime for a set of counters shows that, especially for maximum UMTS RTWP, daytime noise is slightly higher than other groups, see Table 3.9 and Figure 3.17 .

3.5.2 LTE radio network counter statistics

For the period 2014-02-22 to 2014-05-23, values of hourly LTE average UL interference, measured in dB, form a skewed distribution, see Figure 3.18(a) and Table 3.11. Outliers do exist, but are in

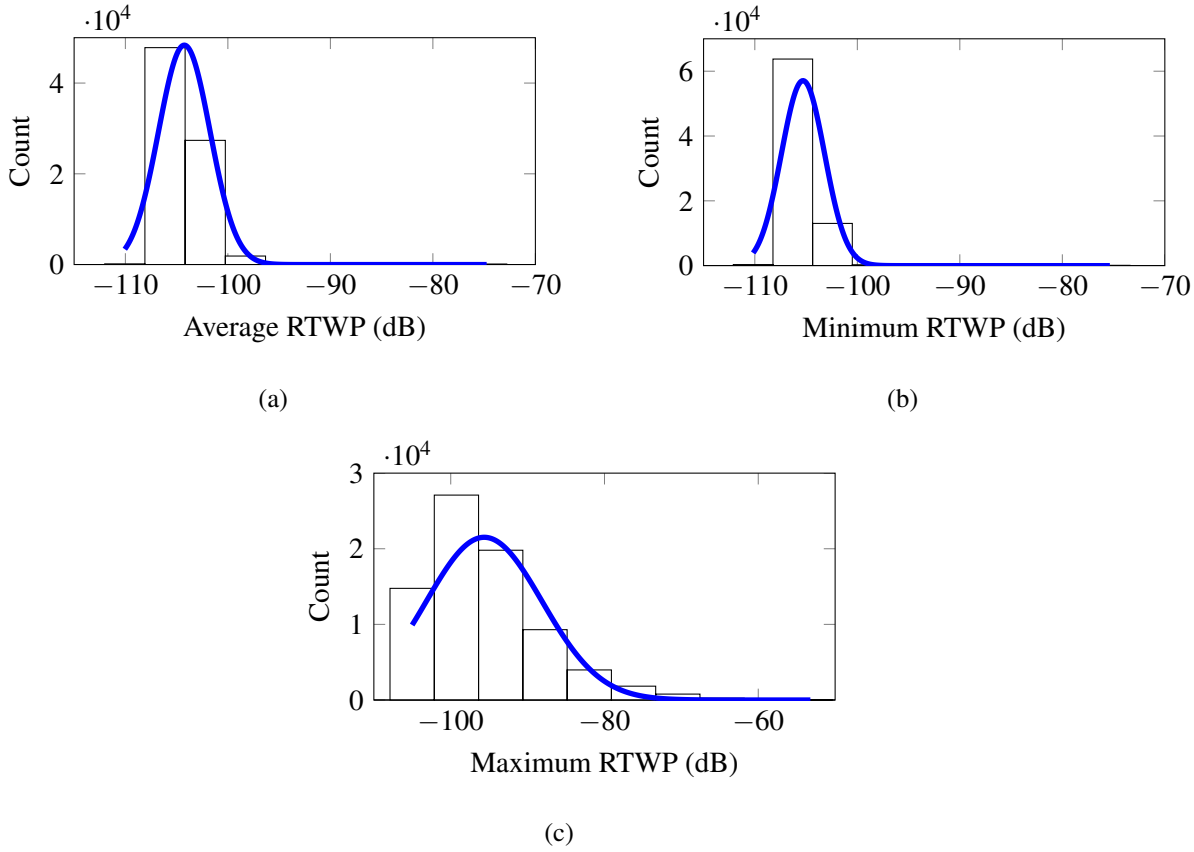

Figure 3.16: Histogram of hourly UMTS RTWP for the period 2014-02-22 to 2014-05-23 with overlaid Gaussian curve and zero values excluded. (a) Average interference following a seemingly Gaussian distribution. (b) Minimum UL interference following a seemingly Gaussian distribution.(c) Maximum UL interference potentially follows a Z distribution.

Table 3.10: Descriptive statistics for UMTS RTWP separately for day and nighttime hours.

	Avg. Day	**Avg. Night**	**Min. Day**	**Min. Night**	**Max. Day**	**Max. Night**
Mode	-105.90	-105.90	-105.90	-105.90	-95.70	-105.80
Median	-104.43	-105.04	-105.50	-105.80	-94.90	-99.50
Mean	-104.01	-104.55	-105.20	-105.42	-93.54	-98.13
Max	-72.79	-73.96	-73.40	-74.60	-50.80	-50.30
Min	-112.02	-108.41	-112.10	-112.10	-107.10	-107.90
Standard Deviation	2.59	2.45	2.22	2.02	7.65	6.59

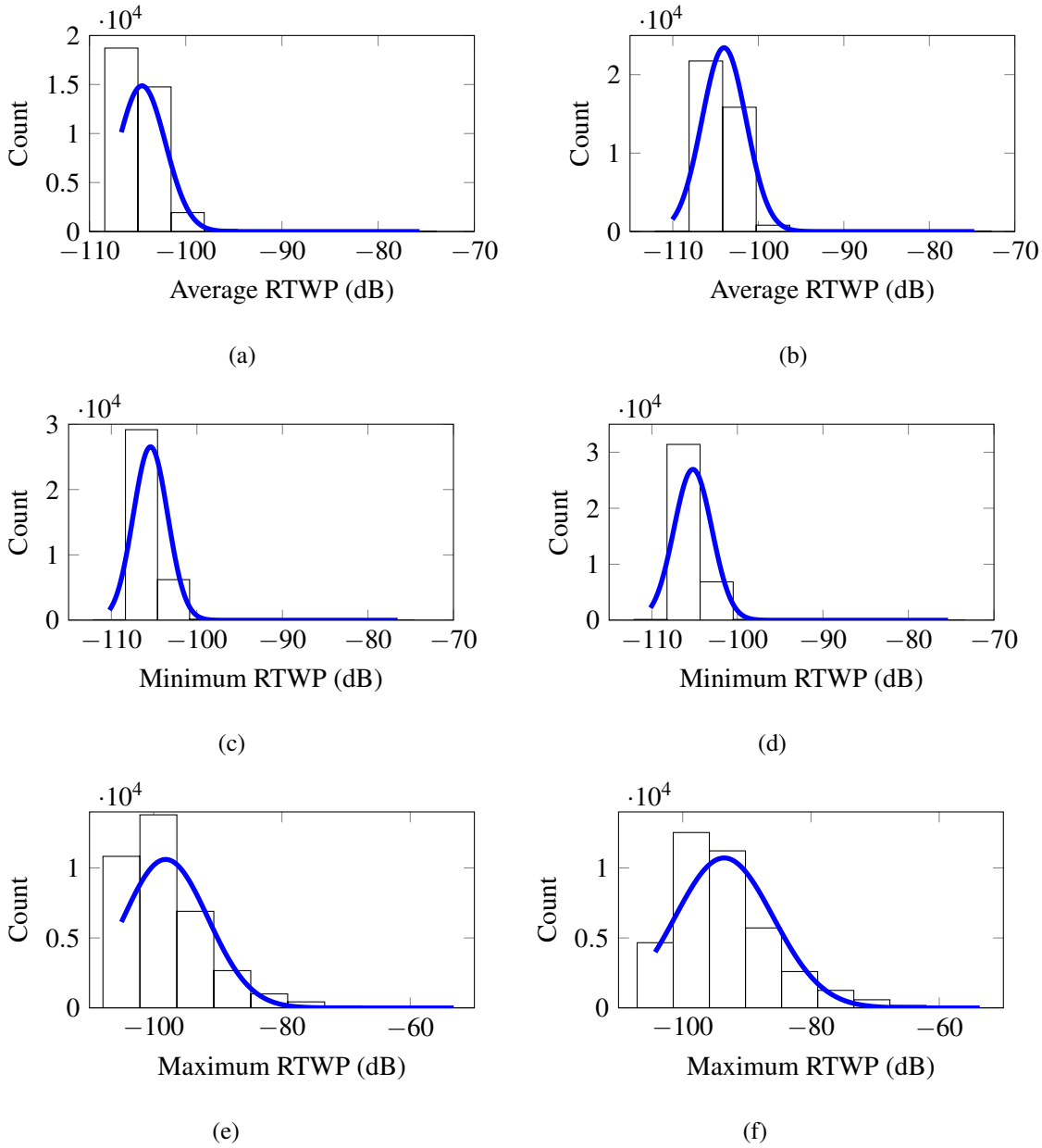

Figure 3.17: Histograms of average, minimum and maximum RTWP for separately for daylight and night hours with Gaussian fits. Distributions appear chi-squared or Gaussian. (a) Average RTWP nighttime distribution. (b) Average RTWP daytime distribution. (c) Minimum RTWP nighttime distribution. (d) Minimum RTWP daytime distribution. (e) Maximum RTWP nighttime distribution. (f) Maximum RTWP daytime distribution.

the lower dB and zero levels, meaning that the outliers would probably not cause an impact. Zero values are assumed to be erroneous, as some cells produce the values for long periods. LTE maximum UL interference in Figure 3.18(b) is more Gaussian, but no outliers appear, excluding the erroneous

zero values. The sample size for both average and maximum UL interference is 32 sectors with 2154 samples each.

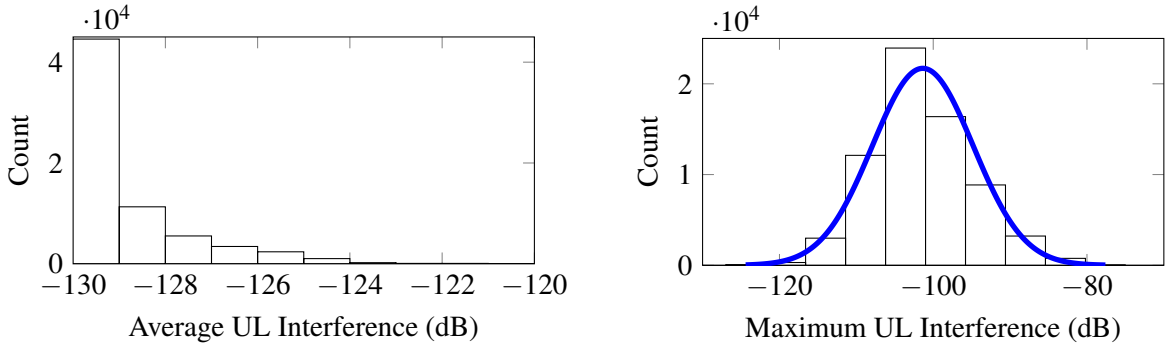

Figure 3.18: Histogram of hourly LTE UL interference for the period 2014-02-22 to 2014-05-23 with overlaid Gaussian curve and zero values excluded. (a) Average interference appears to follow a distribution similar to a chi-squared distribution. (b) Maximum UL interference appears Gaussian.

Table 3.11: Descriptive statistics for average and maximum LTE UL interference in dB for the period 2014-02-22 to 2014-05-23.

	Average	**Maximum**
Mode	-129.00	-102.00
Median	-129.00	-101.36
Mean	-128.39	-101.36
Max	-120.00	-75.00
Min	-130.00	-127
Standard Deviation	1.37	6.56

A comparison of LTE UL interference during the daytime versus nighttime for the set of values shows a small difference in the case of the maximum UL interference. Visually, distributions of the maximum or average UL interference counter are similar, though the distribution of maximum values has a lower average during the night, see Table 3.12 and Figure 3.19.

Table 3.12: Descriptive statistics for LTE UL interference separately for day and nighttime hours.

	Avg. Day	**Avg. Night**	**Max. Day**	**Max. Night**
Mode	-129.00	-129.00	-100.00	-107.00
Median	-129.00	-129.00	-99.00	-105.00
Mean	-128.22	-128.60	-98.59	-104.62
Max	-120.00	-120.00	-75.00	-77.00
Min	-130.00	-130.00	-117.00	-127.00
Standard Deviation	1.45	1.20	5.74	5.97

3.5.3 Microwave backhaul transmission counter statistics

An increase in RSSI may indicate an increase in the noise floor, affecting the system, see Figure 3.20. It does appear that there are some periods with higher than normal RSSI, see Table 3.13. Since the counters are post-processed and the calculation process is unclear, an assumption is made that sampling times differ for minimum, maximum and average counters, hence the observed -500 dB values in the case of maximum and average RSSI, but not minimum RSSI.

Table 3.13: Descriptive statistics for average, minimum, and maximum RSSI (dB).

	Average RSSI	Minimum RSSI	Maximum RSSI
Mode	-64.00	-66.00	-63.00
Median	-64.33	-66.00	-63.00
Mean	-73.95	-68.20	-69.50
Max	-62.00	-63.00	-47.00
Min	-500.00	-88.00	-500.00
Standard Deviation	58.32	6.78	53.57

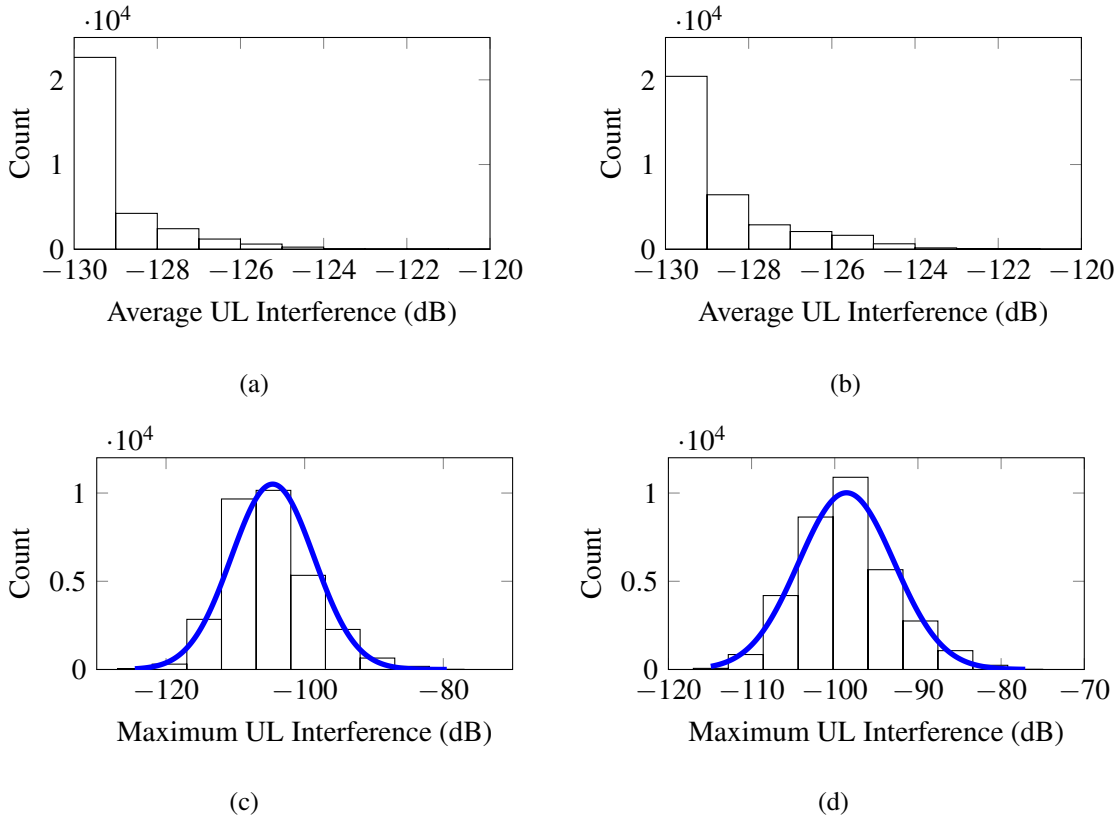

Figure 3.19: Histograms of average and maximum UL interference, separately for daylight and night hours. The average distributions appear to follow a chi-squared distribution and maximum distributions a Gaussian distribution. It is suspected that the skewing of the distribution in the case of the average UL interference may be an artifact of the averaging process. (a) Average UL interference, nighttime. (b) Average UL interference, daytime. (c) Maximum UL interference, nighttime. (d) Maximum UL interference, nighttime.

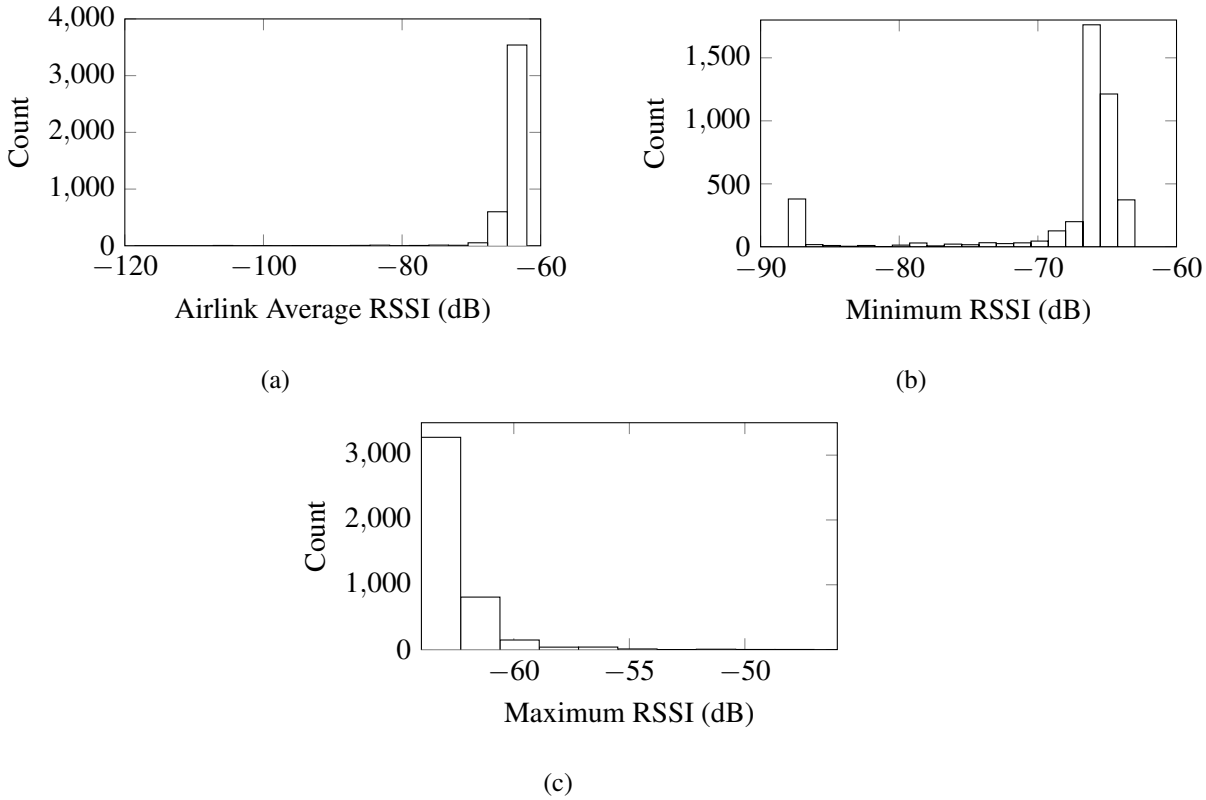

Figure 3.20: Histogram of microwave backhaul transmission HT site RSSI summarised daily for the period 2013-02-07 to 2014-04-01. (a) Average RSSI with extreme outliers below -120 dB omitted. (b) Average RSSI with zero value outliers excluded. (c) Maximum RSSI seems to indicate some periods with high signal strength. The distribution appears to be possibly chi-squared.

3.6 CORRELATION BETWEEN SPACE WEATHER AND CELLULAR NETWORK COUNTERS

Correlation is performed by matching the hour or day (in the case of Received Signal Strength Indicator (RSSI)) in which an event occurred with the hour or day (in the case of RSSI) for when telecommunications counters were collected. Correlation is between values of all eight telecommunication counters and the magnitude of X-ray flare or flux density of solar radio burst. Correlation is a mutual relationship between two variables. The Pearson's population correlation coefficient,

$$\text{corr}(X,Y) = \frac{\text{cov}(X,Y)}{\sigma_X \sigma_Y} = \frac{E[(X-\mu_X)(Y-\mu_Y)]}{\sigma_X \sigma_Y}, \tag{3.2}$$

of two random variables X and Y is the covariance of the variables divided by the product of the standard deviations. X and Y have expected values of μ_X and μ_Y and standard deviations of σ_X and σ_Y, respectively. E indicates expected value.

The p-value confirms whether the relationship found by means of correlation between X and Y is reliable or not. A low p-value (close to zero) would indicate that the relationship is reliable. P-values for Pearson's correlation are calculated using Student's t-distribution, where r = $\mid corr(X,Y) \mid$, and n is the sample size, the t-value is calculated as

$$t = r(\sqrt{(n-2)/(1-r^2)}). \tag{3.3}$$

Using the t-distribution critical value table, it is possible to determine for the decided p-value or alpha value and degrees of freedom (n-2) , what the required r-value should be in order for dependence of X and Y to be considered significant.

Correlation is performed by matching the hour or day (in the case of RSSI) when an event occurred with the hour or day (in the case of RSSI) when telecommunications counters were collected, excluding times where the sun was calculated not to be in line of sight with an antenna. Visually, it can be represented by a plot where x and y coordinates are cellular network counter and space weather indicator, respectively.

Correlation was performed between cellular network counters for the following hours:

- All.
- Only for sun incident hours as identified by Figure 3.5(a) and 3.6(a).
- Only for sun incident hours as identified by Figure 3.5(b) and 3.6(b).

Results were considered not significant if the p-value of the correlation coefficient was larger than 0.05 and if the absolute value of the correlation coefficient was not larger than or equal to 0.7. For the p-value, the null hypothesis is that the solar radio indicator does not relate to the cellular noise indicator. Results are shown in Table 4.4.

The null hypothesis is that the solar radio indicator does not relate to the cellular noise indicator or that r = 0. The null hypothesis is accepted if the p-value of the correlation coefficient was larger than 0.05. Correlation was performed by matching the hour or day (in the case of RSSI) when an event occurred with the hour or day (in the case of RSSI) for when telecommunications counters were collected. Overall, the null hypothesis was accepted even when the correlation was found to be high, therefore the results are not significant.

CHAPTER 4

RESULTS

4.1 CHAPTER OVERVIEW

An analysis was performed to determine if interference with cellular radio equipment was elevated during solar events, based on: system design, considering day and night time hours and also line of sight of antenna radiation patterns with the sun.

It was determined that both basestations and handsets are potentially susceptible to interference due to solar radio flux, given observed noise levels and equipment sensitivity. Bandwidth potentially has a larger impact on noise reception than frequency. Distributions of LTE and UMTS network counters show that solar radio noise can be higher than the mean level of received noise. Microwave backhaul specifications were not available. Finally, correlation was performed between space weather and cellular telecommunications network indicators.

4.2 COMPARISON OF DISTRIBUTIONS

Using the 20 dB down antenna radiation pattern, histograms of cellular radio noise counters during all hours, daylight hours[1] and incident hours[2]. Histograms are scaled to indicate proportion of cells relative to the total. It appears that for UMTS (maximum and minimum RTWP) and LTE that, during solar events, higher interference levels occur during incident hours than during all and daylight hours. Daylight hours show higher interference than all hours. Results for X-Class flares and 2695 MHz radio bursts did not contain enough data points and were omitted. In all cases, Kolmogorov-Smirnov

[1]The hours between 06:00 and 18:59:59.

[2]Hours when towers are in line of sight with the sun during times of solar events, see Figure 3.5 may indicate interference due to the solar events, see 4.1, 4.2, 4.3, 4.4 and 4.5

tests, using a five percent confidence interval, between the all day hours, day hours and incident hours distributions rejected the null hypothesis that the distributions are different.

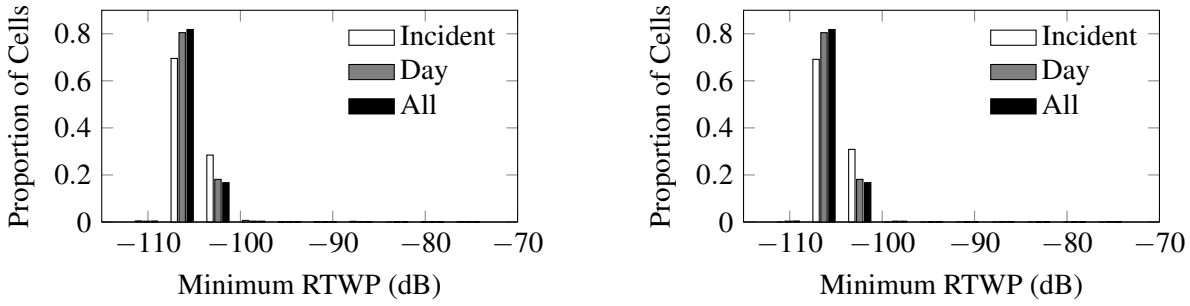

(a) (b)

Figure 4.1: Minimum UMTS RTWP histograms for all, daylight and sun incident hours coinciding with 245 MHz solar radio and M-class X-ray flare events. Results are not granular enough to allow a conclusion to be drawn. (a) Results for 245 MHz radio bursts indicate that for higher dB levels, higher interference occurs during radio events than normally. (b) Results for M-class flares indicate that for higher dB levels, higher interference occurs during radio events than normally.

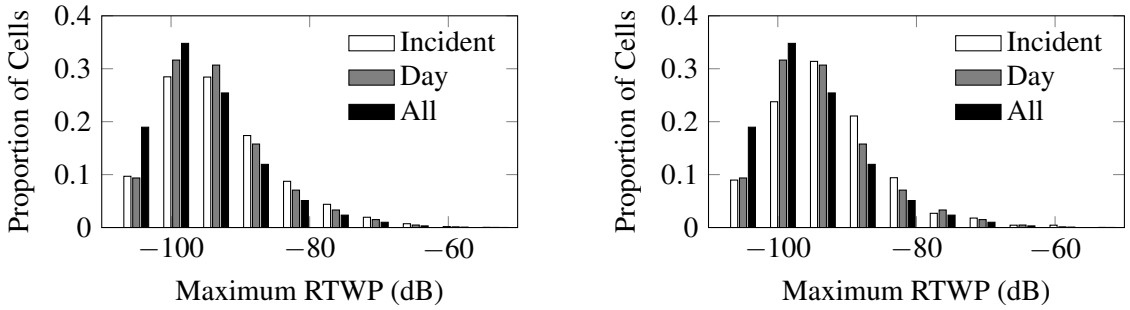

(a) (b)

Figure 4.2: Maximum UMTS RTWP histograms for all, daylight and sun incident hours coinciding with 245 MHz solar radio and M-class X-ray flare events. (a) Results for 245 MHz radio bursts indicate that for higher dB levels, higher interference occurs during radio events than normally. (b)Results for M-class flares generally indicate that for higher dB levels, higher interference occurs during radio events than normally.

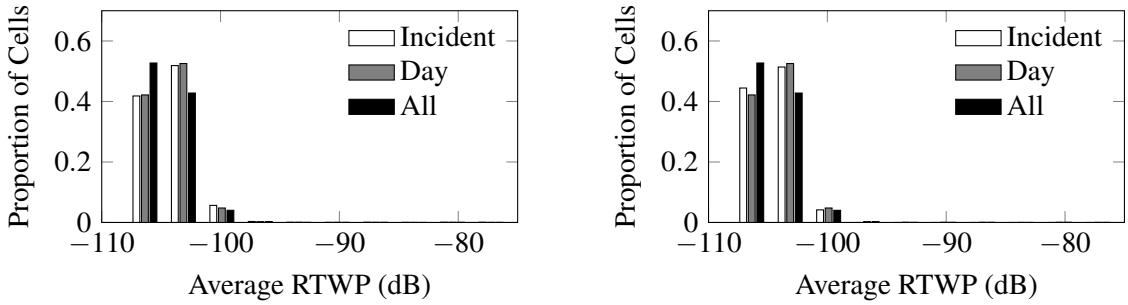

(a) (b)

Figure 4.3: Average UMTS RTWP histograms for all, daylight and sun incident hours coinciding with 245 MHz solar radio and M-class X-ray flare events. Results are not granular enough to allow a conclusion to be drawn. (a) The results for 245 MHz bursts indicate that for higher dB levels, higher interference occurs during radio events than normally. (b) The results for M-class flares indicate that for higher dB levels, lower interference occurs during radio events than normally, excluding the buckets at $\sim$ -100 dB.

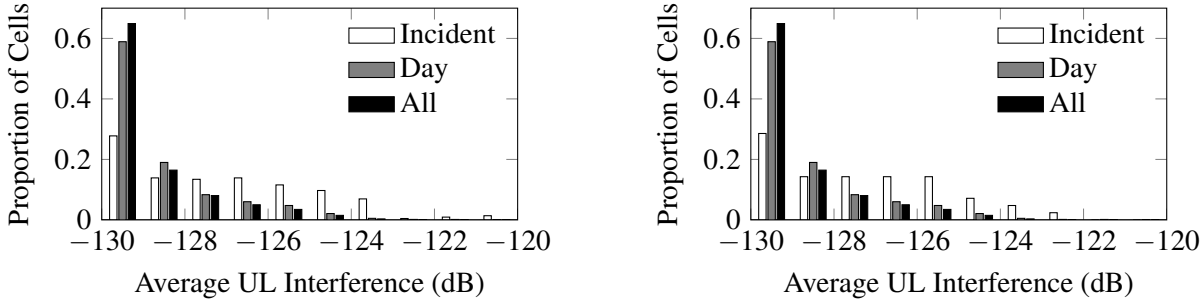

(a) (b)

Figure 4.4: Average LTE UL Interference histograms for all, daylight and sun incident hours coinciding with 245 MHz solar radio and M-class X-ray flare events. (a) Results for 245 MHz radio bursts indicate that for higher dB levels, higher interference occurs during radio events than normally. (b) Results for M-class flares indicate that for higher dB levels, higher interference occurs during radio events than normally.

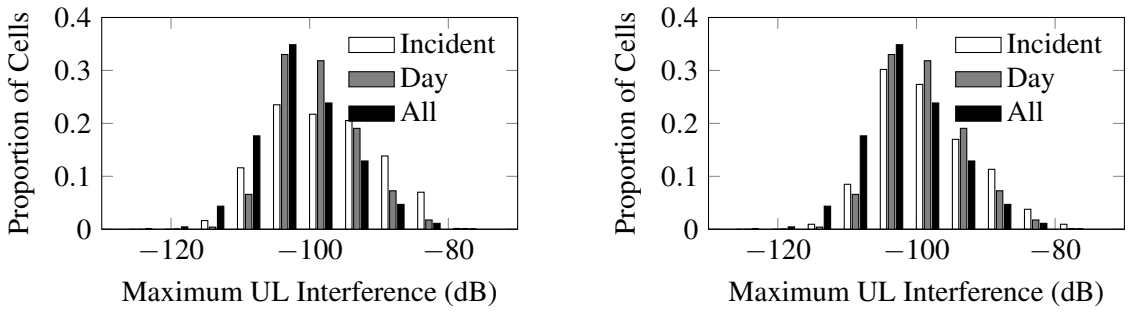

(a) (b)

Figure 4.5: Maximum LTE UL interference histograms for all, daylight and sun incident hours coinciding with 245 MHz solar radio and M-class X-ray flare events. Assuming Gaussian distributions, the all and daylight hour distributions are characterised by means and standard deviations of -101, 6.5 and -98, 5.7 respectively. (a) Maximum UL interference results for 245 MHz radio bursts indicate that for higher dB levels, higher interference occurs during radio events than normally. The mean and standard deviation for incident hours are -97 and 7.7 respectively. (b) Interference for maximum UL interference during M-class flares indicates that higher interference occurs during solar flares than normally. The mean and standard deviation for incident hours are -98 and 6.88 respectively.

4.3 THEORETICAL SENSITIVITY TO SOLAR FLUX

Lowering operating frequency and increasing channel bandwidth causes higher susceptibility to radio noise in the form of solar flux, see Figure 4.6. For example, LTE on 900 MHz with 20 MHz bandwidth is susceptible relative to other technologies. In many cases thermal noise is much lower than the solar flux density. An order magnitude change in bandwidth has half the influence (in dBm) of an order of magnitude change in frequency, see Table 4.1.

Table 4.1: The table contains power due to a flux density of 1000 SFU as a function of bandwidth and central frequency. Given flux density of 1000 SFU, an order magnitude increase in central frequency produces a 20 dBm decrease in power due to the solar interference. An order magnitude increase in bandwidth produces a 10 dBm increase in power due to flux density.

Central Frequency	**1 GHz**	**10 GHz**	**100 GHz**
0.1 GHz BW	-131.5 dBm	-151.5 dBm	-171.5 dBm
1 GHz BW	-121.5 dBm	-141.5 dBm	-161.5 dBm
10 GHz BW	-111.5 dBm	-131.5 dBm	-151.5 dBm
100 GHz BW	-101.5 dBm	-121.5 dBm	-141.5 dBm

Reference handset receiver sensitivities (minimum detectable power at the antenna port of the handset) compared to the required order of magnitude of flux density for solar radio noise to be detected, see Table 4.2, indicates that system design makes it plausible that solar radio bursts could be detected by cellular telecommunications systems. For example, in the case of UMTS, since handsets are required to have high sensitivity (-117 dBm), bursts of 1000 SFU could be detected.

Table 4.2: Minimum flux density that could be detected by a handset, as per the technology design specification, assuming a 0 dBi antenna and based on the results of Figure 4.6

Technology	**Sensitivity (dBm)**	**Required Flux (SFU)**
GSM 1800	-104 to -95 [82]	>>100 000
GSM 900	-104 to -102 [82]	> 10 000
UMTS	-117 to -114 [83]	>1000
LTE	-106.2 to -91[84]	>10 000

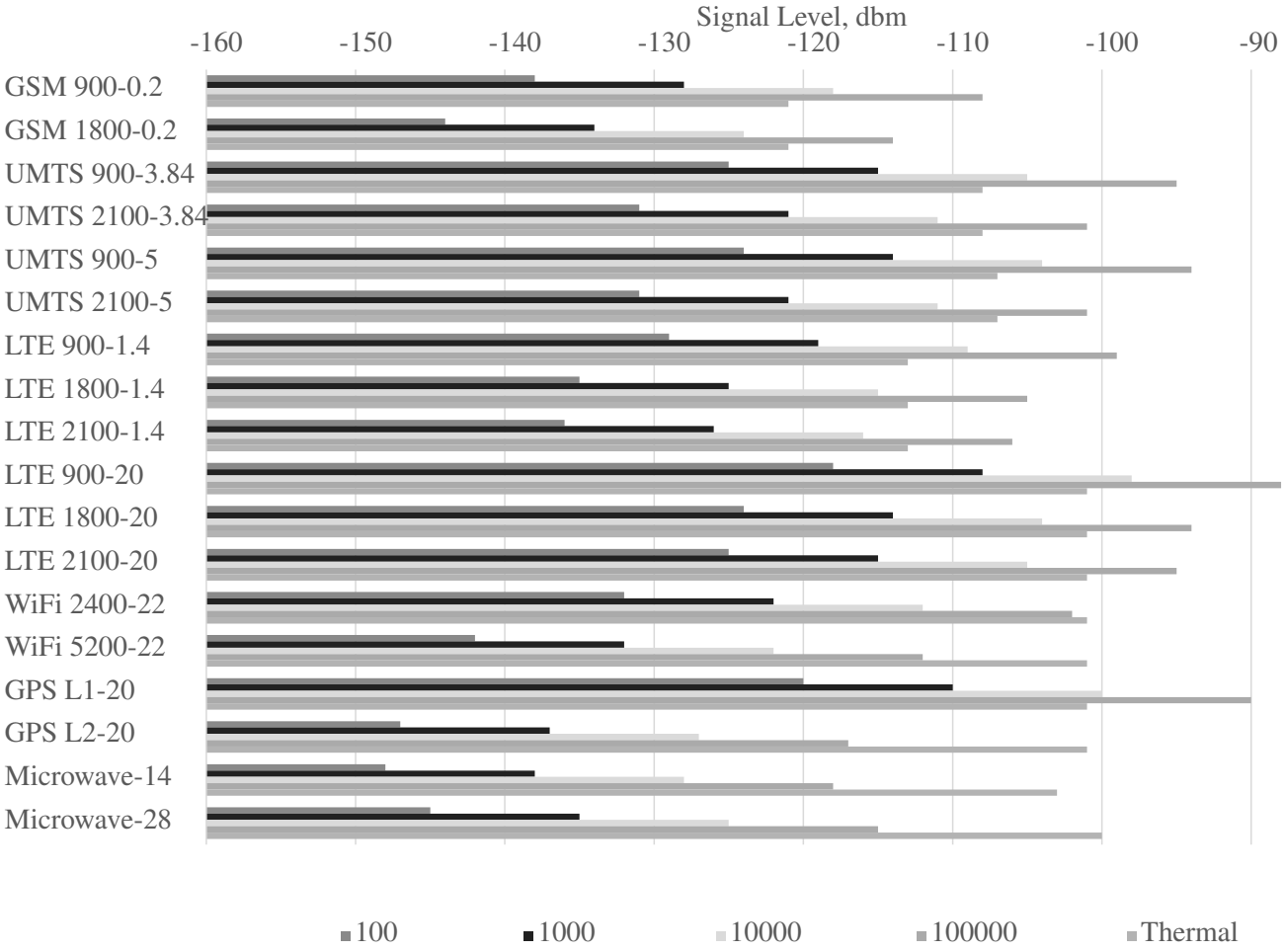

Figure 4.6: The legend indicates noise due to either solar flux level in SFU or thermal noise at 300 K. The top to bottom order shown in each technology group corresponds to the left to right order in the legend. The bars indicate the signal level in dB due to the solar flux for a given technology. The majority of configurations show at least one case where thermal noise is below solar radio noise. Microwave towers should have 3 dBm subtracted from interference level if the assumption is made that the antenna does not have a cross-polarised configuration, see Section 2.5.2. Results were calculated with Equation 3.1 and values are available in Table A.1 in the appendix. Technologies are listed in no particular order.

In the case of a base station, making use of real world values and assuming the worst case scenarios of largest bandwidth and lowest frequency per technology, LTE appears most susceptible of the technologies, see Table 4.3, especially considering how often solar radio events could occur, see Table 3.3, Figure 3.7 and 3.8.

Table 4.3: Base station sensitivity as specified by manufacturers and typically configured in a network compared to the order of magnitude of flux density (with and without the mean base station antenna gain of 16 dBi) that could be detected for typically used settings (supplied by the network operator), based on the results of Table A.1.

Technology	Sensitivity	Typical Configuration	SFU (0 dBi)	SFU (16 dBi)
GSM	-110 dBm	-102 dBm	>>100 000	10 000
UMTS	-115 dBm	-105 dBm	>10 000	>100
LTE	-140 dBm	-120 dBm	100	10

Distributions for LTE and UMTS noise indicators, see Figure 4.7, show that measured interference is in the same range as that which could be caused by solar radio flux, see Figure 4.6. For example, for a flux density of 10 000 SFU, LTE 900 with 20 MHz bandwidth experiences noise just over 3 dBm higher than the mean of the maximum UL interference counter (-101.36 dB, see Table 3.11).

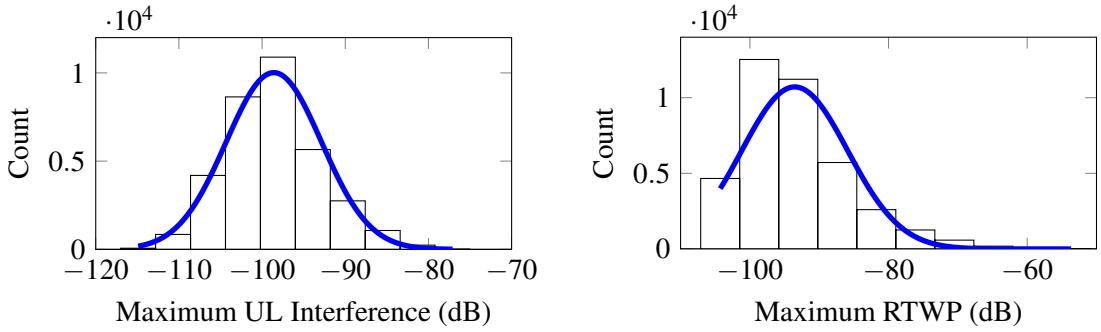

(a) (b)

Figure 4.7: Maximum UL interference for LTE and maximum RTWP for UMTS. (a) Daytime maximum UL interference distribution with Gaussian fit. (b) Maximum RTWP daytime distribution with Gaussian fit.

4.4 CORRELATION BETWEEN SPACE WEATHER AND CELLULAR NETWORK COUNTERS

Using the method as defined in Section 3.6, the null hypothesis[3] was accepted even when correlation was found high, therefore the results are not significant. For the all hours set, no correlation is found,

[3]The solar radio indicator does not relate to the cellular noise indicator

see Table 4.4. When applying the 3 and 20 dB down hour masks, results show -0.7 correlation coefficient between Bad RxQual and M-Class flares, however the p-values are high (1 and 0.73), thus the result is not significant. Application of the 3 and 20 dB down masks to good RxQual correlated against M-Class flares produces correlation coefficients of -0.56 and -0.7, but high p-values in both cases (0.44 and 0.51), the result is not significant. In both cases the result is due to low numbers of samples.

In summary, results of the correlation in Table 4.4 are:

- RSSI does not appear to correlate with space weather indicators and the p-value is larger than 0.05 in all cases. A benefit of all hours being used is that many samples are available.
- Bad RxQual shows some correlation (correlation coefficient -0.58 in the case of 2695 MHz radio bursts, but the p-value is too large (0.13), as too few values exist, therefore the correlation is not meaningful.
- Maximum RTWP for all hours shows some negative correlation (correlation coefficient of -0.38 to X class flares and with a p-value of 0.
- LTE UL interference shows small negative correlation in the case of 2695 MHz radio bursts and X class flares with small p-values.

The negative correlation coefficients which were found are counter intuitive and mean that when the size of space weather events increase, noise measurements on cellular network equipment are seen to be smaller than for small events.

Further investigation of correlation was performed by means of scatter plots to identify potential links between the various sets and to try to identify cases where a non-linear correlation seemed possible. No potential correlation was found using the scatter plots. Figure 4.8 shows typical results for the scatter plots, no evidence of non-linear relationships was found. Furthermore as can be seen in the analysis of the individual parameters, the samples are highly clustered, meaning that the sample diversity is not high.

Table 4.4: The result (correlation coefficient, p-value and number of samples) for correlation of magnitude of solar radio activity with cellular network counter statistics. Rows labeled with 20 dB and 3 dB indicate 20 dB down and 3 dB down antenna radiation patterns respectively. Those without dB in the label indicate correlation results without filtering hours based on line of sight with the sun.

Telecommunications Counter	Solar Radio Burst 245 MHz	Solar Radio Burst 2695 MHz	Solar Flare X-Class	Solar Flare M-Class
(μwave) Ave. RSSI	0.01 0.20 10971	-0.08 0.20 287	0.07 0.41 164	-0.04 0.15 1069
(μwave) Min. RSSI	0.00 0.61 10971	0.11 0.06 287	-0.06 0.47 164	0.03 0.29 1069
(μwave) Max. RSSI	0.01 0.17 10971	-0.09 0.15 287	0.06 0.47 164	-0.03 0.26 1069
(UMTS) Ave. RTWP	-0.01 0.15 18568	-0.13 0.02 324	-0.23 0.01 108	-0.01 0.86 936
(UMTS) 20 dB Ave. RTWP	-0.01 0.70 4104	-0.04 0.69 81	–	0.04 0.54 189
(UMTS) 3 dB Ave. RTWP	-0.02 0.48 324	–	–	0.00 1.00 13
(UMTS) Max. RTWP	-0.01 0.17 18568	-0.15 0.01 322	-0.38 0.00 108	0.00 0.91 934
(UMTS) 20 dB Max. RTWP	-0.00 0.83 4104	-0.08 0.44 81	–	-0.04 0.53 162
(UMTS) 3 dB Max. RTWP	-0.05 0.13 324	–	–	0.00 1.00 13
(UMTS) Min. RTWP	-0.01 0.46 18580	-0.10 0.08 324	-0.14 0.15 108	0.00 0.99 936
(UMTS) 2 dB Min. RTWP	-0.00 0.90 4104	-0.04 0.65 81	–	0.00 0.97 189
(UMTS) 3 dB Min. RTWP	-0.03 0.43 324	–	–	0.00 1.00 13
(LTE) Max. UL Int.	-0.02 0.03 15990	0.02 0.73 283	-0.26 0.01 95	-0.04 0.21 799
(LTE) 20 dB Max. UL Int.	-0.05 0.00 3624	-0.29 0.00 75	–	-0.04 0.53 162
(LTE) 3 dB Max. UL Int.	0.05 0.17 296	–	–	0.00 1.00 11
(LTE) Ave. UL Int.	0.01 0.35 15990	-0.01 0.92 283	0.01 0.92 95	-0.03 0.32 799
(LTE) 20 dB Ave. UL Int.	0.01 0.46 3624	-0.28 0.01 74	–	-0.04 0.54 162
(LTE) 3 dB Ave. UL Int.	0.07 0.03 296	–	–	0.00 1.00 11

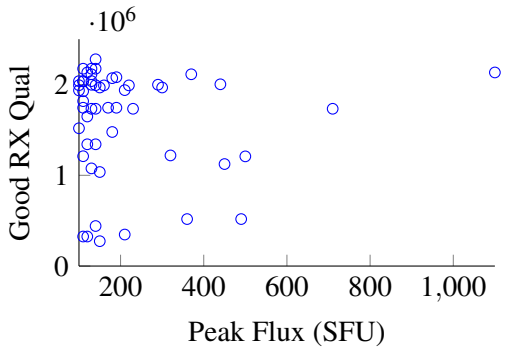

Figure 4.8: Good RxQual plotted against 245 MHz solar flux does not appear to indicate a correlation.

CHAPTER 5

DISCUSSION

The study supports the hypothesis that there may be a link between solar radio noise and interference on cellular networks, based on calculations of noise signal strength as a function of bandwidth and frequency, and making use of device specifications of typical cellular network technologies, as well as given observed values of operational counters (UMTS RTWP and LTE UL interference) in cellular networks. Because of the lower level of antenna gain, handsets appear less vulnerable to solar radio noise than the base station (Table 4.2).

A GSM base station, with a 16 dBi gain antenna, operating at 900 MHz carrier frequency and 200 KHz bandwidth, would need to be exposed to between 1 and 10 million SFU to be affected by interference at a level of -80 to -70 dBm, see Section 2.5.1 for details. Assuming a base station with a 16 dBi gain antenna and UMTS 900 with 5 MHz bandwidth, 1000 SFU would be sufficient to cause detectable interference, given the system specification of sensitivity of -117 dBm; however degradation is reported at levels of -100 to -95 dBm, thus flux density of 10 000 SFU may be necessary to produce performance degradation. As little as 10 SFU can be detected by LTE, at the base station, assuming a gain of 16 dBi. Even at 20 dB down, a 100 times reduction in sensitivity, susceptibility to solar radio noise is possible; a burst of 1000 SFU would be detectable as 10 SFU. If microwave systems in use are singly polarised and the operating frequencies are high (tens of GHz), susceptibility to solar radio noise is much lower than for systems using a cross-polarised antenna configuration and lower operating frequencies ($\sim$1–$\sim$3 GHz), as is the case for GSM, UMTS and LTE. Microwave backhaul high sites have much broader coverage than end nodes, but would typically face horizontally; thus they would be limited in total duration of line of sight interference from the sun. Microwave backhaul end nodes would face upwards or horizontally to high sites, however, beam widths would be very narrow as the links are point to point, limiting solar noise exposure for line of sight interference from

the sun. Of all of the technologies investigated, LTE is the most susceptible from a theoretical point of view, as it operates at a low carrier frequency and with high bandwidth, see Table 4.1.

As per Table 4.6, in all cases, where the carrier frequency was 900 MHz, thermal noise is lower than noise which would be caused by radio bursts. The radio bursts may not currently be considered as part of the noise floor, yet are significant and should be considered when specifying it.

Initially, it appeared that because of base station antennas typically being oriented downwards, away from the sun, and excluding the possibility of multi-path reflections, the time period for interference would be limited to sunrise and sunset hours, which is true when considering a typical 3 dB down antenna radiation pattern. It is evident that for the standard beam width of 3 dB, approximately three percent of cells come into direct line of sight with the sun per day; however $\sim$22 – $\sim$25 percent are in direct line of sight with the sun when considering the antenna radiation pattern of 20 dB down, therefore large events could cause interference over a much larger portion of the day than initially thought. Naturally, the susceptibility will be a function of the radiation pattern of the antenna. It is interesting that for the particular antenna in question, side lobes were much more pronounced than expected, leaving room for unexpected interference at midday.

Solar radio and X-ray flare events occur in decreasing frequency as the event magnitude increases, see Table 3.6. Radio burst events at 245 MHz are observed more often than at 2695 MHz, see Table 3.3. No 2695 MHz events of larger than 10 000 SFU were observed and no flares of magnitude greater than X6 were observed. Large solar radio events (>10 000 SFU) do occur infrequently, but on average (mean) one event was observed per year at 245 MHz and nearly one 1000 SFU event at 2695 MHz.

Microwave backhaul counters were not granular enough to be useful in the study, but the hourly resolution for GSM, UMTS and LTE is suitable; however higher time resolution would have been more desirable in order to establish a causal link between solar radio noise and interference on cellular networks. For the period 2013-04 to 2014-07-11, on average (mean), X-ray flare durations were 19.1 and 23.43 minutes for M and X-class events, respectively, with standard deviations of 12.21 and 15.82 respectively. On average (mean), radio burst durations were 6.8 and 11.88 minutes, for 245 and 2695 MHz events, respectively, with standard deviations of 42.66 and 12.73 respectively; however some events of many hours have occurred. Cellular disturbance of the longer duration X-ray flares do not seem to be more pronounced than those of solar radio bursts, at least visually, see Section 4.2.

Cellular phone counters that were aggregated by means of maximum value appeared visually to be Gaussian in distribution. Maximum UL interference and RTWP are good examples, with UL interference appearing most Gaussian. These counters have bigger differences between day an nighttime distributions than other aggregation methods (seen in Chapter 3), which was also evident in the analysis in Chapter 4. The difference in interference level between day and nighttime may be, in part, due to higher network traffic levels during the day. Particularly in the case of maximum LTE, as was expected from the results of the theoretical calculations, it does appear that an increase in interference occurs during sun incident hours compared to daylight and nighttime hours, though correlation between counters was not found and Kolmogorov-Smirnov tests between the distributions show that although five percent of samples differ, the distributions are the same.

An antenna with large secondary vertical lobes, combined with a cellular technology operating at low frequency and at a large bandwidth, is likely to be the most susceptible combination, providing more opportunities for line of sight with the sun and higher sensitivity to noise. For example, LTE with a carrier frequency of 900 MHz and 20 MHz bandwidth appears most susceptible. Technologies making use of wideband approaches to minimise interference at any particular frequency could be more affected by solar radio noise, since solar radio noise is wideband.

Assuming a large solar event, the overall potential effect of the sun during the day can be reduced if the side lobes of an antenna are small. An antenna design with small side lobes and/or shielding from above would stop potential interference problems to all but boresight. As technologies become more data-intensive and bandwidths become bigger, there may be increased susceptibility. High bandwidth technologies such as LTE could be operated at high rather than low frequencies as a precaution.

It is important to distinguish between perceived and actual impact of noise on a telecommunications system. Noise may cause minor problems on the physical layer that are not noticed by the end user. A dropped call is an example of user-perceived interference. Increased radio noise may not actually cause any user-perceived negative impact on the radio network, as wireless communication systems are designed to compensate for noise by deploying mitigating measures. The measures however will ultimately reduce throughput. Aggregated, the efficiency of the network could be reduced, which would have an associated cost. Currently, the impact of solar radio events could possibly be concealed by general network noise. An exceptionally large solar radio event, which was not available during the study period, would be needed to determine the full effect.

Milestones for the project that were reached are:

- Investigate the potential effect of space weather on cellullar telecommunications networks.
- Obtain solar flux data and become familiar with data by performing an initial analysis.
- Obtain proxy data, which can give a good indication of solar flux density and become familiar with data by performing an initial analysis.
- Obtain timestamped cellular network counters from a telecommunication network.
- Obtain solar flux, and radio noise data measurements for a comparable period to cellular network counters.
- Create a database of clean data.
- Gain an understanding of cellular network counters data.
- Determine if distributions for hours where cells were in line of sight with the sun experienced higher interference levels than otherwise.
- Determine if a correlation exists between solar events and degradations in network performance overall.
- Determine if a correlation exists between solar events and degradations in network performance for sun-facing hours.

CHAPTER 6

CONCLUSION AND FURTHER WORK

The contribution of the study is the determination that cellular communication networks are potentially susceptible to solar radio noise. Design and manufacturer specifications as well as network operator specified values were used in the determination. The methods for characterising solar interference on cellular telecommunications networks were presented. Requirements for further analysis have been determined. Cellular operators are constrained by network vendor and system designs, therefore it is difficult to increase data granularity of one system without affecting supporting systems. A cellular network is an ideal source of the required data, but operational constraints make it difficult to impossible to produce the data at the desired granularity and time periods. More granular data is required. The results are inline with expectations and indicate that 1 hour cadence is not good enough.This study provides the approach for future studies regarding solar interference in the cellular radio bands.

Calculations show that it is possible that solar radio noise could interfere with technologies used in cellular radio networks, especially in low frequency and high bandwidth applications, such as LTE and future high bandwidth systems. However, the data used for an initial investigation do not indicate a correlation owing to low granularity of cellular network data and lack of large solar events. Furthermore, solar events last on average (mean) fractions of hours, any positive correlation may be diluted. It is suggested that further studies collect solar event data for flux density of greater than 1000 SFU and cellular telecommunications performance data, for the bands of 900 – 2100 MHz, at minute granularity for periods around solar events. The overall potential effect of the sun during the day can be reduced if antennas are designed with small side lobes and/or shielding from above would stop potential interference problems to all but times of direct alignment with the sun, assuming that multi-path is not a factor.

Further work requires good quality, high granularity cellular and space weather data for long time periods and may include:

- Improving the equation used to calculate dBm from flux density by using the manufacturer specified aperture of antennas used in the cellular network, rather than an isotropic antenna.
- Selection of antennas that have radiation patterns uniform in azimuth would make results easier to understand. The experiment could be simplified by making use of a monopole antenna.
- Cellular telecommunication counters are available for short periods, but space weather data span tens of years. A long period and higher time resolution cellular counters would allow better analysis of known events. A number of years of data would be desirable.
- Network traffic is affected by many factors (service outages on numerous systems could affect other systems, pricing, convenience), thus some indicators may provide deceptive results, as the true source of interference is not known, therefore it would be beneficial to have a controlled experimental environment, rather than using a live network.
- Telecommunications counters in this study are similar, but not exactly equivalent, as technologies are different. Higher time resolution counters would be conducive to more precise analysis.
- Telecommunications counters of unprocessed signal or noise level would be useful, making comparison across technologies easier. Out-of-band measurements may not be fully indicative of in-band noise. The problem could be approached by recording wideband signal or noise level across the band 800 MHz to 3 GHz or in cellular networks frequency bands and making use of network counters. A standard cellular network multi-band antenna could be used and the signal noise level could be logged.
- The effect of multi-path or reflections of solar radio noise could be considered in future investigations.
- GPS was partially investigated theoretically and an overview presented, Section A.1. Future work could include an analysis of GPS data for interference and comparison to solar radio noise, since GPS operates in a similar band to cellular communications and data seems to be abundant.
- A number of dedicated cellular network antennas should be erected as per typical configuration on a cellular network. A further antenna could be adjusted to face or track the sun. Radio signal level can be measured on cellular network bands. A number of years' worth of data should be captured. This will allow initial study of the band in question. Further research making use of high time resolution cellular network counters could be performed if the initial investigation is

successful.

- A predictive model is likely to be based on a popular space weather indicator, such as $F_{10.7}$ or sunspot number. The space weather indicators investigated do not appear to correlate with $F_{10.7}$, see Section A.4. Further investigation is required for a suitable indicator.
- An approach making use of extreme value statistics may be a good continuation to this study.
- Non-thermal noise interference, especially considering typically experienced background noise at basestation sites as well as SNR requirements of the various modulation schemes could be further considered.

REFERENCES

[1] D. E. Gary *et al.*, "Effects of solar radio bursts on wireless systems," *Effects of Space Weather on Technology Infrastructure*, vol. 176, p. 203, 2004.

[2] P. Cannon, M. Angling, L. Barclay, C. Curry, C. Dyer, R. Edwards, G. Greene, M. Hapgood, R. B. Horne, D. Jackson *et al.*, *Extreme space weather: impacts on engineered systems and infrastructure*. Royal Academy of Engineering, 2013.

[3] Y. K. Tulunay and P. A. Bradley, "The impact of space weather on communication," *Annals of Geophysics*, vol. 47, no. 2-3 Sup., 2009.

[4] L. J. Lanzerotti, "Space weather effects on communications," in *Space Weather-Physics and Effects*. Springer, 2007, pp. 247–268.

[5] Z. Chen *et al.*, "Evaluation of solar radio bursts' effect on GPS receiver signal tracking within international GPS service network," *Radio Science*, vol. 40, no. 3, 2005.

[6] A. P. Cerruti *et al.*, "Observed solar radio burst effects on GPS/wide area augmentation system carrier-to-noise ratio," *Space Weather*, vol. 4, no. 10, p. S10006, 2006.

[7] L. J. Lanzerotti *et al.*, "Solar radio burst event (6 April 2001) and noise in wireless communications systems," *Bell Labs Technical Journal*, vol. 7, no. 1, pp. 159–163, 2002. [Online]. Available: http://dx.doi.org/10.1002/bltj.30

[8] J. M. Goodman, *Space weather and telecommunications*. Springer, 2005.

[9] R. Simon and S. Teperman, "The world trade center attack: lessons for disaster management," *Critical Care*, vol. 5, no. 6, p. 318, 2001.

[10] L. K. Comfort *et al.*, "Coordination in rapidly evolving disaster response systems the role of information," *American Behavioral Scientist*, vol. 48, no. 3, pp. 295–313, 2004.

[11] D. Tipper, T. Dahlberg, H. Shin, and C. Charnsripinyo, "Providing fault tolerance in wireless access networks," *Communications Magazine, IEEE*, vol. 40, no. 1, pp. 58–64, 2002.

[12] ETSI, "GSM Technical Specification. Digital cellular telecommunications system (Phase 2+); Radio subsystem link control (GSM 05.08)," ETSI, Tech. Rep., July 1996.

[13] NOAA/ Space Weather Prediction Center, "NOAA space weather scales," 2005, http://www.swpc.noaa.gov/NOAAscales/index.html. Last accessed on 07 August 2014.

[14] D. Guidice and J. Castelli, "Spectral distributions of microwave bursts," *Solar Physics*, vol. 44, no. 1, pp. 155–172, 1975. [Online]. Available: http://dx.doi.org/10.1007/BF00156853

[15] T. Takakura, "Microwave bursts of solar radio emission," *Publications of the Astronomical Society of Japan*, vol. 12, p. 55, 1960.

[16] G. M. Nita *et al.*, "Statistics of solar microwave radio burst spectra with implications for operations of microwave radio systems," *Space Weather*, vol. 2, no. 11, 2004.

[17] P. M. Kintner, B. O'Hanlon, D. E. Gary, and P. M. S. Kintner, "Global Positioning System and solar radio burst forensics," *Radio Science*, vol. 44, no. 1, pp. n/a–n/a, 2009. [Online]. Available: http://dx.doi.org/10.1029/2008RS004039

[18] R. L. Arnoldy *et al.*, "Energetic solar flare X-rays observed by satellite and their correlation with solar radio and energetic particle emission," *The Astrophysical Journal*, vol. 151, pp. 711–736, July 1967.

[19] N. Gopalswamy, "Type-I Solar Radio Bursts," *Kodaikanal Observatory Bulletins*, 1986.

[20] J. Schmelz and J. Brown, *The sun: a laboratory for astrophysics*. Kluwer Academic Publishers, 1992, pp. 411–422.

[21] S. M. Wentworth, *Fundamentals of electromagnetics with engineering applications*. Wiley, 2004, pp. 235–237.

[22] R. O. Pepin *et al.*, "The historical record of solar activity," in *The procedings of the Conference on the Historical Record of Solar Activity*, Boulder, Colorado, 1980, pp. 119–134.

[23] J. Beer *et al.*, "Use of 10Be in polar ice to trace the 11-year cycle of solar activity," *Nature*, vol. 347, no. 6289, pp. 164–166, Sep. 1990. [Online]. Available: http://dx.doi.org/10.1038/347164a0

[24] K. Tapping and B. DeTracey, "The origin of the 10.7 cm flux," *Solar Physics*, vol. 127, no. 2, pp. 321–332, 1990. [Online]. Available: http://dx.doi.org/10.1007/BF00152171

[25] J. A. Kennewell, "Solar radio interference to satellite downlinks," in *Antennas and Propagation. ICAP 89, Sixth International Conference*, vol. 2, no. 301. IET, 1989, pp. 334–339.

[26] M. G. Kivelson and C. T. Russell, *Introduction to space physics*. Cambridge University Press, 1995.

[27] K. R. Lang, G. Börner, A. Burkert, W. Burton, M. Dopita, A. Eckart, T. Encrenaz, E. Grebel, B. Leibundgut, J. Lequeux *et al.*, *The Sun from Space*, 2nd ed. Springer, 2009.

[28] S. Kahler, "Solar flares and coronal mass ejections," *Annual Review of Astronomy and Astrophysics*, vol. 30, pp. 113–141, 1992.

[29] T. Forbes, "A review on the genesis of coronal mass ejections," *Journal of Geophysical Research: Space Physics (1978–2012)*, vol. 105, no. A10, pp. 23 153–23 165, 2000.

[30] J. Phillips *et al.*, "Ulysses solar wind plasma observations at high southerly latitudes," 1995. [Online]. Available: http://trs-new.jpl.nasa.gov/dspace/bitstream/2014/30669/1/95-0802.pdf

[31] A. Fokker, "Type IV solar radio emission," *Space Science Reviews*, vol. 2, no. 1, pp. 70–90, 1963. [Online]. Available: http://dx.doi.org/10.1007/BF00174028

[32] IPS AUSTRALIA. Solar radio burst classifications. [Online]. Available: http://www.ips.gov.au/Category/World%20Data%20Centre/Data%20Display%20and%20Download/Spectrograph/Solar%20Radio%20Burst%20Classifications.pdf

[33] H. A. S. Reid and H. Ratcliffe, "A review of solar type III radio bursts," *Research in Astronomy and Astrophysics*, vol. 14, no. 7, p. 773, 2014.

[34] J. Fainberg and R. G. Stone, "Satellite observations of type III solar radio bursts at low frequencies," *Space Science Reviews*, vol. 16, pp. 145–188, Jun. 1974.

[35] V. Zheleznyakov and V. Zaitsev, "The origin of type-V solar radio bursts," *Soviet Astronomy*, vol. 12, p. 14, 1968.

[36] NASA, "File:Structureofthemagnetospheremod.svg," April 2014, https://en.wikipedia.org/wiki/File:Structure_of_the_magnetosphere_mod.svg. Last accessed on 08 April 2014.

[37] Sebman81, "File:IonosphereLayersen.svg," April 2014, https://en.wikipedia.org/wiki/File:Ionosphere_Layers_en.svg. Last accessed on 08 April 2014.

[38] "DONKI space weather database of notifications, knowledge, information," 2014, https://kauai.ccmc.gsfc.nasa.gov/DONKI. Last accessed on 01 April 2014.

[39] K. Tapping *et al.*, "Solar magnetic activity and total irradiance since the maunder minimum," *Solar Physics*, vol. 246, no. 2, pp. 309–326, 2007. [Online]. Available: http://dx.doi.org/10.1007/s11207-007-9047-x

[40] K. F. Tapping, "The 10.7 cm solar radio flux (F10.7)," *Space Weather*, vol. 11, pp. 394–406, July 2013.

[41] K. Tapping and D. Charrois, "Limits to the accuracy of the 10.7 cm flux," *Solar Physics*, vol. 150, no. 1-2, pp. 305–315, 1994.

[42] Government of Canada, "Solar radio flux - Archive of measurements," 2013, http://www.spaceweather.gc.ca/data-donnee/sol_flux/sx-5-eng.php. Last accessed on 15 April 2013.

[43] Space Weather Prediction Center (SWPC), "Radio bursts event list," 2010, http://www.swpc.noaa.gov/ftpdir/lists/radio/README2. Last accessed on 07 August 2014.

[44] G. P. Wiid *et al.*, "Radio frequency interference and lightning studies of a square kilometer array demonstrator structure," in *IEEE Transactions on electromagnetic compatibility*, vol. 53, no. 2, 2011, pp. 543–547.

[45] L. J. Lanzerotti, D. J. Thomson, and C. G. Maclennan, "Wireless at high altitudes environmental effects on space-based assets," *Bell Labs Technical Journal*, vol. 2, no. 3, pp. 5–19, 1997.

[46] C. Ho *et al.*, "Interference effects of deep space network transmitters on IMT-2000/UMTS receivers at s-band," *The Telecommunications and Mission Operations Progress Report 42-142, April–June 2000*, pp. 1–21, 2000.

[47] A. Eisenblatter, H.-F. Geerdes, and M. Grotschel, "Planning UMTS radio networks," *OR/MS Today*, vol. 35, pp. 41–46, 2008.

[48] J. Raza *et al.*, "Spatial filtering of RF interference in radio astronomy," *Signal Processing Letters, IEEE*, vol. 9, no. 2, pp. 64–67, 2002.

[49] P. A. Fridman and W. A. Baan, "RFI mitigation methods in radio astronomy," *Astronomy & Astrophysics*, vol. 378, pp. 327–344, 2001.

[50] Cisco, "Cisco visual networking index: global mobile data traffic forecast update, 2012-2017," 2013, http://www.cisco.com/en/US/solutions/collateral/ns341/ns525/ns537/ns705/ns827/white_paper_c11-520862.html. Last accessed on 23 April 2013.

[51] S. Prasad *et al.*, "Performance analysis of OFDMA in LTE," in *Computing Communication & Networking Technologies (ICCCNT), 2012 Third International Conference on*. IEEE, 2012, pp. 1–7.

[52] FCC, "First report and order in the matter of revision of part 15 of the commission's rules regarding ultra-wideband transmission systems," Federal Communication Commission, ET Docket 98-153 FCC 02-48, April 2002.

[53] M. Hamalainen, R. Tesi, and J. Iinatti, "UWB coexistence with IEEE 802.11 a and UMTS in modified Saleh-Valenzuela channel," in *Ultra Wideband Systems, 2004. Joint with Conference on Ultrawideband Systems and Technologies. Joint UWBST and IWUWBS. 2004 International Workshop on*. IEEE, 2004, pp. 45–49.

[54] M. Hamalainen, V. Hovinen, R. Tesi, J. H. Iinatti, and M. Latva-aho, "On the UWB system coexistence with GSM900, UMTS/WCDMA, and GPS," *Selected Areas in Communications, IEEE Journal on*, vol. 20, no. 9, pp. 1712–1721, 2002.

[55] B. T. Ahmed and M. C. Ramon, "On the impact of ultra-wideband (UWB) on macrocell downlink of UMTS and CDMA-450 systems," *Electromagnetic Compatibility, IEEE Transactions*

on, vol. 50, no. 2, pp. 406–412, 2008.

[56] M. A. Al-Adwany, A. Ali, E. Najim, and A. M. Younis, "A study on the effect of UWB interference on downlink UMTS system," in *Energy, Power and Control (EPC-IQ), 2010 1st International Conference on*. IEEE, November 2010, pp. 107–110.

[57] B. Taha-Ahmed, M. Calvo-Ramon, and L. Haro-Ariet, "Impact of ultra wide band (UWB) on macrocell downlink of DCS-1800 and GSM-900 systems," *Radioengineering*, vol. 14, no. 1, pp. 51–55, April 2005.

[58] K. E. Lonngren, S. V. Savov, and R. J. Jost, *Fundamentals of electromagnetics with MATLAB*, 2nd ed. Scitech Publishing, 2007, ch. 8, p. 451.

[59] D. Levin. (2014, April 16), "*Cell signal receive angle*," [Online]. Available e-mail: david.levin@digitata.com Message: Cell Signal Receive Angle.

[60] Kathrein Scala Division, *Multiband directional antenna*, Kathrein Scala Division, Medford, OR 97501 USA.

[61] K. Chetty. (2013, April 19), "*Masters thesis discussion*," [Online]. Available e-mail: Chetty_K@mtn.co.za Message: Masters Studies: Dropped Call Data and Frequency Allocations.

[62] ICASA, "Legislation and regulations - Engineering and technology - Radio frequency spectrum management - Frequency spectrum usage and availability spectrum usage Q1 2013," 2013, https://www.icasa.org.za/. Last accessed on 30 April 2013.

[63] B. Bala *et al.*, "Noise in wireless systems produced by solar radio bursts," *Radio Science*, vol. 37, no. 2, p. 1018, 2002.

[64] L. Lanzerotti *et al.*, "Noise in wireless systems from solar radio bursts," *Advances in Space Research*, vol. 36, no. 12, pp. 2253–2257, 2005.

[65] C. S. Carrano, C. T. Bridgwood, and K. M. Groves, "Impacts of the December 2006 solar radio bursts on the performance of GPS," *Radio Science*, vol. 44, no. 1, pp. n/a–n/a, 2009. [Online]. Available: http://dx.doi.org/10.1029/2008RS004071

[66] M. Stasiak, M. Głąbowski, A. Wiśniewski, and P. Zwierzykowski, *Modeling and dimensioning of mobile networks from GSM to LTE*. Chichester, UK: John Wiley & Sons, Ltd., 2011, ch. 1.

[67] 3GPP, *Technical specification group GSM/EDGE radio access network; physical layer on the radio path; general description (Release 12)*, 3GPP, 2012.

[68] J. Karlsson and J. Heinegard, "Interference rejection combining for GSM," in *Universal Personal Communications, 1996. Record., 1996 5th IEEE International Conference on*, vol. 1. IEEE, 1996, pp. 433–437.

[69] M. Salmenkaita, J. Gimenez, P. Tapia, and M. Fernandez-Navarro, "Optimizing the GSM/EDGE air interface for multiple services with dynamic frequency and channel assignment," in *Vehicular Technology Conference, 2002. Proceedings. VTC 2002-Fall. 2002 IEEE 56th*, vol. 4. IEEE, 2002, pp. 2215–2219.

[70] K. Heiska, *GSM, GPRS and EDGE Performance: Evolution towards 3G/UMTS*, 2nd ed. Wiley Online Library, 2003, ch. Appendix D: Interference between GSM/EDGE and Other Cellular Radio Technologies, pp. 587–597.

[71] ITU, "Focus on international regulations for spectrum management and satellite orbits," 2010, http://www.itu.int/net/pressoffice/press_releases/2010/48.aspx. Last accessed on 06 October 2013.

[72] D. Astély, E. Dahlman, A. Furuskar, Y. Jading, M. Lindstrom, and S. Parkvall, "LTE: the evolution of mobile broadband," *Communications Magazine, IEEE*, vol. 47, no. 4, pp. 44–51, 2009.

[73] D. Levin. (2013, June 11), "*Performance counter discussion*," [Online]. Available e-mail: david.levin@digitata.com Message: Performance Counters.

[74] ICASA, "Spectrum usage & spare broadcasting frequencies Q1 - 2012," June 2012, https://www.icasa.org.za/. Last accessed on 5 May 2014.

[75] *Hughes AirReach Broadband 9000 Element EMS, Revision F*, Hughes Network Systems, LLC, 11717 Exploration Lane, Germantown, MD 20876, 2005.

[76] A. Clegg, "RF dialects: Understanding each other's technical lingo," in *Third IUCAF Summer*

School on Spectrum Management for Radio Astronomy, National Science Foundation. IUCAF, June 2010.

[77] A. Schneider, "Find 'missing' elevations with GPS visualizer," 2013, http://www.gpsvisualizer.com/elevation. Last accessed on 15 April 2014.

[78] United States Naval Observatory, "Sun or moon rise/set table for one year," March 2012, http://aa.usno.navy.mil/data/docs/RS_OneYear.php. Last accessed on 18 April 2014.

[79] I. Reda and A. Andreas, "Solar position algorithm for solar radiation applications," Technical report, nREL Report No. TP-560-34302, www.osti.gov/bridge, Tech. Rep., January 2008.

[80] V. Roy, "sun_position.m," 2009, www.mathworks.com/matlabcentral/fileexchange/4605sunpositionm. Last accessed on 16 April 2014.

[81] W. F. Denig, "NOAA/NESDIS/NGDC/STP, boulder-solar radio data," 2003, http://www.ngdc.noaa.gov/stp/solar/solarradio.html. Last accessed on 08 April 2013.

[82] ETSI, "3GPP TS 45.005 v8.8.0. 3rd generation partnership project; technical specifaction group GSM/EDGE radio access network; radio transmission and reception (Release 8)," ETSI, Tech. Rep., March 2010.

[83] ——, "ETSI TS 125 101 V11.9.2 Universal Mobile Telecommunications System (UMTS); user equipment (UE) radio transmission and reception (FDD) (3GPP TS 25.101 version 11.9.2 Release 11)," ETSI, Tech. Rep., April 2014.

[84] ——, "ETSI TS 136 101 V8.4.0 LTE; evolved universal terrestrial radio access (E-UTRA); user equipment (UE) radio transmission and reception (3GPP TS 36.101 version 8.4.0 Release 8)," ETSI, Tech. Rep., January 2009.

[85] E. D. Kaplan and C. J. Hegarty, *Understanding GPS: principles and applications*. Massachusetts, USA: Artech House, 2005.

[86] P. Daly, "Navstar GPS and GLONASS: global satellite navigation systems," *Electronics & Communication Engineering Journal*, vol. 5, no. 6, pp. 349–357, 1993.

[87] Lockheed Martin, "U.S. Air Force awards Lockheed Martin GPS III flight operations con-

tract," May 2012, http://www.lockheedmartin.com/us/news/press-releases/2012/may/0531-ss-gpsIII.html. Last accessed on 19 October 2013.

[88] J. Aarons, "Global morphology of ionospheric scintillations," *Proceedings of the IEEE*, vol. 70, no. 4, pp. 360–378, 1982.

[89] F. A. Khan and A. G. Dempster, "Impacts of GPS-based synchronization degradation on cellular networks," in *International Global Navigation Satellite Systems Society (IGNSS) Symposium*, 2007.

[90] A. Vallat and D. Schneuwly, "Clock synchronization in telecommunications via PTP (IEEE 1588)," in *Frequency Control Symposium, 2007 Joint with the 21st European Frequency and Time Forum. IEEE International*. IEEE, 2007, pp. 334–341.

[91] "IEEE standard for a precision clock synchronization protocol for networked measurement and control systems," IEEE Instrumentation and Measurement Society, Tech. Rep., July 2008.

[92] The Mathworks Inc. Matlab Product Help [program]. Version 7.12.0 (R2011a), Mathworks 2011.

APPENDIX A

FURTHER ANALYSIS

A.1 GLOBAL NAVIGATIONAL SATELLITE SYSTEM

GPS is a global navigation satellite system constellation of satellites providing freely available location services on a standard positioning service with a horizontal accuracy of typically 13 m and 22 m for altitude for single frequency receivers. The Precise Positioning Service is primarily for US government use. The system makes use of triangulation and timing advance or time of arrival [85] (corrected for relativistic effects) to calculate position. Four satellites are required for location calculation (latitude, longitude, altitude, receiver clock offset) if the receiver time is not precisely calibrated [86]. If only the altitude is desired, only three visible satellites are required.

GPS operates close to cellular networks in frequency. The antenna used is right-hand circularly polarised. The separation of GPS signal into L1 at 1575.42 MHz and L2 at 1227.60 MHz is designed to estimate and compensate for ionospheric group path delay [8] and a spread spectrum signal, Code Division Multiple Access (CDMA), is used to transmit signal at 10.23 Mbps. Spread spectrum gives the system some immunity from jamming. CDMA codes are chosen so that cross correlation and therefore interference is minimised between satellites. The carrier modulation is binary phase shift keying . A minimum received signal power requirement is -158.5 dB, -161.5 dB and -164.5 dB for L1 C/A, L1 P and L2 respectively.

A short or C/A (course/acquisition) (on L1) and long or P(Y) (precision code) signals (on L1 and L2) are currently used for calculating location. GPS III, with first satellites due in 2014 [87], will provide more precision and robustness by means of L2C (essentially M, P(Y) and C/A code on L2 frequency) and L5 (P(Y) code on 1176,45 MHz) [85]. M is a more robust code developed for military

applications.

Interference with GPS includes that of ionospheric origin. The ionospheric scintillation index, S_4, which describes intensity fading [88], is derived from rapidly sampled GPS signals. Strong scintillation can cause receivers to malfunction. Single frequency users are more affected [8].

GPS may be more sensitive to interference than thought [5][6]. At 1.415 GHz, 4000 – 12000 SFU can cause in-band interference resulting in loss of lock on the L2 signal. On 2003-10-28, a strong radio burst was observed between 11:02 – 11:12 and 11:42 - 12:00 UT. Solar flux magnitude reached 7000 and 12000 respectively. Ionospheric total electron content increased on the sun-facing side of the planet at the equator during the events. Total electron content fluctuations had a secondary impact on the system.

Although it is not related to radio noise, noise experienced by GPS systems may be an indicator of noise in other systems. It is possible that at a given time, even though GPS may experience interference, a cellular radio network may not, as antennas should be oriented towards the sun to experience negative effects. Coded GPS receivers may perform better than uncoded ones, especially since L1 and L2 noise components are not additive.

The ability of GPS to function depends on carrier-to-noise ratio. As the ratio becomes smaller, performance decreases. GPS signal is affected by interference, multipath and scintillation [85]. Interference is more likely to be unintentional and from out-of-band signal from other communication systems. Jamming (malicious interference) needs to be wideband to interfere with the CDMA used in GPS. Systems are designed to be resistant to interference from systems of the same type (intra-system or self-interference). The band in which L2 operates is co-primary, meaning that other services also operate in the band, such as high-powered pulsed radar systems. Solar radio noise is expected to occur as wideband noise for short periods and likely pulses. GPS is resilient to pulsed interference owing to clipping in the receiver analogue-to-digital converter, assuming quick response from automatic gain control and that the A/D does not saturate.

Historically, cellular networks rely on GPS for governing synchronisation of timing for GSM, UMTS [89] and LTE. If GPS systems lose lock, timing may be affected, because systems in the core and radio network lose synchronisation. This could cause user-perceived call quality decreases as well as quality of service, especially during cell handover and calls may be dropped. However, IEEE 1588v2 (IEEE 1588-2008) or precision timing protocol (PTP) [90] is designed to provide timing

synchronisation more accurately than network time protocol and more cost-effectively than dedicated GPS devices. PTP can use IP as a transport [91].

A.2 THEORETICAL SENSITIVITY TO SOLAR FLUX

Table A.1: SFU and the equivalent power in dBm as would be detected at a receiver for cellular technologies and primary frequencies (Freq) and bandwidth (BW), in MHz. Microwave towers can have 3 dBm subtracted from interference level if the assumption is made that the antenna does not have a cross-polarised configuration, see Section 2.5.2. Results were calculated with Equation 3.1. Thermal indicates thermal noise at 300 K. Technologies are listed in no particular order.

	Freq	**BW**	**100 SFU**	**1 000 SFU**	**10 000 SFU**	**100 000 SFU**	**Thermal**
GSM 900	900	0.2	-138 dBm	-128 dBm	-118 dBm	-108 dBm	-121 dBm
GSM 1800	1800	0.2	-144 dBm	-134 dBm	-124 dBm	-114 dBm	-121 dBm
UMTS 900	900	3.84	-125 dBm	-115 dBm	-105 dBm	-95 dBm	-108 dBm
UMTS 2100	2100	3.84	-131 dBm	-121 dBm	-111 dBm	-101 dBm	-108 dBm
UMTS 900	900	5	-124 dBm	-114 dBm	-104 dBm	-94 dBm	-107 dBm
UMTS 2100	2100	5	-131 dBm	-121 dBm	-111 dBm	-101 dBm	-107 dBm
LTE 900	900	1.4	-129 dBm	-119 dBm	-109 dBm	-99 dBm	-113 dBm
LTE 1800	1800	1.4	-135 dBm	-125 dBm	-115 dBm	-105 dBm	-113 dBm
LTE 2100	2100	1.4	-136 dBm	-126 dBm	-116 dBm	-106 dBm	-113 dBm
LTE 900	900	20	-118 dBm	-108 dBm	-98 dBm	-88 dBm	-101 dBm
LTE 1800	1800	20	-124 dBm	-114 dBm	-104 dBm	-94 dBm	-101 dBm
LTE 2100	2100	20	-125 dBm	-115 dBm	-105 dBm	-95 dBm	-101 dBm
WiFi 2400	2400	22	-132 dBm	-122 dBm	-112 dBm	-102 dBm	-101 dBm
WiFi 5200	5200	22	-142 dBm	-132 dBm	-122 dBm	-112 dBm	-101 dBm
GPS L1	1577.5	20	-120 dBm	-110 dBm	-100 dBm	-90 dBm	-101 dBm
GPS L2	1227.6	20	-147 dBm	-137 dBm	-127 dBm	-117 dBm	-101 dBm
Microwave	26000	14	-148 dBm	-138 dBm	-128 dBm	-118 dBm	-103 dBm
Microwave	26000	28	-145 dBm	-135 dBm	-125 dBm	-115 dBm	-100 dBm

A.3 $F_{10.7}$

In order to understand the data better, $F_{10.7}$ flux values and sunspot number were combined into a single data set. $F_{10.7}$ and sunspot number datasets with data from 1947–2007, reported correlation of 0.82.

The $F_{10.7}$ data were stratified into three groups:

- Max - Dates that fall within two years of solar maximum.
- Min - Dates that fall within two years of solar minimum.
- Neither - Dates that fall into neither of the above.

Descriptive statistics have been calculated, see Table A.2, and box plots of the groups, see Figure A.1, plotted. The grouping appears to be consistent with the fitted distributions. The groups are skewed to the right. Whiskers are calculated as per Matlab defaults and correspond to roughly 2.7σ. Whiskers encompass values larger than Q3+1.5×(Q3-Q1) and smaller than Q1-1.5×(Q3-Q1). Q1 and Q3 are the 25th and 75th percentiles [92].

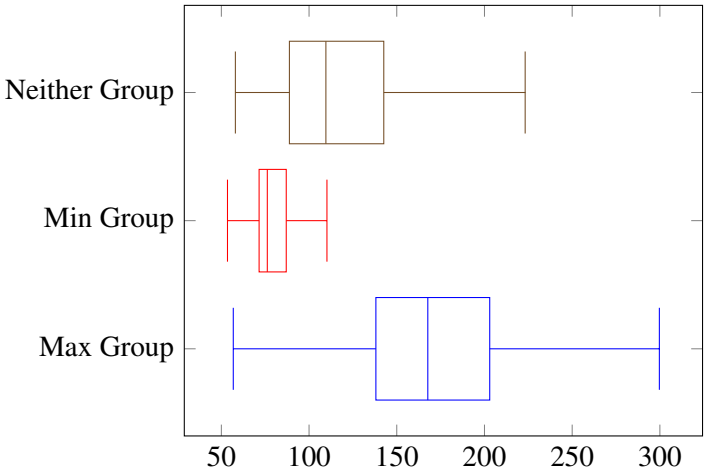

Figure A.1: It appears that the groups are acceptable, even though there are some outliers.

Histograms of the three groups were fitted to distributions by making use of Matlab dfitool, Figure A.2. The datasets are distributed as expected with the minimum set containing low values; the 'neither' group intermediate values and the maximum group the highest values. Some overlap between groups does exist, which is reasonable, given the noisy characteristics of the data.

$$f(n) = \sim 3^n * 11 \tag{A.1}$$

The system has been described by:

$$f_{full}(x) = 150 + f_1(x) + f_2(x) + f_a(x) + f_b(x) + f_c(x) \tag{A.2}$$

$$f_{basic}(x) = 150 + f_1(x) + f_2(x) + f_3(x) \tag{A.3}$$

The individual components are:

$$d_f = 365 * 7 + 2/\pi \tag{A.4}$$

$$\begin{aligned} f_a(x) &= 20 * sin(d_f * x/365/3.0619 \\ f_1(x) &= 42 * sin(d_f * x/365) \\ f_c(x) &= 36 * sin(d_f * x/365/5.6104) \\ f_2(x) &= 88 * sin(d_f * x/365/2.6669) \\ f_3(x) &= 13.8 * sin(d_f * x/365/7.9983) \end{aligned} \tag{A.5}$$

(A.6)

The fundamental component representing the 11-year cycle is Equation A.2. The equation for f_{full}, Equation A.5, uses all of the major components identified by the Fourier transform and f_{basic} makes use of only the three most prominent frequencies. A shift of seven years was decided on based on visual inspection, Equation A.4.

A problem with this model is that the lower than expected third solar cycle in the graph complicates the modelling. Ideally, all maximums and minimums should be normalised, resulting in a more general model. This requires more investigation, but is currently unnecessary. The benefit of using a spline for interpolation and of removing anomalies, which may cause high frequency noise components, appears to be minimal when comparing frequency analysis results, Figure A.4, A.5 and A.6.

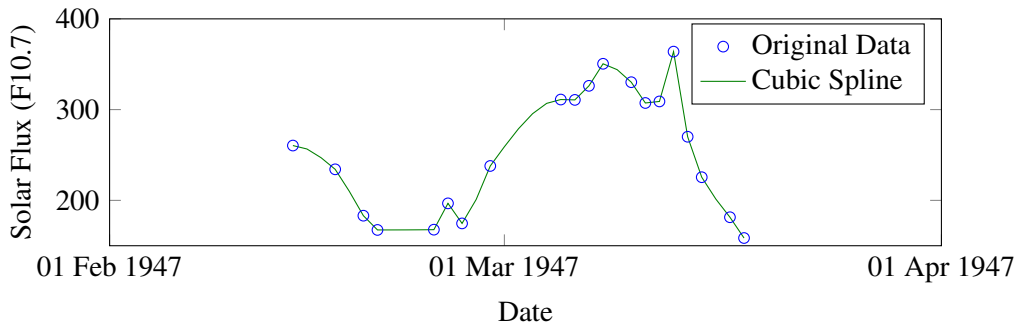

Figure A.3: First 30 interpolated values from cubic spline showing intersection with actual measurements.

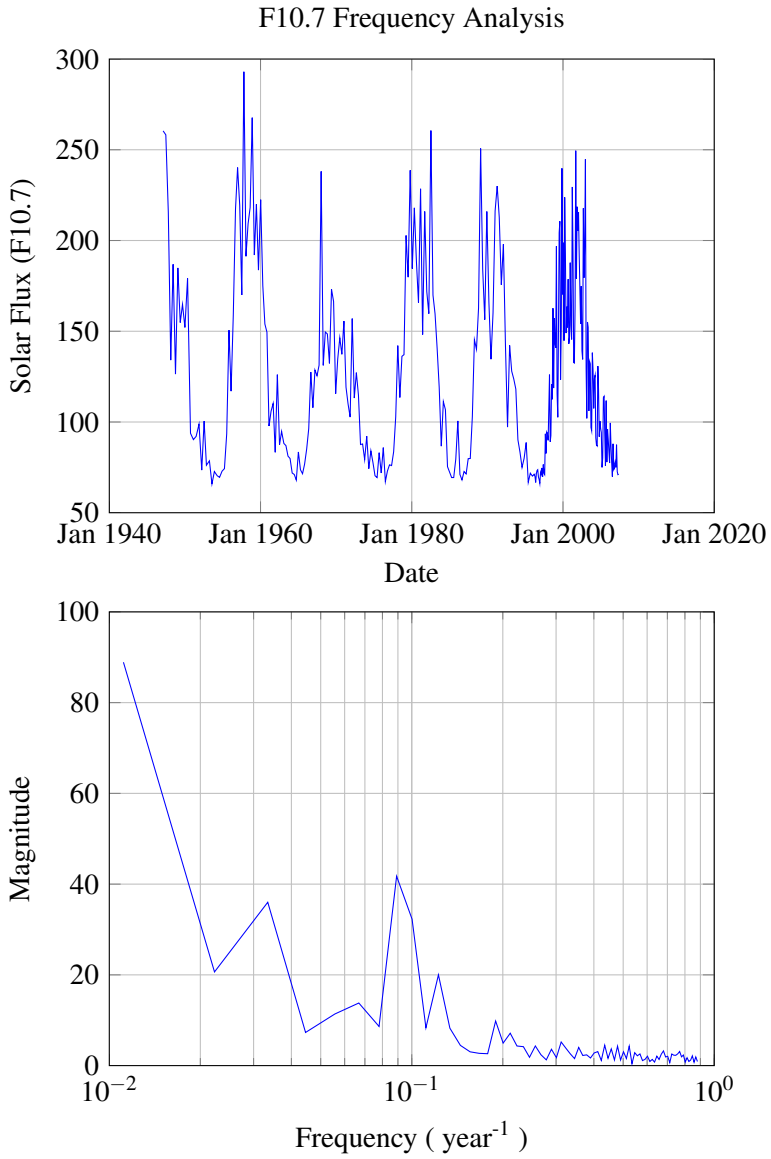

Figure A.4: A frequency analysis of solar flux data shows the most significant components are at approximately 89, 29 and 11 years. The 11-year cycle agrees with the literature.

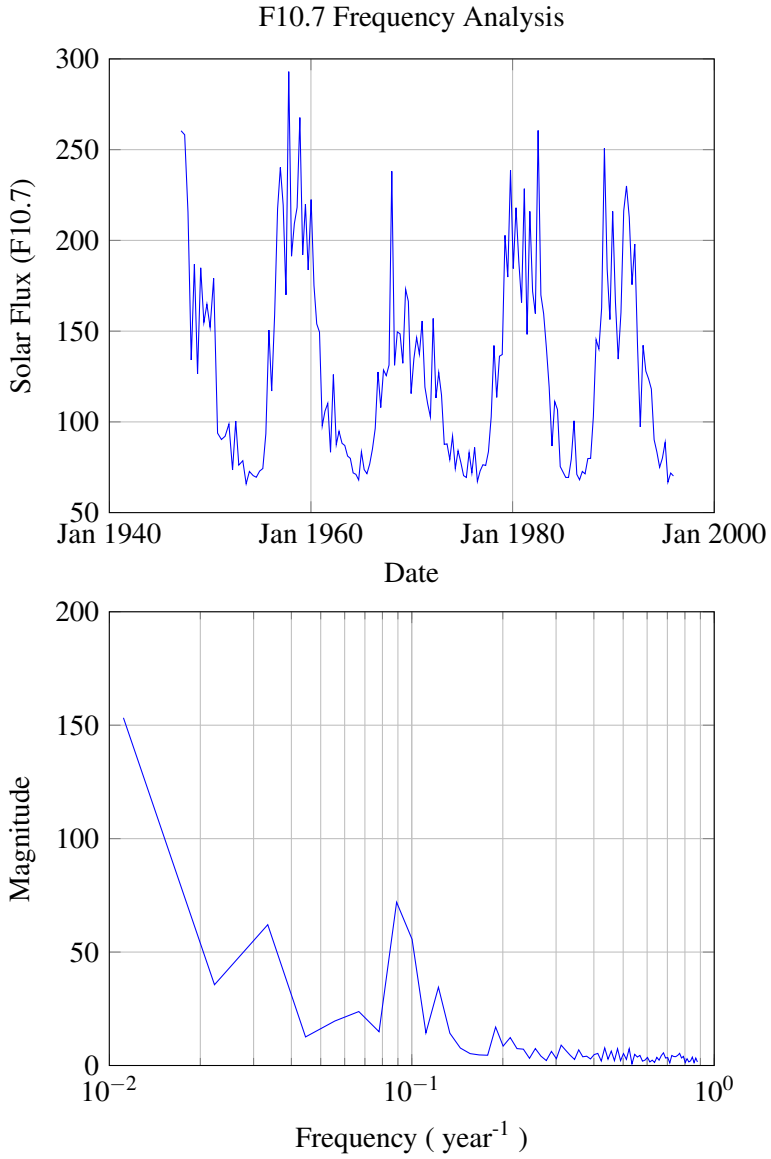

Figure A.5: A frequency analysis of solar flux data shows the most significant components are at approximately 89, 29 and 11 years. Spiky data have been removed in an effort to improve frequency analysis. The 11-year cycle agrees with the literature.

F10.7 Frequency Analysis with Cubic Spline and Moving Average Applied

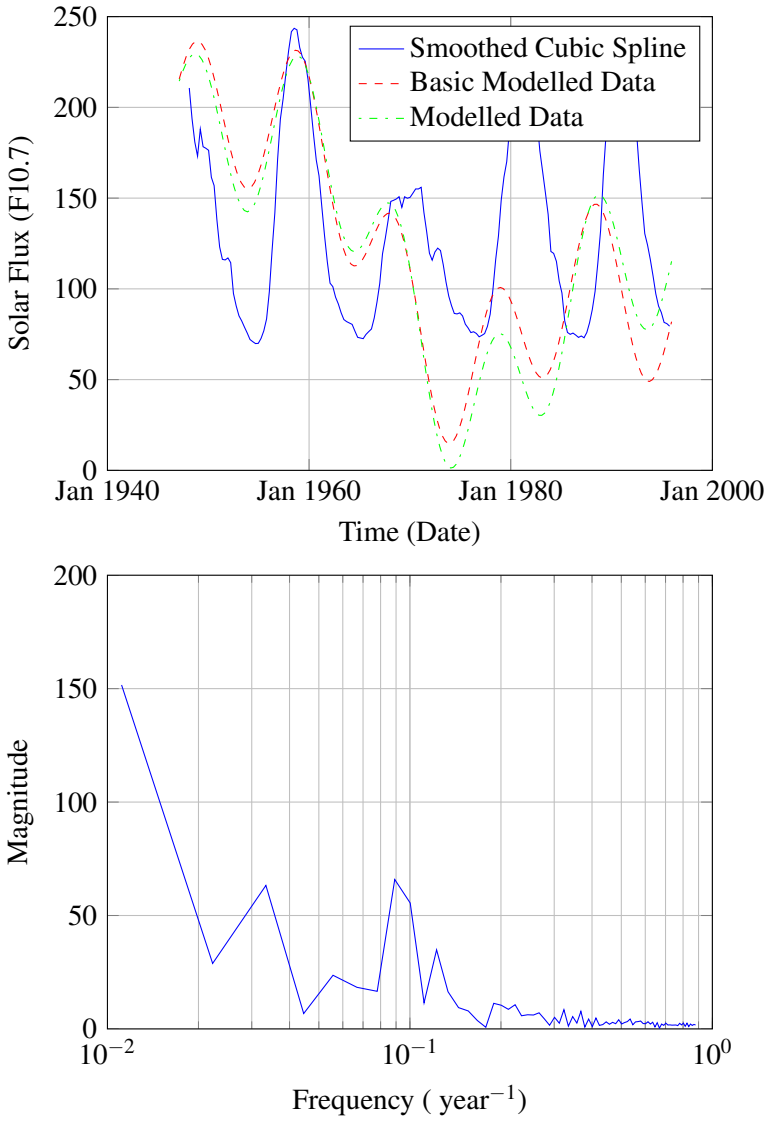

Figure A.6: A frequency analysis of solar flux data post cubic spline interpolation shows the most significant components are at approximately 89, 29 and 11 years. The 11-year cycle agrees with the literature.

A.4 CORRELATION BETWEEN SPACE WEATHER INDICES

Figures showing plots of correlation between data sources where correlation was found are presented. Plots of data used in the correlation between RxQual and M-class flare can be seen in Figure A.7. No significant relationship appears to exist between radio bursts and X-ray flares for the period 2014-02-22 to 2014-05-23. Data were used according to Table A.3 to perform correlation between the space weather indices. Figure A.8 investigates the possibility of a correlation between $F_{10.7}$ noon flux and solar flares, as well as between $F_{10.7}$ noon flux and peak flux. Correlation was also performed between solar flux and solar flare data, see Figure A.9. No correlation was found. The data used to correlate X-ray flare, solar radio bursts and $F_{10.7}$ are described by Table A.3.

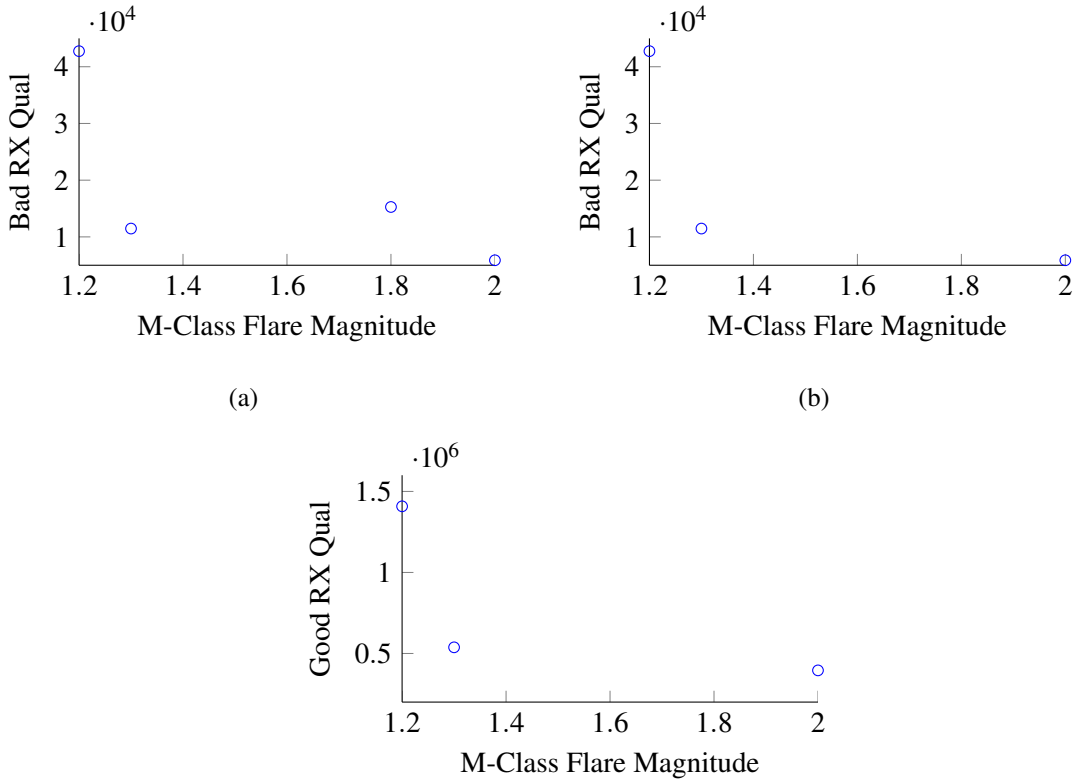

Figure A.7: Scatter plots of M-class X-ray flare magnitude against RxQual. Correlation is not evident because of insufficient samples. (a) M-class flare versus bad RxQual for 20 dB down. (b) M-class flare versus bad RxQual for 3 dB down. (c) M-class flare versus good RxQual for 20 dB down.

Table A.3: Particulars of data used for correlation of $F_{10.7}$ with X-ray flares and solar radio bursts.

Source	Data	Samples	Granularity	Period
NOAA SWPC	Solar radio bursts	Per event	Second	1996-07-13 to 2014-04-16
NOAA SWPC	GOES-8 GOES-15 SEM/XRS 1.0-8.0	Per event	Second	1997-02-02 to 2013-10-10
NOAA SWPC	$F_{10.7}$ Noon Flux	Daily	Noon	1996-07-13 to 2014-04-16

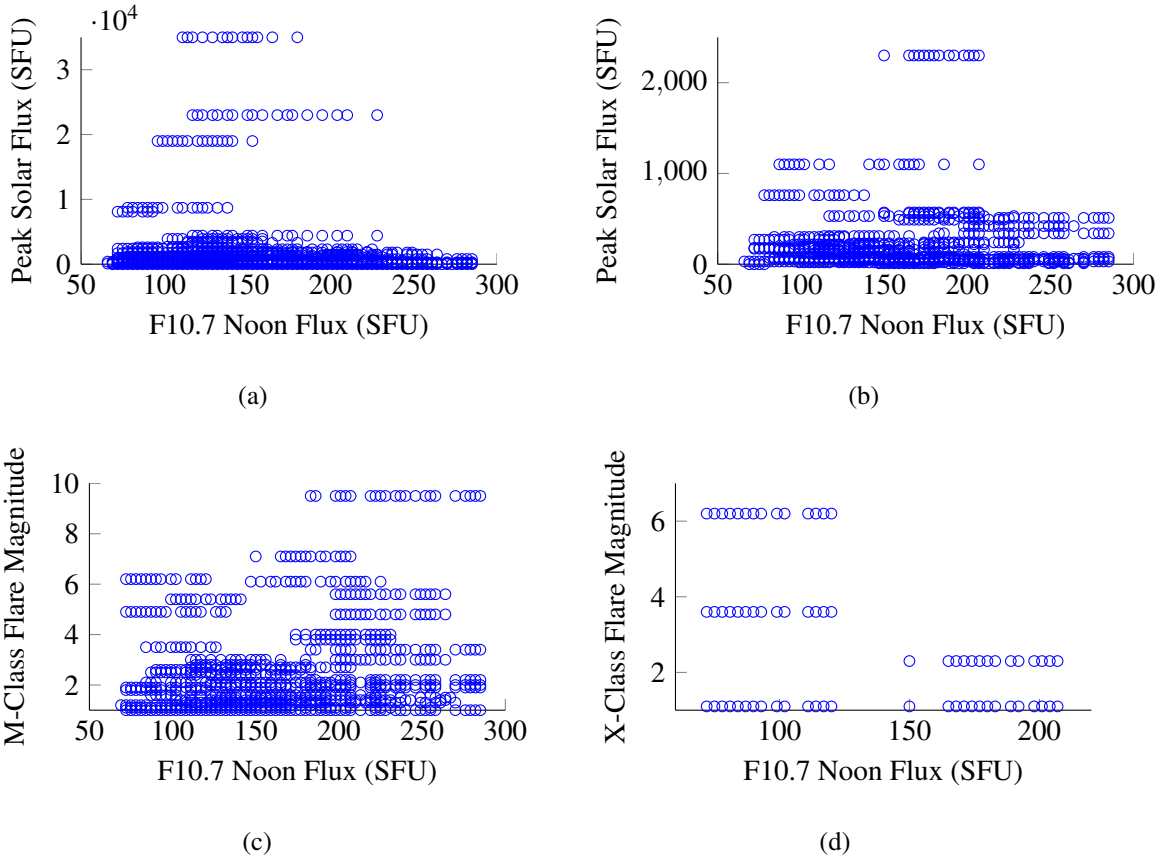

Figure A.8: Scatter plots of peak solar flux and X-ray flare magnitude against $F_{10.7}$ noon flux investigating correlation. Correlation is not evident. (a) Peak solar flux for 245 MHz versus $F_{10.7}$ noon flux for the period 1996-07-13 to 2014-04-16. (b) Peak solar flux for 2695 MHz versus $F_{10.7}$ noon flux for the period 1996-07-13 to 2014-04-16. (c) M-class solar flare magnitude versus $F_{10.7}$ noon flux for the period 1997-02-02 to 2013-10-10. (d) X-class solar flare magnitude versus $F_{10.7}$ noon flux for the period 1997-02-02 to 2013-10-10.

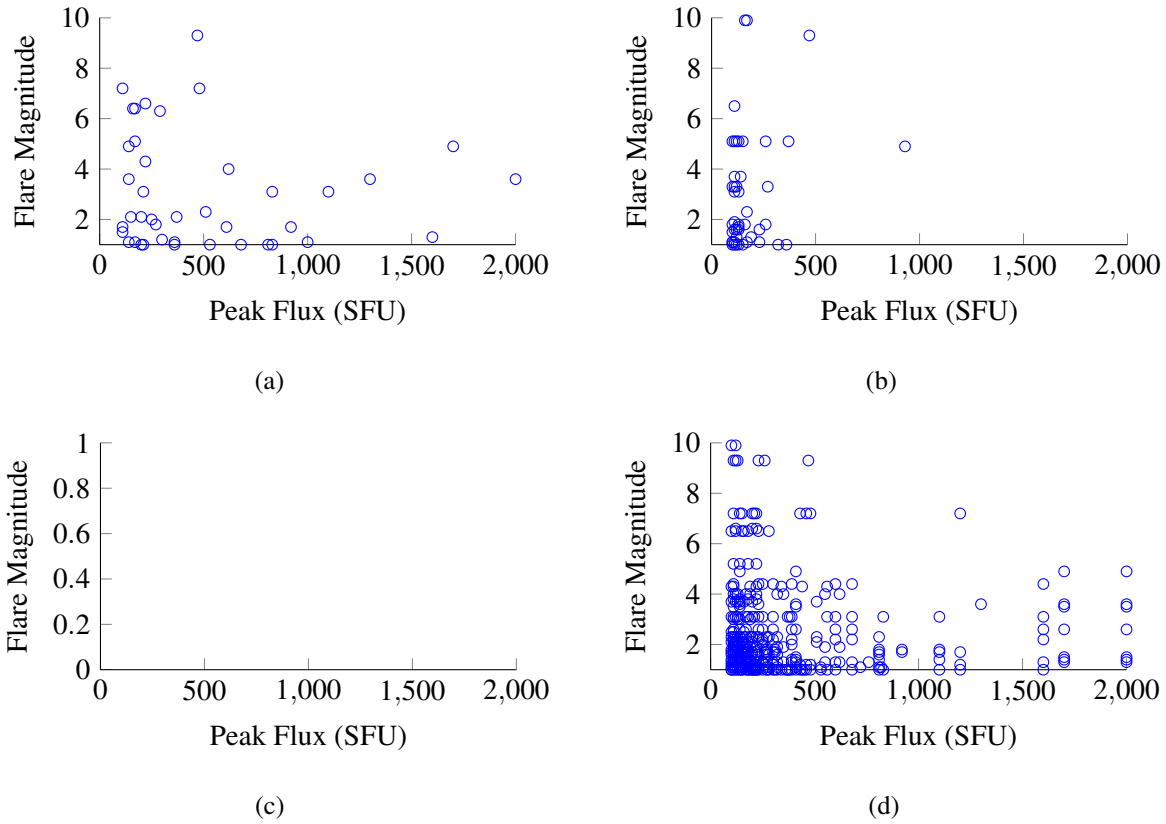

Figure A.9: Solar flare magnitude plotted against peak flux. Outliers above 2000 SFU are excluded for clarity. (a) X-ray flare magnitude versus peak flux for start hours of coinciding events. (b) X-ray flare magnitude versus peak flux for peak hours of coinciding events. (c) X-ray flare magnitude versus peak flux for end hours of coinciding events. No matches exist for the available hours. (d) X-ray flare magnitude versus peak flux matched on coinciding event days. Increasing the time period does not result in correlation.

Department EERC
Course M.ENG
Course Code ERI 890
Student Writing Dissertation Jan Adam Vivian Zieba
Supervisor : Sunil Maharaj
Theses/Dissertation Title : The Characterisation Of Space Weather Effects On Cellular And Microwave Telecommunication

Book/Journal Title	Author/Editor	Chapter/Article title	Author	ISBN/ISSN	Publisher	Page numbers
1) Kathrein:Scala Division		Multiband Directional Antenna	Kathrein Inc.	742 241	*Kathrein inc. Scala Division.*	Figures : 824–960 MHz and 1710–2170 MHz : Vertical pattern ±45°-polarization 0.5°–7° electrical downtilt
2) Kathrein:Scala Division		Multiband Directional Antenna	Kathrein Inc.	742 241	*Kathrein inc. Scala Division.*	Figures : 824–960 MHz and 1710–2170 MHz : Horizontal pattern ±45°-polarization
3) The Sun From Space	Kenneth R. Lang	Chapter 6		3540769528	*Springer*	Page 267, Figure 6.9
4) The Sun From Space	Kenneth R. Lang	Chapter 6		3540769528	*Springer*	Page 279, Figure 6.12
5) The Sun From Space	Kenneth R. Lang	Chapter 6		3540769528	*Springer*	Page 310, Figure 6.28